

Aus der Klinik und Poliklinik für Hals-, Nasen-, Ohrenkrankheiten, Kopf- und
Halschirurgie
(Direktor/in Univ.- Prof. Dr. med Werner Hosemann)
der Universitätsmedizin der Ernst-Moritz-Arndt-Universität Greifswald

**Proteome dynamics of non-thermal atmospheric plasma
treated airway epithelial cells**

Inaugural - Dissertation

zur

Erlangung des akademischen
Degrees

Doktor der Zahnmedizin
(Dr. med. dent.)

der

Universitätsmedizin

der

Ernst-Moritz-Arndt-Universität

Greifswald

2012

vorgelegt von: Philipp Emicke
geb. am: 09.10.1985
in: Hamburg

Dekan: Prof. Dr. rer. nat. Heyo K. Kroemer

1. Gutachter: Prof. Dr. med. Werner Hosemann

2. Gutachter: Jun.-Prof. Dr. rer. nat. Lars Leichert

Ort, Raum: Greifswald, Hörsaal Zentrum für Zahn-, Mund- und Kieferheilkunde

Tag der Disputation: 28.08.2012

1. Index

1. Index	3
2. Abbreviations.....	5
3. Table of figures	7
4. Abstract	9
5. Introduction	11
5.1. Non-thermal atmospheric plasma	11
5.2. Possible applications of non-thermal atmospheric plasma.....	12
5.3. Effects on eukaryotic tissues and cells	13
5.4. Proteomic approach provides new insights into adaption mechanisms of cells after non-thermal plasma treatment.....	14
5.5. Possible use of non-thermal plasma in Ear-, Nose- and Throat (ENT) medicine....	14
6. Focus of this thesis	17
7. Material and Methods.....	19
7.1. Cell line and Cell cultivation.....	20
7.2. Non-thermal atmospheric pressure plasma (ENTplas) treatment.....	21
7.3. Wound model	24
7.4. Sample preparation for proteomic analysis	25
7.5. Two-dimensional difference in-gel electrophoresis (2D-DIGE)	26
7.6. Statistical analysis.....	27
7.7. Preparative 2D gel electrophoresis and sample preparation for mass spectrometry 	29
7.8. Matrix-assisted laser desorption-ionization time-of-flight mass spectrometry (MALDI-TOF-MS).....	30
7.9. Network and protein functional analysis using specialized software	31
7.10. Immuno Blot analysis.....	31
8. Results.....	33
8.1. ENTplas treatment improves proliferative activity of S9 airway epithelial cells in an in vitro wound model	33

8.2. Two-dimensional difference in-gel electrophoresis (2D-DIGE) reveals alterations in the proteome of S9 airway epithelial cells triggered by ENTplas treatment	35
8.3. Principal component analysis demonstrates both: experimental quality and the appearance of ENTplas treatment-related effects	41
8.4. Statistical comparison and subsequent network analysis of ENTplas treated samples and their corresponding control (GeneSpring[®]-analysis) give first insights into affected cellular functions and pathways	43
8.5. ENTplas-mediated changes in the proteomic profile displayed by treemaps confirm the appearance of oxidative stress after ENTplas treatment.....	46
8.6. Correlation of protein expression patterns displayed by Hierarchical Clustering...49	
8.7. K-means-Clustering as an assumption-free approach for regulated protein recruitment out of a large data set	51
8.8. Network analysis of calculated K-means Cluster using Ingenuity Pathway Analysis (IPA) suggests underlying molecular functions of likely expressed protein subsets53	
8.9. Immuno Blot analysis of cytosolic Nrf2 expression confirms the involvement of this oxidative stress related regulator	54
8.10. Cytosolic concentrations of full length IL-1beta and IL-33 are decreased in S9 epithelial cells after ENTplas treatment, suggesting processes of stimulation and modulation of immune-related cytokines	56
9. Discussion.....	57
9.1. The influence of non-thermal plasma treatment on wound healing	58
9.2. The role of Nrf2 in ROS-induced intracellular oxidative stress environments after non-thermal plasma treatment	59
9.3. Biomarkers for further analyses, risk assessment and plasma-source designing65	
9.4. Other potential ENT-specific applications of non-thermal plasma.....65	
10. References.....	69
11. Appendix	i
Supplemental material.....	ii
Danksagung	lxiii

2. Abbreviations

Abbreviation	stands for:
2D-SDS-PAGE	two-dimensional sodium dodecylsulfate polyacrylamide gel-electrophoresis
APPJ	atmospheric pressure plasma jet
BSA	bovine serum albumin
CHAPS	3-[(3-Cholamidopropyl)dimethylammonio]-1-propanesulfonate
CTFR	cystic fibrosis conductance regulator
DBD	dielectric barrier discharge
DIGE	difference in-gel electrophoresis
DNA	deoxyribonucleic acid
ENTplas treatment	epithelial cell non-thermal plasma treatment
FGF-2	fibroblast-growth-factor 2
h	hour(s)
HRP	horseradish peroxidase
KEGG	Kyoto Encyclopedia of Genes and Genomes
MALDI-TOF-MS	matrix-assisted laser desorption/ionisation time-of-flight mass-spectrometry
min	minute(s)
mRNA	messenger ribonucleic acid
MRSA	methicillin-resistant <i>Staphylococcus aureus</i>
NO	nitric oxide
PVDF	polyvinylidene fluoride
RNA	ribonucleic acid
RNS	reactive nitrogen species
ROS	reactive oxygen species

sec	second(s)
TBS-T	tris-buffered saline Tween-20
UV	ultraviolet (light)
W	watt(s)

3. Table of figures

Figure 1: Micrographs of cultured S9-epithelial cells.....	21
Figure 2: Scheme of the atmospheric pressure non-thermal plasmajet kINPen 08 used.	22
Figure 3: Non-thermal plasma treatment procedure of the whole cell.	24
Figure 4: Schematic view from above of the cell culture plate.	24
Figure 5: Scheme of the distribution of the punched wounds for one entire 10 cm cell culture plate.....	25
Figure 6: 2D-DIGE experimental setup and workflow.....	27
Figure 7: Effect of ENTplas treatment on S9 epithelial cell wound healing.....	34
Figure 8: Complex fusion gel of 120 s ENTplas treated S9 cells 0 h after treatment.	35
Figure 9: Dual channel fusion images of ENTplas treated S9 epithelial cells versus the corresponding non-treated control.....	36
Figure 10: Classification of all identified proteins by cellular function.	38
Figure 11: 2D-DIGE analyses of ENTplas treated S9 epithelial cells.....	39
Figure 12: Proteinmodifications detected after ENTplas treatment.	40
Figure 13: Principal Component Analysis (PCA).	42
Figure 14: Molecular Function and Toxicity Analysis assessed by IPA (Ingenuity Pathway Analysis).	45
Figure 15: Visualization of large data sets by Voronoi Treemaps.....	48
Figure 16: Hierarchical Clustering of detected 2D-DIGE protein spots by sample condition and expression profile.	50
Figure 17: Protein expression profile analysis by K-means clustering.	52
Figure 18: Validation of by Immuno Blot analyses of Nrf2 and Keap1 cytosolic concentrations after ENTplas treatment.....	55
Figure 19: Cytosolic IL-1 beta and IL-33 levels after ENTplas treatment determined by Immuno Blotting.....	56
Figure 20: Ingenuity Pathway Analysis network of MALDI-TOF-MS identified proteins from statistical analysis.....	62
Figure 21: Hypothetical scheme of non-thermal plasma treatment cell stimulation via the Nrf2-pathway.....	64

4. Abstract

Non-thermal atmospheric pressure plasma has recently been shown to have broad application potential for medical as well as industrial purposes. Improved wound healing and tissue decontamination have been described as consequences of non-thermal plasma treatment. However, thus far the underlying molecular mechanisms in human tissues have only been partially characterized.

In this work a two-dimensional difference in-gel electrophoresis (2D-DIGE) approach was used and an analysis-workflow to study the response of human cells to atmospheric pressure non-thermal plasma was established. Human S9 bronchial epithelial cells were used as a model for airway epithelial cells. They were treated with atmospheric pressure plasma jet (APPJ) for different periods of time. Subsequently, time-resolved comparative proteome analysis was used to study the complex cellular adaptation reactions after a 120 sec plasma treatment, which accelerated wound healing in a clinically relevant model. The results indicate, that intracellular oxidative stress due to the non-thermal plasma treatment either leads to cell death or to proliferation. The oxidative stress response, mediated by Nrf2, appears to play a pivotal role in molecular signalling and might be a key pathway determining the fate of stressed cells. This thesis demonstrates changes in Nrf2-expression after non-thermal plasma treatment. Furthermore, potential protein biomarker candidates for evaluation of oxidative stress after non-thermal plasma treatment were identified.

Finally, it is shown, that the cytosolic concentrations of IL-1 β and IL-33 were decreased following non-thermal plasma treatment. Thus, modulation of innate immune response by non-thermal plasma treatment of epithelial cells (ENTplas treatment) is concluded.

5. Introduction

5.1. Non-thermal atmospheric plasma

Plasma is a specific gaseous state usually considered the fourth state of matter. By applying energy to gases, electrons may be liberated to yield a fully or partially ionized gas, which is referred to as plasma. In nature plasmas are found in lightning and in the magnetosphere [1]. About 99 % of all known visible matter in the universe is in the plasma state. Plasma is normally generated at temperatures far above 1000°C and is therefore dangerous for life. However, it is also possible to create low-temperature artificial plasmas (“non-thermal” or “cold plasma”). Non-thermal plasma of this sort is used for example in TV- plasma screens or in energy-saving lamps [2].

These low-temperature plasmas can be created either under low or atmospheric pressure conditions. A distinction is made primarily between so-called “jet”-sources and the “dielectric-discharge barrier” (DBD)-sources. Both make use of a high-frequency alternating voltage, which are able to excite the surrounding gases and to convert it into the plasma state. Both technical approaches can be used in pulsed and unpulsed modes. Interrupting the voltage source creates pulsed plasmas with decreased output temperatures. DBD-sources are primarily using the surrounding air, while jet-sources can excite gas in capillaries between two electrodes. In this latter case not only ambient but also various gas mixtures and rare gases such as Argon can be converted into plasma and are transported to the origin. The jet-sources have the advantage that the flow-rate of these passing gases can be defined and varied. The electrical excitation leads to the formation of ions, radicals and free electrons in the excited plasma field, which may then interact with surrounding materials. The composition of non-thermal plasmas has been well described by Sensenig et al. and Heinlin et al. [3], [4]. Beside the charged particles, such as ions and electrons, they mentioned electric fields, UVA-, UVB- and UVC-radiation and heat as additional components. Furthermore, reactive oxygen species (ROS) such as O, OH, HO₂, H₂O₂, electrically excited oxygen (O (1D)), O₂ ¹Δ_g and O₃ were detected in non-thermal plasmas. Finally, reactive nitrogen species (RNS), such as NO, NO₂ occurred in the excited plasma field.

5.2. Possible applications of non-thermal atmospheric plasma

The availability of non-thermal atmospheric pressure plasma sources opened a wide field of possible applications not only in technology, but also in the military and last but not least the medical field [5–8]. Nowadays, industrial plasma is frequently used e.g. for staining fibres and plastics, converting fuels into hydrogen, food preservation and surface conditioning [5–7] and air decontamination [8]. The results of these attempts drew the military's attention to this new technology and decontamination of biohazards and biological warfare agents like anthrax became a possible application [9].

However, the most interesting facet of non-thermal atmospheric plasma may be in civil applications. Beside the industrial attempts, first initial observations of biological and medical applications were promising. Investigation of interactions of non-thermal atmospheric plasmas with human body fluids and tissues *in-vitro* and *in-vivo* were the first studies in this field. Fridman et al. showed, that blood coagulates significantly faster after non-thermal plasma treatment of wounds *in-vivo* [10], [11]. Furthermore, they investigated the effect of a non-thermal plasma treatment on wound healing of chronic wounds [8], [12]. They were able to show, that non-thermal plasma has a supporting effect on the wound healing. Furthermore, non-thermal plasma has the ability to kill bacteria, even methicillin-resistant *Staphylococcus aureus* (MRSA) strains, on surfaces and even on patient's skin [13–16].

Based on these observations, two main fields of medical applications of atmospheric-pressure plasma can be envisioned: The first and most innovative field is the direct application onto patient's skin for therapeutic purposes [17] ranging from skin disinfection via treatment of infective skin diseases, stimulation of wound healing [8], [15], [18], dental applications [19–21] to cancer treatment [8], [19], [22], [23]. The second type of application is plasma-based decontamination or sterilization [24–33], or the improvement of biocompatibility of surfaces, materials, devices, or implants for subsequent medical applications [34–37]. In addition to its general antimicrobial activity a main advantage of non-thermal plasma is its ability to inactivate even MRSA and biofilms [16], [31], [32], [38] to resolve recent MRSA and biofilm-related issues. An overview of the published effects of non-thermal atmospheric plasma on eukaryotic cells and tissues will be summarized in the following chapters.

5.3. Effects on eukaryotic tissues and cells

Based on the initial findings, further and more detailed investigations concerning the effects of non-thermal plasma treatment on eukaryotic cells were performed in different working groups. Kalghatgi et al. demonstrated a stimulation of proliferation of human endothelial cells by non-thermal atmospheric plasma [39]. In contrast, they found increased cell damage and the induction of apoptosis in melanoma cells at higher doses of non-thermal plasma [3]. Similar results have been shown by Kim et al. [40]. Colorectal cancer cells showed increased cell growth arrest and initiation of apoptotic activity after a non-thermal plasma treatment.

Sensenig et al. and Kalghatgi et al. were able to demonstrate in melanoma cells as well as in endothelial cells and mammalian cells the increased appearance of reactive oxygen species (ROS) after non-thermal plasma treatment [3], [39], [41]. ROS are believed to be the most potent reactive agents interacting with surfaces and tissues during a non-thermal plasma treatment [42]. ROS appeared elevated in the medium after non-thermal plasma treatment and even in the medium alone, prior to addition to the cell cultures, and caused subsequent effects. Increased activities of Fibroblast-Growth-Factor-2 (FGF-2) in endothelial cells have been associated with increased levels of extra- and intracellular ROS after non-thermal plasma treatment. Removing the short wave UV-light during non-thermal plasma treatment showed no significant differences in the effects achieved, supporting a subordinate role of UV radiation [41].

When much higher doses of plasma have been applied to human tissues, less positive effects of a non-thermal plasma treatment were described [41], [43]. Both studies found DNA damage and cell death after non-thermal plasma treatment.

These observations lead to the conclusion, that the effects of a non-thermal atmospheric plasma treatment on living cells and tissues can be diverse under different conditions and seem to be dose-dependent. Thus, on the one hand overdoses of plasma-treatment leads to cell damage, but on the other hand, lower doses may induce potentially useful effects like cell proliferation [39], [41], [44]. Although many *in-vitro* attempts have been made to modulate cell repair and regeneration using non-thermal plasmas, the underlying molecular mechanisms mediating the effects have not been completely investigated so far. Here, proteomic analyses can provide new insights by providing protein level information of global adaptation reactions.

5.4. Proteomic approach provides new insights into adaption mechanisms of cells after non-thermal plasma treatment

Proteomics deals with changes in the pattern of expressed proteins. Proteins and their modified forms are physically separated and identified. Proteins are the result of an evolutionarily developed system, which follows a central dogma of molecular biology from the reading (transcription) of DNA, the genetic material, to the RNA to the proteins, which are translated from the RNA. With few exceptions (i.e.: reverse transcriptase), this procedure is a one-way street and ends at the proteins and the execution of their functions. The aforementioned components of this system are subject during this cascade to many changes and modifications. And for each of these parts there is a specific area of molecular biology to befriend them.

Quantitation of these changes in response to external stimuli can shed light on changes induced in cell physiology by the stimulus. It is to be expected that non-thermal plasma treatment may well result in alterations of protein levels since protein damaging agents, including ROS, reactive nitrogen species, UV and infrared radiation are generated. This allows both comparison of plasma dosage and the determination of the kinetics of the effects. Interesting protein candidates are identified by mass spectrometry, allowing a subsequent wider network analysis.

By performing time-resolved experiments direct and secondary effects of plasma treatment can be studied. To achieve a better understanding of the effects of cold plasma on human mucosa, ENTplas (Epithelial Non-Thermal Plasma) treatment-related changes on the proteome level of S9 epithelial cells were investigated as a surrogate model for airway medical use. Recent studies by Hellings et al. [45] established a united airways model, considering no relevant molecular biological and physiological differences between upper and lower airways. Thus, results from experiments with S9 epithelial cells should be able to transfer to both levels, allowing conclusions to a broader field of application.

5.5. Possible use of non-thermal plasma in Ear-, Nose- and Throat (ENT) medicine

Various medical applications of non-thermal plasma to skin have been developed and tested over the last years [4], [17]. In order to define special requirements for possible

ENT applications, some specific properties of oral and airway-specific mucosa have to be considered. The mucosae of the upper airways and the oral cavity are different from skin surfaces elsewhere on the human body and are much more sensitive to external plasma applications. Furthermore, the mucosa of the oral cavity in particular has a different resident bacterial population from the dermis [46–48]. *Staphylococcus aureus*, however, colonises both oral and airway mucosa as well as the skin and can lead to severe infection after tissue injury [49], [50]. Extensive bacterial colonization and biofilms may inhibit wound healing [51], [52], which in turn requires biofilm removal or prevention strategies. It is commonly assumed that low dose non-thermal atmospheric pressure plasma could potentially satisfy these needs: Recent studies by Winter et al. [53] actually showed impacts of low temperature gas plasma on vegetative bacteria on protein level. Treatment with non-thermal argon plasma led to severe DNA and cell wall damages. Comparable studies with human cells have not been done so far, but are necessary to verify the safety of an appropriate treatment.

However, if non-thermal plasma treatment of human tissues can be shown to be harmless at defined doses, many possible applications can be envisaged ranging from the stimulation of wound healing to tissue decontamination.

6. Focus of this thesis

The application of non-thermal plasma showed promising results for different purposes in the medical field. Phenomena, such as the accelerated clotting of blood or the support of wound healing *in vivo* have already been described. The effects of non-thermal plasma treatment emerged to be dose dependent. Thus, higher applied doses resulted in tissue damage and apoptotic reactions.

Although more and more applications are being sought, the basic effects of non-thermal treatment are still not understood on the cellular and subcellular level for eukaryotic cells. Because of this, risk assessment and source design cannot be optimally performed at this time.

The aim of this work is to examine the effects of non-thermal plasma application on protein levels in an epithelial cell model. For this purpose, a physiological relevant system had first to be established as well as an experimental wound-healing protocol. After that, molecular effects of the non-thermal plasma treatment were examined using a proteomic approach consisting of a high-resolution two-dimensional difference in-gel polyacrylamide gel electrophoresis (2D-DIGE-PAGE) and subsequent identification of proteins by MALDI-TOF-mass-spectrometry. Statistical methods for quantitative analyses had to be established and selected for the resulting large data sets. Furthermore, visualization of large data sets had to be tested and modified.

Finally, the detected biological effects on proteins and their expression have to be understood in terms of cell physiology.

7. Material and Methods

In order to investigate the intracellular effects of a non-thermal plasma treatment on upper airway epithelial cells, a proteomic approach was chosen. After cell cultivation and non-thermal plasma treatment, protein extraction and labelling was carried out using a protocol developed for the difference in-gel electrophoresis methodology (DIGE). This method, previously described by Westermeier et al. [54], [55], uses an internal standard, which permits normalization of spot intensities from different gels. This 2D gel procedure shows approximately 1500 protein spots per gel in the region between pI 4 to 7 and a molecular weight from 10 kDa up to 120 kDa. The major advantage of this two-dimensional gel-based method is the ability to directly detect protein modifications, which result in changes of pI or molecular weight. Oxidation of proteins due to ROS, dimerization and methylation show characteristic spot patterns on the gels and can therefore be easily visualized. The gel-preparation and the electrophoresis were performed according to the protocols described by Junker et al. [56] and Farajzadeh et al. [57]. Subsequent identification of protein spots was achieved by a combination of matrix-assisted laser desorption/ionization time-of-flight mass-spectrometry (MALDI-TOF-MS) followed by sequencing of isolated peptides by MS/MS experiments. Briefly, protein spots were cut out of the gels, digested with trypsin and co-crystallized with a special organic matrix on analytical targets. The spotted peptides are released using high-energy laser light and are accelerated in an electrical field towards a detection unit, where the time of flight of the fragment-ions can be determined. The time-of-flight and the mass of the accelerated fragments correlate according to the following formula: $\frac{m}{z} = \frac{2 \cdot eU}{L^2} \cdot t^2$ (t=time-of-flight; m=mass; z=charge number; e=elementary charge (constant); U=voltage; L=length of acceleration way). Thus, fragments of different weights can be separated by their specific mass. Proteins can now be identified via their specific “fingerprint” of tryptic fragments. Additional MALDI-TOF-MS/MS was used to confirm separated peptide ions by additional fragmentation and sequencing of the peptide fragment. This method allows the detection of multiple proteins in one excised spot or of proteins present in low concentration.

After identification of the two-dimensional separated proteins in plasma treated samples, their quantification and statistical analysis of their expression was compared to that in non-treated controls.

Proteins with altered expression after treatment were further analysed for their biological functions and involvement in metabolic networks.

Western Blots were used for validation of possible protein biomarker, characterizing the effects of the non-thermal plasma treatment.

7.1. Cell line and Cell cultivation

Epithelial cells were isolated from the bronchus of a seven-year-old patient with cystic fibrosis [58]. This parent cell line IB3 showed the typical one-gene defect, which affects functionality of chloride channels. The defect was corrected by transforming IB3 with recombinant adenovirus (adeno-12-SV 40) containing a functional cystic fibrosis conductance regulator (CTFR) gene. This generated the S9 cell line [59]. S9 cells (ATCC CRL-2778) were incubated with 10 ml standard cell cultivation medium (93% MEM Earl Standard w/o L-Glutamin, 4% FCS, 2% Glutamin, 1% non-essential amino acids) in a cell culture plate in an atmosphere of 95% air and 5% CO₂ at 37°C. Micrographs are shown in **Figure 1**.

Sub cultivation was performed at an approximate cell density of 1x10⁷ cells/cm² by removing the cell cultivation medium, washing with 5.0 ml PBS (8.0 g NaCl, 0.2 g KCl, 1.44 g Na₂HPO₄*2H₂O, 0.24 g KH₂PO₄, Aqua dest. ad 1000 ml) and overlaying with 1.0 ml trypsin-solution (0.05% trypsin, 0.02% EDTA) for 5 to 15 minutes to detach cells from the surface [51], [60]. Then, 3 ml standard cell cultivation medium was added, cells were repeatedly pipetted and afterwards divided into aliquots in new cell culture plates each with 9 ml fresh cell cultivation medium with a sub-cultivation ratio of 1:4, which corresponded to approximately 1x10⁷ viable cells per cell culture plate. These subcultures were incubated as described above until sufficient numbers of cells for ENTplas treatment were reached.

ATCC Number: **CRL-2778**
Designation: **S9**

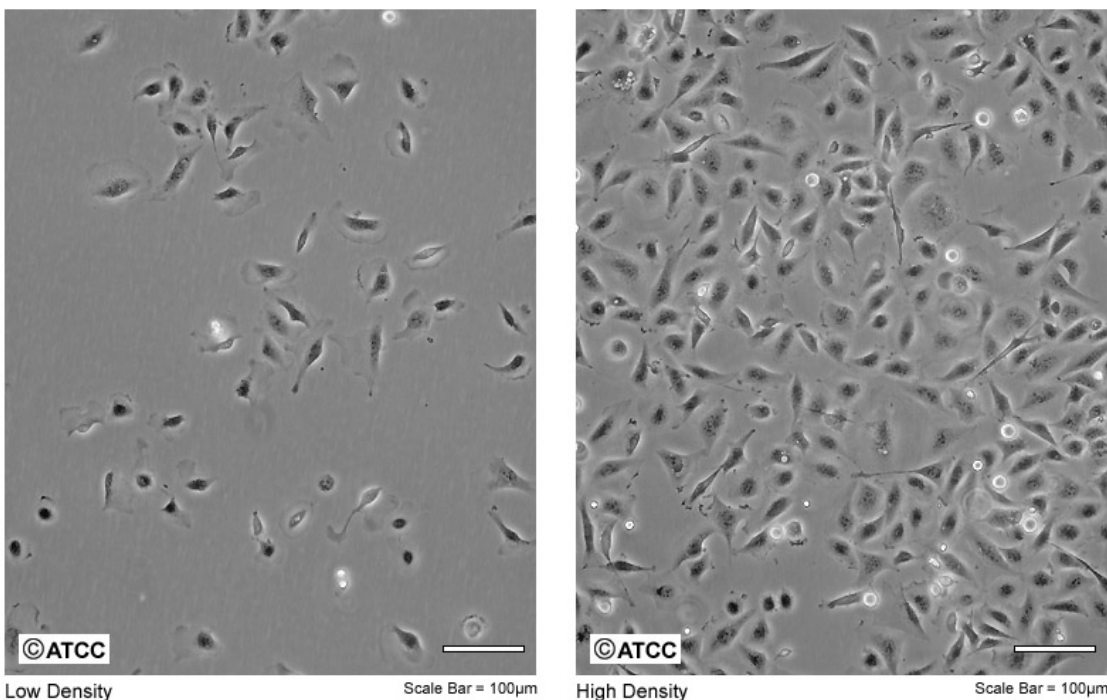


Figure 1: Micrographs of cultured S9-epithelial cells. S9 cells are an immortal cell line derived from a patient with cystic fibrosis. The one gene defect was corrected with an adenovirus. Growth phase cells are displayed on the left. Cell culture near confluence is displayed on the right. The micrographs were kindly provided by the manufacturer (ATCC; www.atcc.org).

7.2. Non-thermal atmospheric pressure plasma (ENTplas) treatment

For ENTplas treatment the kINPen 08, an atmospheric pressure plasma jet developed by the INP (Leibniz Institute for Plasma Science and Technology) in Greifswald, was used: It consists of a quartz capillary (1.6 mm diameter), which surrounds a pin-type electrode (1 mm diameter). Argon gas passes the quartz capillary with a steady flow rate of 5 standard litres per minute (slm) and flows around the electrode (see **Figure 2**). A high-frequency (HF) voltage of 2-6 kVpp., 1.1 MHz was applied to the pin-type electrode.

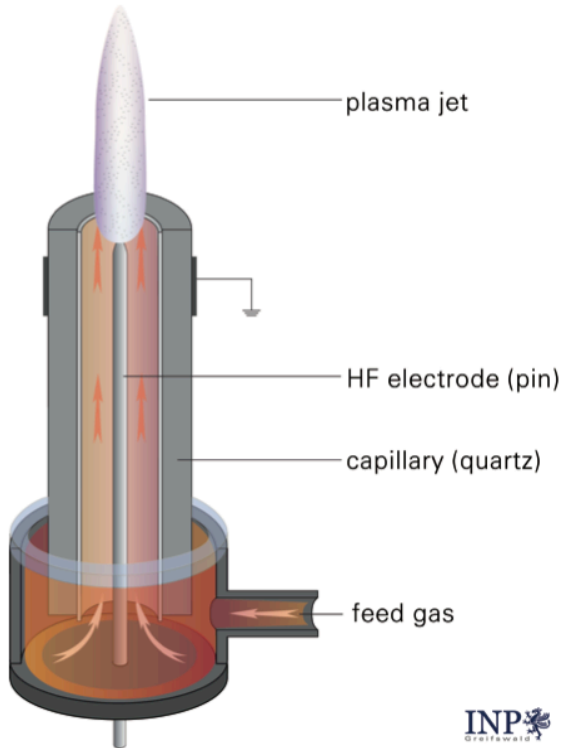


Figure 2: Scheme of the atmospheric pressure non-thermal plasma jet kINPen 08 used. (The scheme is taken from Landsberg et al. [61] and kindly provided by the manufacturer: Leibniz Institute for Plasma Science and Technology; Greifswald, Germany).

By this mechanism, the plasma is generated from the top of the centred electrode and expands to the surrounding air forming a visible plasma-jet with a length of up to 12 mm. The length of the jet depends on voltage and flow rate of the gas applied. At the tip of this plasma jet, temperatures measured were more or less constant between 37°C and 48°C (depending on the operating power between 1,9 W and 3,2 W) with a constant thermal output of about 150 mW [6]. Plasma was operated at 2,8 W and a temperature of about 39°C to 41°C at the tip, which was cooled down immediately during application by the medium covering the cells. These parameter set up was used in order to ensure comparability with results from other working groups like Sensenig et al. [3].

Table 1 shows the physical parameters of the ENTplas treatment for the different treatment time periods of 30 s, 60 s, 120 s, 240 s and 360 s. Values were calculated based on the measurements from Weltmann et al. [6].

Table 1: Physical parameters of the applied plasma on S9 airway epithelial cells using the plasma-jet device for different operating times. The kINPen 08 was used at 2,8 W and the plasma tip was guided over the entire cell culture plate following parallel offset lines within the different treatment times. The resulting physical parameters can be taken from the table.

Treatment time for the entire cell culture plate ($78,54 \text{ cm}^2$) in seconds (s)	Corresponding treatment time for 1 cm^2 in seconds (s)	Maximum corresponding discharge power at 3,2 W in J/cm^2	Corresponding thermal output at 150 mW in J/s
30	0,382	1,222	0,057
60	0,764	2,445	0,115
120	1,528	4,889	0,229
240	3,056	9,778	0,458
360	4,584	14,668	0,688

For ENTplas treatment, cell cultures were split. In comparison to untreated controls, applied ENTplas treatment varied between 30 sec and 360 sec for the entire cell culture plate to monitor the effects on wound healing for different ENTplas doses. Finally, a 120 sec ENTplas treatment was chosen for the analysis of short and long-time observations on protein level after ENTplas treatment in a 2D-DIGE approach. The visible tip of the plasma jet was oriented vertically to the cell culture surface (see **Figure 3**) and moved in lines with parallel offsets over the cell layer within the culture plate (see **Figure 4**), while cells were covered with 1 ml standard cell medium.

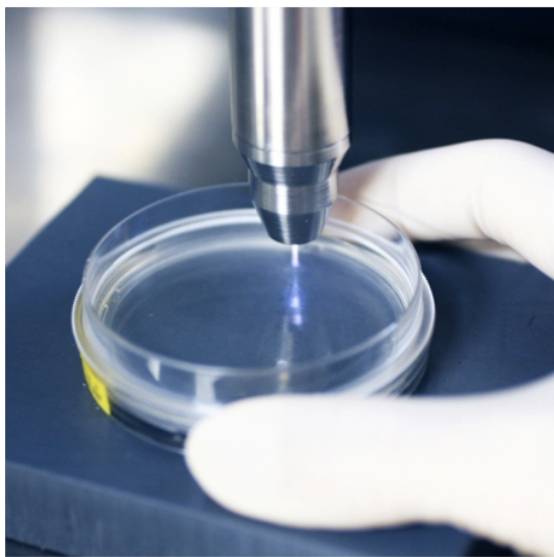


Figure 3: Non-thermal plasma treatment procedure of the whole cell. Cells are covered with medium in the cell culture plate and the tip of the plasma jet is vertically positioned to the cell culture surface. (Picture taken with kindly permission from Landsberg et al. [61])

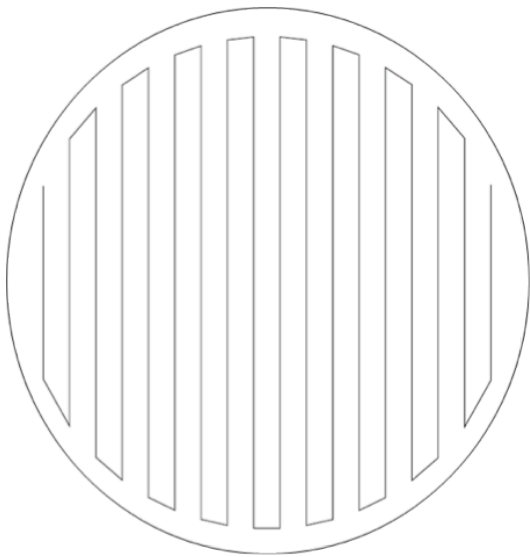


Figure 4: Schematic view from above of the cell culture plate. The tip of the non-thermal plasma jet follows the line with parallel offsets in order to treat the entire area of the cell culture plate.

After ENTplas treatment for 120 sec, treated and control cell cultures were either harvested immediately (0 h) or incubated for different time periods enabling assessment of recovery (incubation for 24 h, 48 h, 72 h, 96 h, or 120 h) before proteome analysis. Time-resolved proteome analyses (short-time: 0, 0.5, 1 h and long-time: 24, 48, 72 h) were performed on controls and samples.

7.3. Wound model

In order to study effects of ENTplas treatment on wound healing, cell cultures of S9 airway epithelial cells in a cell culture plate of 10 cm diameter were used as a surrogate model for airway epithelial cells. Confluent cell cultures were treated using an established wound model, previously described by Beule et al. [60] and Roth et al. [51]. Briefly, S9 epithelial cells in their 16th passage were seeded at a density of 10^6 cells/cell culture plate and grown under similar conditions as described above. When confluence was reached, 21 circular wounds per 10 cm diameter cell culture plate were created (see **Figure 5**) using a 4 mm sterile biopsy punch (pfm AG, Cologne, Germany) and cells were flushed away using an Eppendorf pipette.

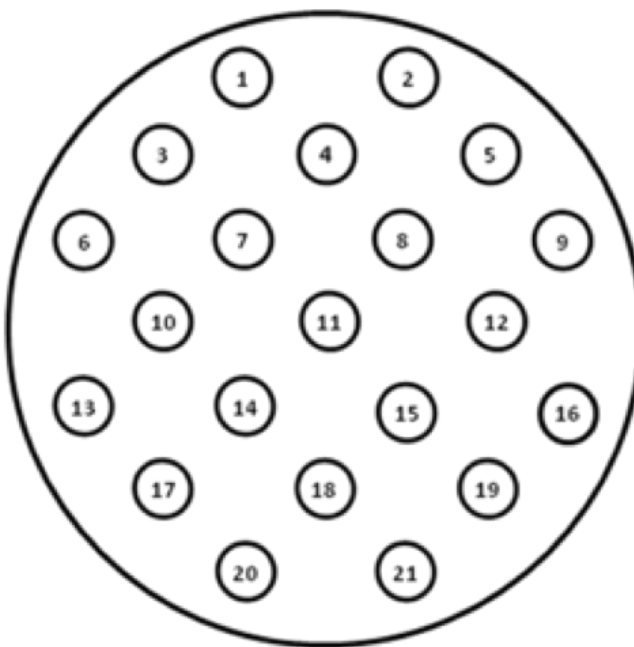


Figure 5: Scheme of the distribution of the punched wounds for one entire 10 cm cell culture plate. Wounds are distributed equally over the available area.

All wounds were documented photographically and subsequently plasma treated using the kINPen 08 device as described above (see **Figure 4**) for 30 sec, 60 sec, 120 sec, 240 sec and 360 sec. Untreated wounds (controls) were kept in the dark for the same period. Wound areas were documented at 4-fold magnification using an inverted microscope (Nikon Eclipse) either directly after treatment (0h), or after a 24 h, 48 h, 72 h, 96 h and 120 h recovery period in cell culture. The size of six wounds per treatment condition was measured on the photographs by using an area-calculating tool of Photoshop CS5 (Adobe, San Jose, Calif., USA). Medians for each condition were calculated. Each of the different treatment groups was compared with the untreated control group. Effects between the two factors “group” and “time” were considered statistically significant for $p < 0.05$ using Anova. Sphericity of wounds was assumed.

7.4. Sample preparation for proteomic analysis

For harvesting of cells, the cell culture medium was removed and cells were washed with 5 ml 1x phosphate buffered saline (PBS). After PBS removal, cells were incubated with 1.8 ml sample buffer (8 mol/L urea, 2 mol/L thiourea) and detached with a cell scraper (Greiner BioOne). Prior to disruption, cells were shock-frozen in liquid nitrogen and stored at -70°C. For disruption, cells were defrosted in a thermomixer (Eppendorf, Hamburg, Germany) at 1400 rpm at 30°C for 10 minutes and again shock-frozen. After

five freeze and thaw-cycles, samples were centrifuged (20,000 x g, 60 min, 4°C) to remove cell debris. Supernatants were transferred into new tubes and stored at -70°C prior further processing. Protein concentrations were estimated using a Bradford assay (Bio-Rad, Munich, Germany) as previously described [62].

7.5. Two-dimensional difference in-gel electrophoresis (2D-DIGE)

Samples were labelled before separating by two-dimensional difference in-gel electrophoresis. The methodological principle is shown in **Figure 6**. Cy-dyes were used and added to the samples following the manufacturer's instructions (GE Healthcare, Munich, Germany). Briefly, samples were adjusted to pH 8.5 using 50 mmol/L NaOH and labelled by adding 400 pmol of dye (Cy3 or 5) per 50 µg of protein on ice for 30 minutes. To stop the reaction 10 mmol of lysine were added and incubation on ice was continued for 10 minutes. If necessary, labelled samples were stored at -70°C. In order to improve sample-to-sample comparisons, an internal standard consisting of aliquots of all samples was generated and labelled with the Cy2-dye as described above. This standard was loaded onto every gel to permit normalisation of different gels. From all samples, four technical replicates labelled either with Cy3-dye or with Cy5-dye were analysed.

For two-dimensional difference in-gel electrophoresis, two labelled samples (Cy3 and Cy5, each 50 µg) were mixed with the corresponding internal standard (Cy2, 50 µg) in rehydration buffer (for 10 units: 80.0 mg CHAPS, 17.5 mg DTT, 52.5 µl Pharmalyte pH 3-10, some grains Bromphenolblau, ad 400.0 µl sample buffer) and used to rehydrate immobilized pH gradient strips with a pH range from 4 to 7 (24 cm; GE Healthcare, Munich, Germany). After rehydration, the first dimension isoelectric focussing was performed as described earlier by Thiele et al. [63]. Subsequently, the second dimension separated the proteins on 12.5% SDS-polyacrylamide gel between low-fluorescent glass plates (GE Healthcare) in a Dodeca system (Bio-Rad). Every 2D-PAGE gel was scanned with a laser scanner (Typhoon 9400; GE Healthcare) at 488/520 nm for Cy2, 532/670 nm for Cy3 and 633/670 nm for Cy5. The resulting images (3 per gel) were processed with dedicated software as described below. Proteome analysis was performed for two separate experimental series independently, one for short-time observations (0 min, 30 min, 60 min) and one for long-time observations (24 h, 48 h,

72 h). For data analysis short-term and long-term observations were initially treated separately, but then merged for joint time-resolved data analysis.

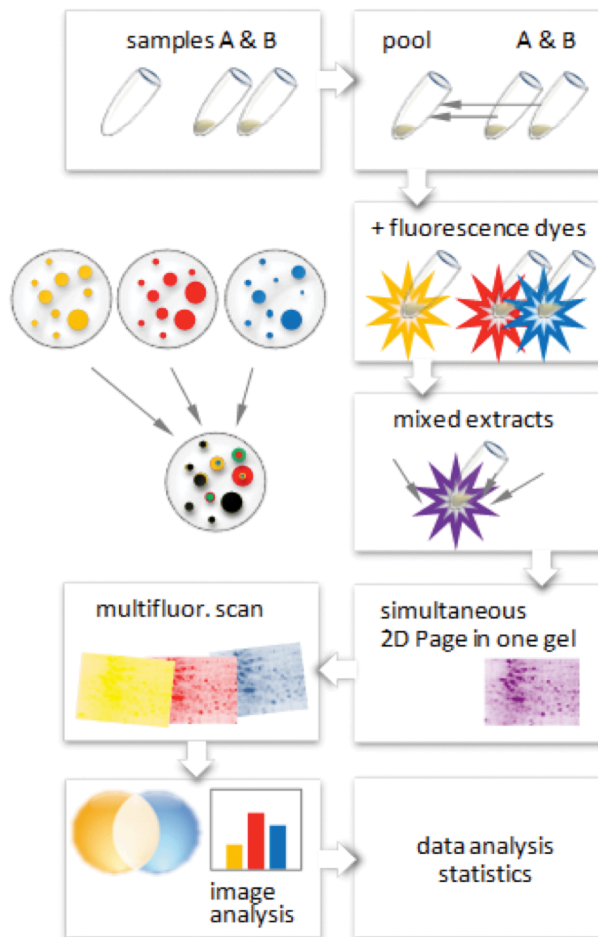


Figure 6: 2D-DIGE experimental setup and workflow. First step is the creation of the internal standard, which is pooled from all samples. Second step is the fluorescent labelling of the different protein samples and the internal standard. Subsequent 2D-PAGE separates the proteins from two different samples (Cy-3 and Cy-5 labelled) and the internal standard (Cy-2 labelled) by their pI and their molecular weight. After scanning and image analyses, expression data can be analysed via statistics.

7.6. Statistical analysis

Analysis of the scanned gel images was performed with the software packages Delta2D (Version 4.2, Decodon GmbH, Greifswald, Germany), data analysis with GeneSpring® GX (Version 7.3.1, Agilent Technologies, Waldbronn, Germany). Initially, all image sets were positionally aligned via the corresponding Cy2-channel (internal standard). Secondly, all samples were merged in order of increasing observation time to create a fused image (2D proteome map – Luhn et al. [64]) in union fusion mode. Spot detection

and editing were done with the Delta2D software on the union fused image and then spots and spot labels were transferred onto all other images included in the analysis.

GeneSpring[®] GX (Agilent Technologies) and TMeV-software (implemented in Delta 2D) were used for statistical analysis and graphical display of expression profiles. Acquired spot expression values were transferred to GeneSpring GX and normalized by a two-level procedure. The first step corrected differences between intensities of different gels by dividing the background-corrected values of the spot volumes by the median of all spots of the corresponding channel (Cy2, Cy3 or Cy5). Secondly, intensity calibration with the internal standard (Cy2-channel) of each spot was performed by dividing the median normalized spot volumes of the Cy3 and Cy5 channels by the corresponding value of the internal standard (Cy2 channel of the spot).

In order to identify differences in spot intensity, the values of plasma treated samples were divided by the corresponding baseline values of the untreated control using GeneSpring[®] GX. Stringent selection criteria were employed in order to reduce false positive results and changes were only considered significant when the following three criteria were fulfilled: (i) the change of the intensity ratio had to exceed a factor of 1.5 (ii) the p-value of the corresponding analysis of variance test had to be lower than 0.05 (One-way-ANOVA) and (iii) raw values of each spot had to exceed 0.3, avoiding calculation of ratios of spots close to background intensities.

This procedure had to be performed for each data set (short and long term) separately. Since identical normalizations were used for both sub-projects, candidate lists were subsequently merged with GeneSpring[®] GX.

For TMeV-analysis both separate projects were initially merged and spot detection was optimized. pI-range and molecular weight range were cropped to the maximum interpretable common region. Normalization was performed as described above and then principle component analysis (PCA) was performed to validate reproducibility of experimental conditions and identify possible outliers (compare with **Figure S-1**). After removal of an obvious outlier of one gel image, caused by a hardware failure of the scanning device, a hierarchical clustering by the Euclidean distance was performed. A k-means-clustering resulting in ten different clusters visualized the different expression patterns observed in the time-resolved proteome analysis, which were lastly assigned to

metabolic pathways and cellular physiology by network analysis using Ingenuity Pathway Analysis (Ingenuity Systems; www.ingenuity.com).

7.7. Preparative 2D gel electrophoresis and sample preparation for mass spectrometry

Preparative two-dimensional gel electrophoresis was performed as previously described [63]. Briefly, 450 µg of protein was pooled from treated and untreated samples of each condition (75 µg each) and added to the rehydration buffer.

Resulting 2D-PAGE gels were stained with colloidal Coomassie brilliant blue according to the manufacturer's instructions (GE Healthcare). Gel image documentation was performed by a transmission light scan. Gel image analyses were performed with the Delta-2D software package (Decodon GmbH) as described above.

Spots of interest were processed for identification as described by Eymann et al. [65]. Briefly, spots were excised manually or using a spot cutter (Proteom Works, Bio Rad) with a picking head diameter of 2 mm. Excised protein spots were transferred into 96-well-microplates, which were loaded with 100 µl of Lichrosolv water in each well. Tryptic digestion was performed automatically in an Ettan Spot Handling Workstation (Amersham Biosciences) as well as the subsequent spotting of peptide-solution onto MALDI targets. Cutted gel pieces were washed twice with 100 µl 50 mM ammoniumbicarbonate/ 50% v/v methanol for 30 min and once with 100 µl 75% v/v ACN for 10 min. In the next step samples were dried for 17 min and then incubated with 10 µl trypsin solution (20 ng/ml trypsin (Promega, Madison, WI, USA) in 20 mM ammoniumbicarbonate) at 37°C for 120 min. For peptide extraction gel pieces were covered with 60 µl 50% v/v ACN/ 0.1% w/v TFA and incubated for 30 min at 37°C. Supernatants containing peptides were transferred into new microtiter plates. Again peptide extraction was performed with 40 µl of the same solution. Joined supernatants were now completely dried at 40°C for 220 min. Peptides were dissolved in 2.2 µl of 0.5% w/v TFA/ 50% v/v ACN. MALDI targets were spotted directly with 0.7 µl of this solution. Then, this sample solution was mixed with 0.4 µl of matrix solution (50% v/v ACN/ 0.5% w/v TFA saturated with α-cyano-4-hydroxycinnamic acid (CHCA)) by aspirating five times. After drying for 10-15 min, samples were measured using the MALDI-TOF/TOF instrument.

7.8. Matrix-assisted laser desorption-ionization time-of-flight mass spectrometry (MALDI-TOF-MS)

MALDI-TOF-MS measurements were performed with a Proteome-Analyzer 4800 (Applied Biosystems, Foster City, CA, USA). Reflector mode was used in order to record the spectra in a mass range from 900 to 3700 Da with a mass focus to 2000 Da. Twenty-five subspectra with 100 shots per subspectrum were accumulated for one main spectrum using a random search pattern. An automatic internal two-point calibration was performed, when the autolytic fragments of trypsin with the mono-isotopic ($M+H$)¹⁺ m/z at 1045.564 and 2211.104 reached a signal-to-noise ratio (S/N) of at least 10. Although the standard peptide search tolerance was 50 ppm, the effective standard deviation was between 2 and 15 ppm. Less than 1% of the samples with failed auto-calibration had to be calibrated manually. Using GPS-Explorer software package (Applied Biosystems, Foster City, CA, USA), the peak lists were created and searched automatically. The following GPS-Explorer settings were selected: mass range from 900 to 3700 Da; peak density of 50 peaks per range of 200 Da; minimum area of 100 and maximum 200 peaks per protein spot and minimum S/N ratio of 6. These peak-lists were compared to a UniProt SwissProt database (Rel. 51.5 restricted to human taxonomy) by the MASCOT search engine (Version 2.1). Positive identifications had to reach the following specifications: sequence coverage of at least 30% and twice a MOWSE-score of at least 49. Proteins and peptides, which failed the 30% sequence coverage barrier, were reanalysed with more accurate MALDI-MS/MS. The MALDI-TOF-TOF analysis was used for the five strongest peaks of the previous MS-spectrum. Here, 20 subspectra with 125 shots per subspectrum were accumulated using a random search pattern. The internal auto-calibration was performed if the mono-isotopic arginine ($M+H$)¹⁺ m/z at 175.119 or lysine ($M+H$)¹⁺ m/z at 147.107 reached an S/N of at least 5. Settings for GPS-Explorer setup were: mass range from 60 Da to a mass that was 20 Da lower than the precursor mass; peak density of 5 peaks per 200 Da; minimum area of 100 and maximum 20 peaks per precursor and a minimum S/N ratio of 5.

For peak list interpretation, the database mentioned above was used with the MASCOT search engine (Version 2.1). Results reaching a MOWSE-score of at least 49 in reflector mode (MALDI-TOF-MS) and being confirmed by subsequent measurement of the strongest peaks (MS/MS), were regarded as positively identified proteins. The

confirmation by subsequent measurements (MS/MS) was particularly useful for protein-identification in spots, which contained multiple proteins.

Protein identifications and statistically relevant data were combined via unique spot-IDs using the MSRepo database software (Decodon, Greifswald, Germany). Categorization of the identified proteins was achieved by using the Panther Classification System (<http://www.pantherdb.org/>) [66].

7.9. Network and protein functional analysis using specialized software

Expression profiles of statistically significant changing spots were exported from GeneSpring® and TMeV. Data were combined with identification-lists from mass-spectrometry and then imported into Ingenuity Pathway Analysis (Ingenuity Systems; www.ingenuity.com). Using this program, it was possible to create protein networks and pathways, which contained the proteins displaying changes in intensity and thereby placing individual protein data into physiological context.

Additionally, Voronoi Treemaps [67] were used for data analysis and visualization. Identified proteins were assigned to adapted KEGG Brite orthology hierarchies and subsequently displayed with corresponding normalized expression values for each time point.

7.10. Immuno Blot analysis

Ten micrograms of protein from each time point (0 h, 0.5 h, 1 h, 24 h, 48 h, and 72 h) were separated by 12.5% SDS-PAGE and transferred onto a Immobilon-P polyvinylidene fluoride (PVDF) membrane (Millipore) for Immuno Blotting with specific antibodies using a conventional semi-dry blotting device (Milliblot Graphic Electrophoresis II, Millipore, Billerica, MA, USA) for 2 hours. Prior antibody binding, membranes were blocked in a solution of 5% non-fat dry milk in tris-buffered saline Tween-20 (TBS-T buffer; TBS-Tween, 137 mM Tris-HCl, 2.68 mM NaCl, and 0.1% Tween 20) for 90 min at room temperature. Immediately after this step, the membranes were incubated with the different primary antibodies overnight at 4°C. To detect nuclear factor erythroid 2-related factor 2 (Nrf2), Interleukin 1beta (IL-1β), Interleukin 33 (IL-33) and Kelch-like ECH-associated protein 1 (Keap1), rabbit polyclonal IgG anti-Nrf2, anti-IL-1β, anti-IL-33 and anti-Keap1 antibodies (Santa Cruz Biotechnology, USA) were used in a dilution of 1:100 (2 µg/ml) in TBS-T buffer containing 5% bovine serum

albumin (BSA). Membranes were washed six times in TBS-T buffer before the incubation with the secondary antibodies at room temperature for 1 h. Stabilized goat anti-rabbit horseradish peroxidase (HRP)-conjugated secondary antibody (Santa Cruz Biotechnology) was used in dilution 1:2,500 in 5% non-fat dry milk in TBS-T buffer. After six washing steps with TBS-T buffer, membranes were incubated with SuperSignal West Femto Maximum Sensitivity Substrate (Pierce; Thermo Fisher) for 5 min. Signals were detected with a Fusion-SL-3500.WL instrument for fluorescence and chemo luminescence applications (Vilber Lourmat, Eberhardzell, Germany). Band intensities were quantified using the ImageQuant software version 5.0 (GE Healthcare). Statistical significance was determined using a two-sided t-test.

8. Results

8.1. ENTplas treatment improves proliferative activity of S9 airway epithelial cells in an in vitro wound model

The analysis of changes in wound areas after ENTplas treatment revealed statistically significant differences. **Figure 7** illustrates the time-dependent development of wound areas for non-treated control samples (green) and those exposed to different doses of ENTplas treatment. Lower doses of ENTplas (30 sec up to 120 sec) result in stronger proliferation, thus less residual wound area over time. ENTplas treatment for 120 sec (red) showed the strongest effect on wound closure activity 24 h to 120 h after treatment ($p < 0.005$) (**Figure 7-A**). In contrast, higher doses of non-thermal plasma treatment resulted either in significantly lower wound closure activities compared to the control (240 sec) or even completely blocked the capacity for regeneration and closure of the wound area (360 sec). Thus, non-thermal atmospheric pressure plasma treatment showed clear effects on S9 airway epithelial cells and caused differences in proliferation and cell migration activities, which resulted in dose dependent alterations of wound closure.

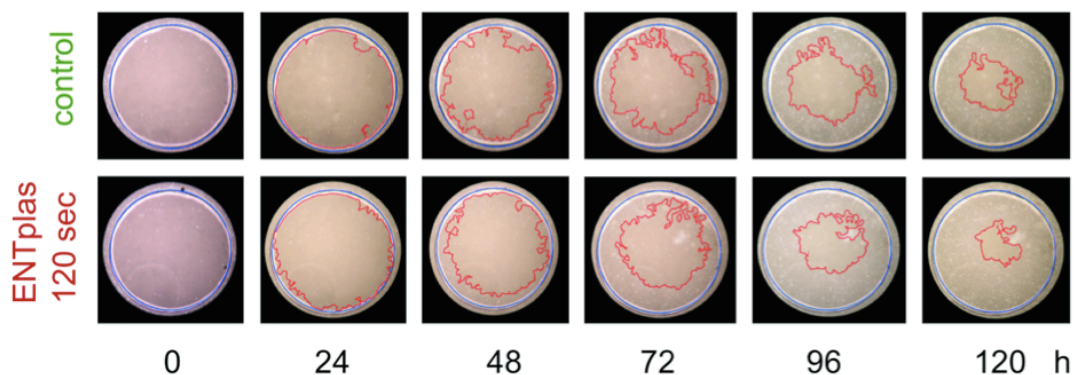
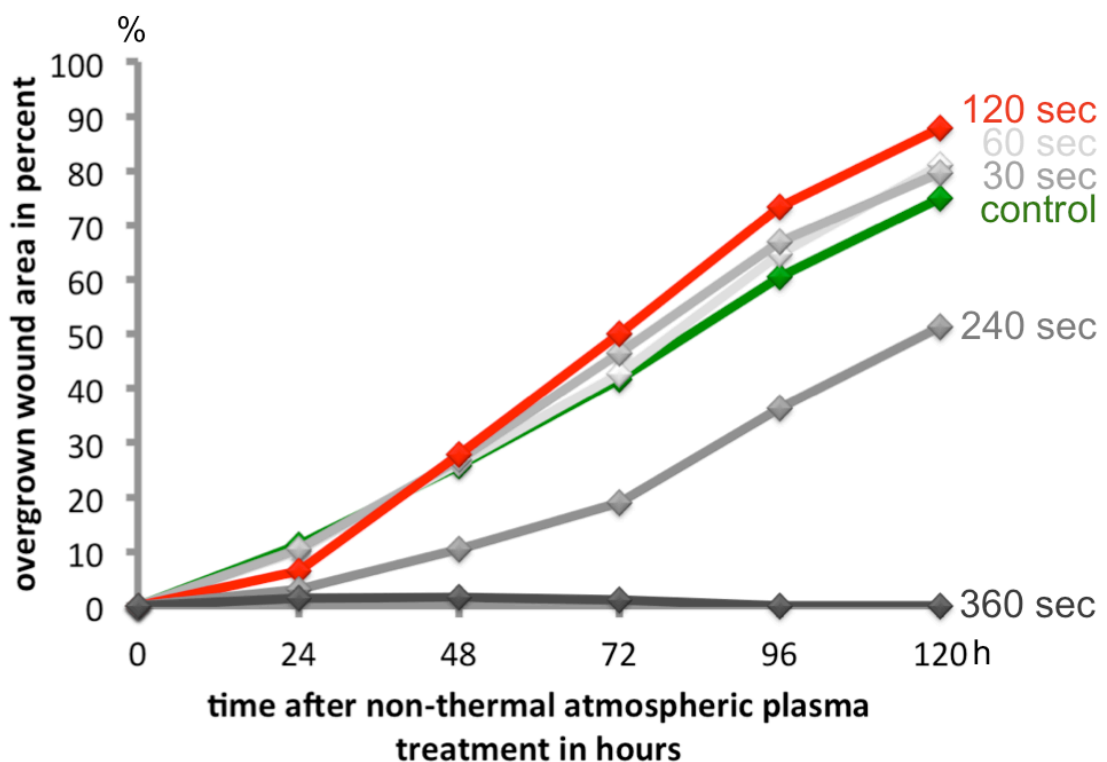
A**B**

Figure 7: Effect of ENTplas treatment on S9 epithelial cell wound healing. Time course of overgrown wound area after ENTplas treatment of S9 epithelial cells observed after applying an in-vitro wound model (A) Photographically documented wound areas for each time point (0 h, 24 h, 48 h, 72 h, 96 h and 120 h) after ENTplas treatment (120 sec) and untreated control are shown. The blue circle displays the original punched wound border and the red line displays the current cell borderline. (B) The median percentages of the overgrown wound area from six observed wounds per condition for different ENTplas treatment durations (30 – 360 sec) at each observation time point are displayed.

In the cell culture system tested, a duration of 120 sec ENTplas treatment might be therapeutically beneficial, because S9 cells seemed to be clearly affected after 24 h of incubation compared to the control, while still displaying improved proliferative potential and wound healing after 120 h (**Figure 7-A**). Therefore, S9 cells exposed 120 sec to non-thermal plasma were subject to comparative proteome analysis with non-treated controls cells to explore the mechanisms responsible for these alterations.

8.2. Two-dimensional difference in-gel electrophoresis (2D-DIGE) reveals alterations in the proteome of S9 airway epithelial cells triggered by ENTplas treatment

S9 cells treated with ENTplas for 120 sec and non-treated controls cells were harvested either directly after end of treatment or at different time points of a subsequent cultivation in MEM. Protein extracts of treated samples and corresponding controls were analysed by 2D-DIGE in a pI-range from 4 – 7. In 48 gel images, 1505 detectable protein spots could be analysed with respect to ENTplas treatment induced alterations.

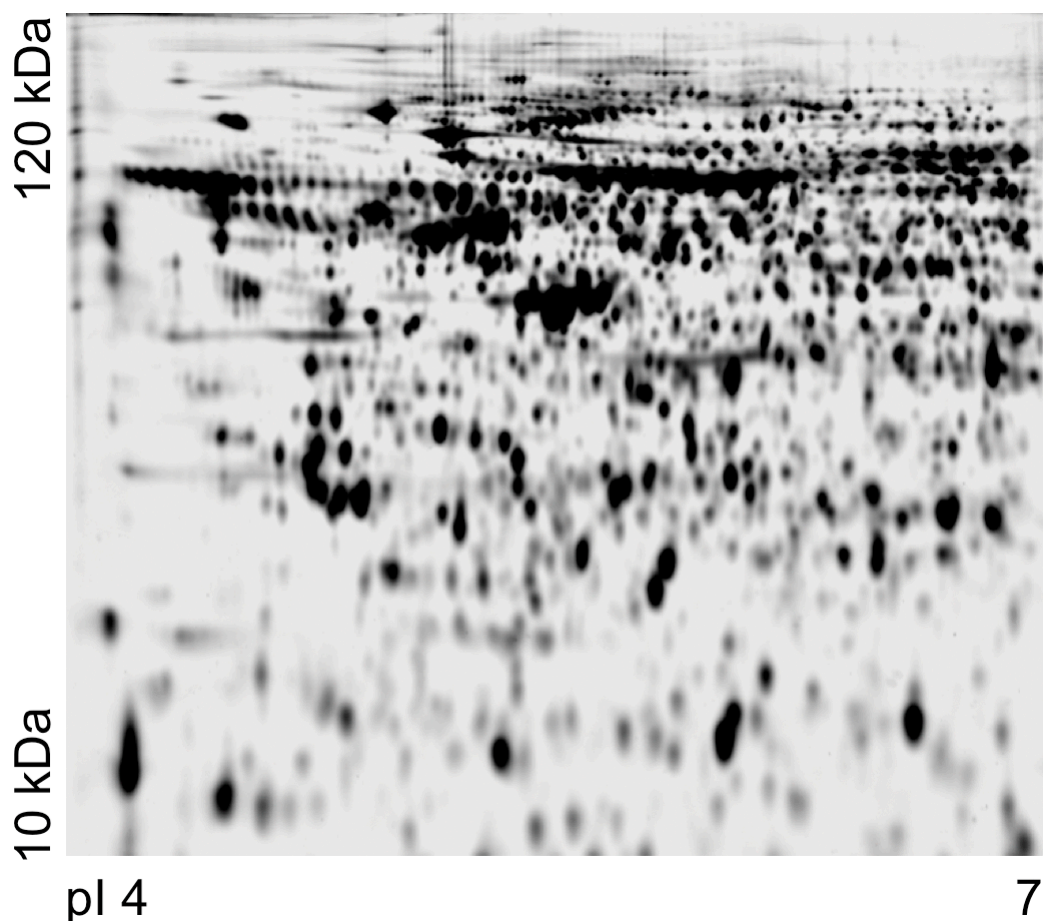


Figure 8: Complex fusion gel of four technical replicates of 120 s ENTplas treated S9 cells 0 h after treatment. Shades of grey indicate the spot intensities.

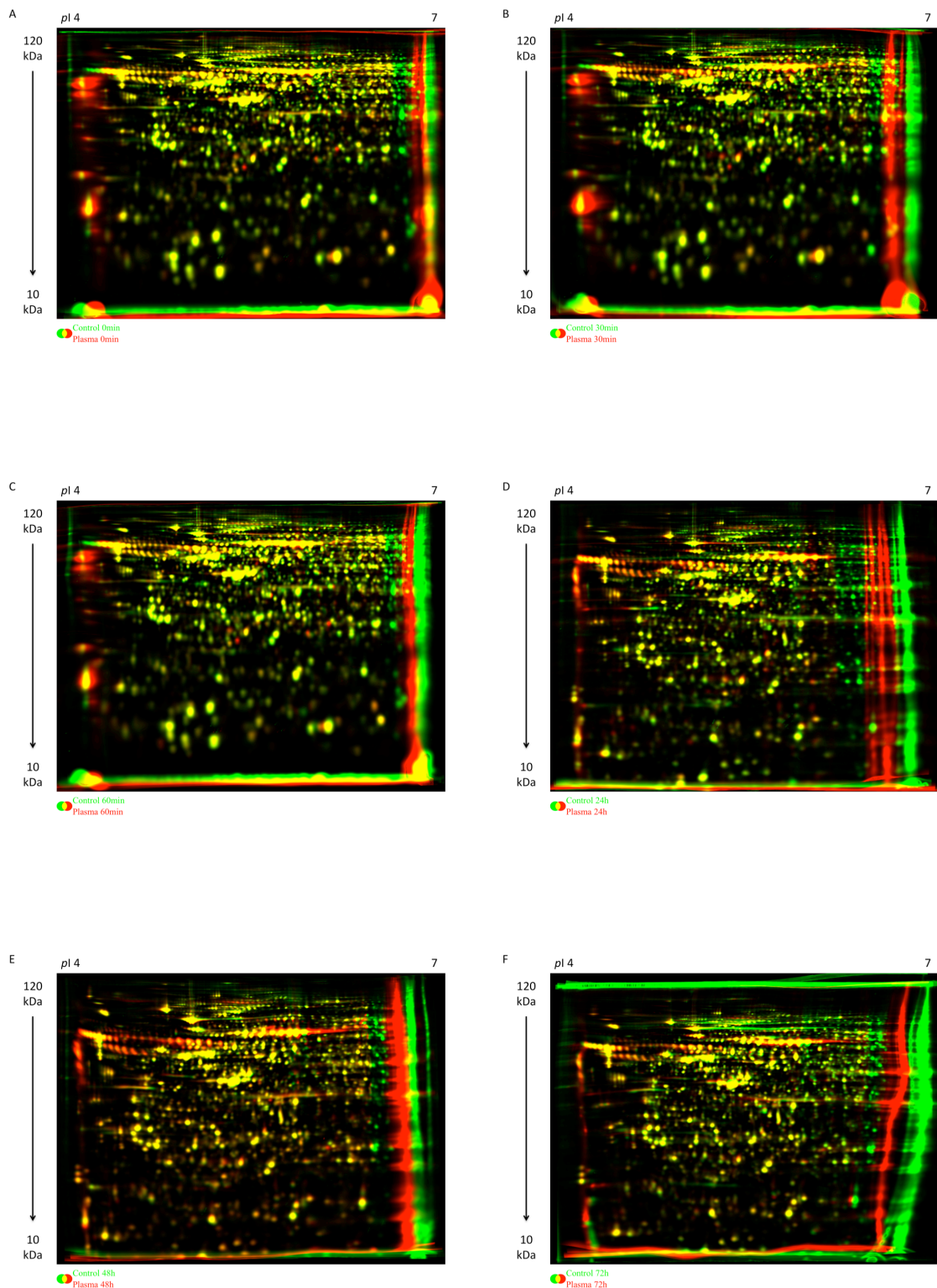


Figure 9: Dual channel fusion images of ENTplas treated S9 epithelial cells compared to the corresponding non-treated control. Protein samples were analysed by a 2D-DIGE approach covering a *pI*-range of 4-7 and a molecular weight range from 10 - 120 kDa. Fused gel images of all four technical replicates were calculated by using 'average' fusion mode. Green spots represent dominantly expressed proteins in a non-treated control. Red spots represent spots, which are higher expressed in ENTplas treated S9 epithelial cells and yellow protein spots are expressed nearly similarly in

controls and plasma treated cells. (A) Cells were harvested directly after treatment (0 h), (B) 0.5 h after treatment, (C) 1 h, (D) 24 h, (E) 48 h and (F) 72 h after treatment. Self-evidently, corresponding controls have not been treated, but incubated the same time as ENTplas treated samples outside the cell culture incubator.

Qualitative image analyses of dual channel comparison already showed multiple ENTplas treatment-related changes of intensities of protein spots. However, although 2-DE-based proteomic approaches can precisely identify treatment-related alterations in the intensity of protein spots they need complementary mass spectrometry approaches to reveal protein identities. In an effort to comprehensively characterize the effect of ENTplas treatment on S9 epithelial cells, MALDI-TOF-mass spectrometry was used to perform 1218 protein-identifications in 722 spots. Many proteins, especially structural ones were represented by more than one protein spot and therefore our proteome analysis covered proteins coded by 499 different genes. These proteins were categorized using “Panther-Gene Ontology” into different functional groups. Two proteins out of 499 assigned with “unknown function” in the Panther-Gene Ontology. The remaining 497 proteins were first assigned to 16 main groups of biological processes as displayed in **Figure 10**. In conclusion 1071 processes were found. Second, the 497 proteins were assigned to 11 different main molecular functions, while a total of 586 affected functions are demonstrated.

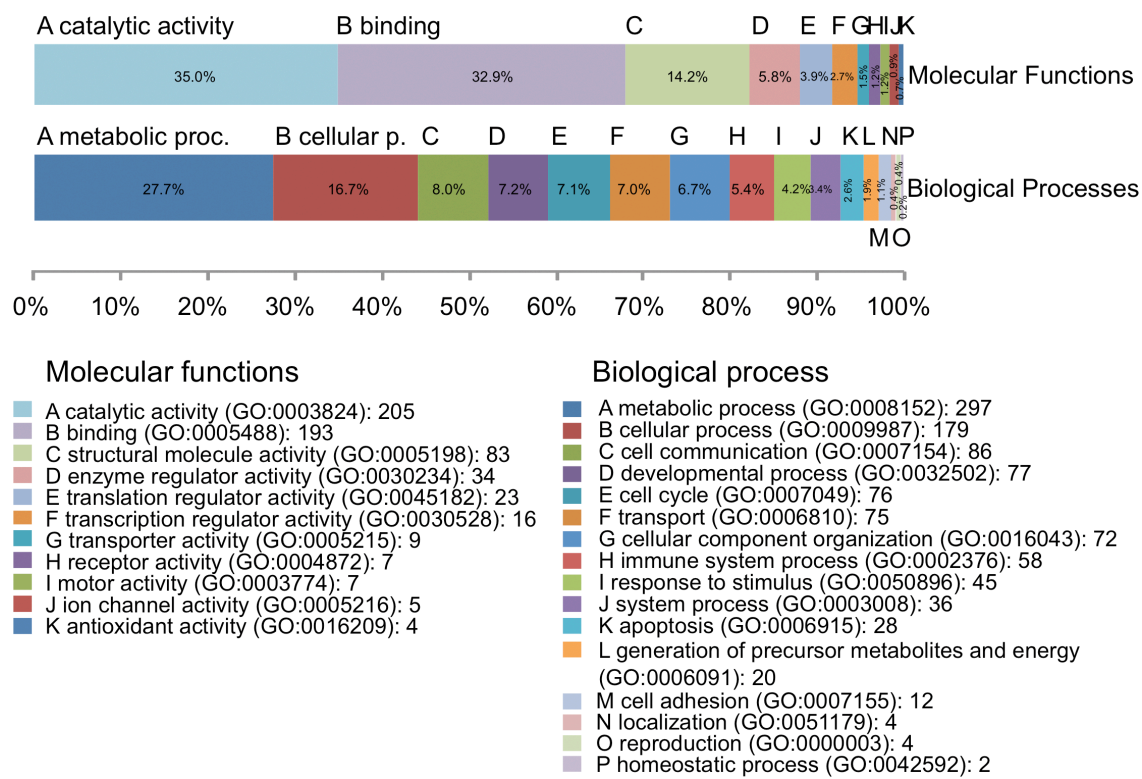


Figure 10: Classification of all identified proteins by cellular function. Subsets of protein-identifications from MALDI-TOF-MS/MS are illustrated by bar charts. 497 different proteins were characterized and assorted to 16 biological processes and 11 molecular function categories. Classification of proteins was performed with Gene Ontology Categories (Panther; www.pantherdb.org). Numbers of assorted proteins are attached to the specific classifications.

Compared to peptide-based LC-MS proteomic approaches, 2-D gel electrophoresis offers the ability to monitor protein modifications that alter protein mobility (processing, degradation, post translation modifications at individual positions), because separation occurs at the protein level. Protein modifications due to the ENTplas treatment appear as changes in intensity in multiple spots with the same protein identification by MALDI-TOF-MS (selected examples are highlighted in **Figure 11**). **Figure 12** illustrates the four selected examples for modifications triggered by ENTplas treatment resulting in changes of spot patterns of the same identified protein. Such modifications may occur due to the natural protein function in response to a changed environment. The cytosolic thioredoxin reductase 1 for example reduces oxidized sites (among others: ribonucleotide-reductase). Different forms of this protein with specific pIs and molecular weights accumulate in separated protein spots in the two-dimensional gel. Other proteins, like CLIC4 (chloride intracellular channel protein 4) or HSPB1 (heat shock protein beta-1) likely shifted due to protein modifications, namely oxidation

of methionine or cysteine, leading to the appearance of sulfonic acids and the creation of disulfide bonds. Posttranslational modifications have been identified by MALDI-MS (e.g. CLIC4: spot_1: AGSDGESIGNCPFSQR (m/z 1680.725) vs. spot_2: AGSDGESIGNC_{3ox}PFSQR (m/z 1728.695). These modifications are not physiological and often result in permanent and sometimes irreversible structural changes, which may affect protein function and necessitate replenishment by new synthesis. As expected, modifications due to oxidation were dominating. Such modifications are in agreement the property of non-thermal plasma to trigger formation of free radicals, electrons and ions.

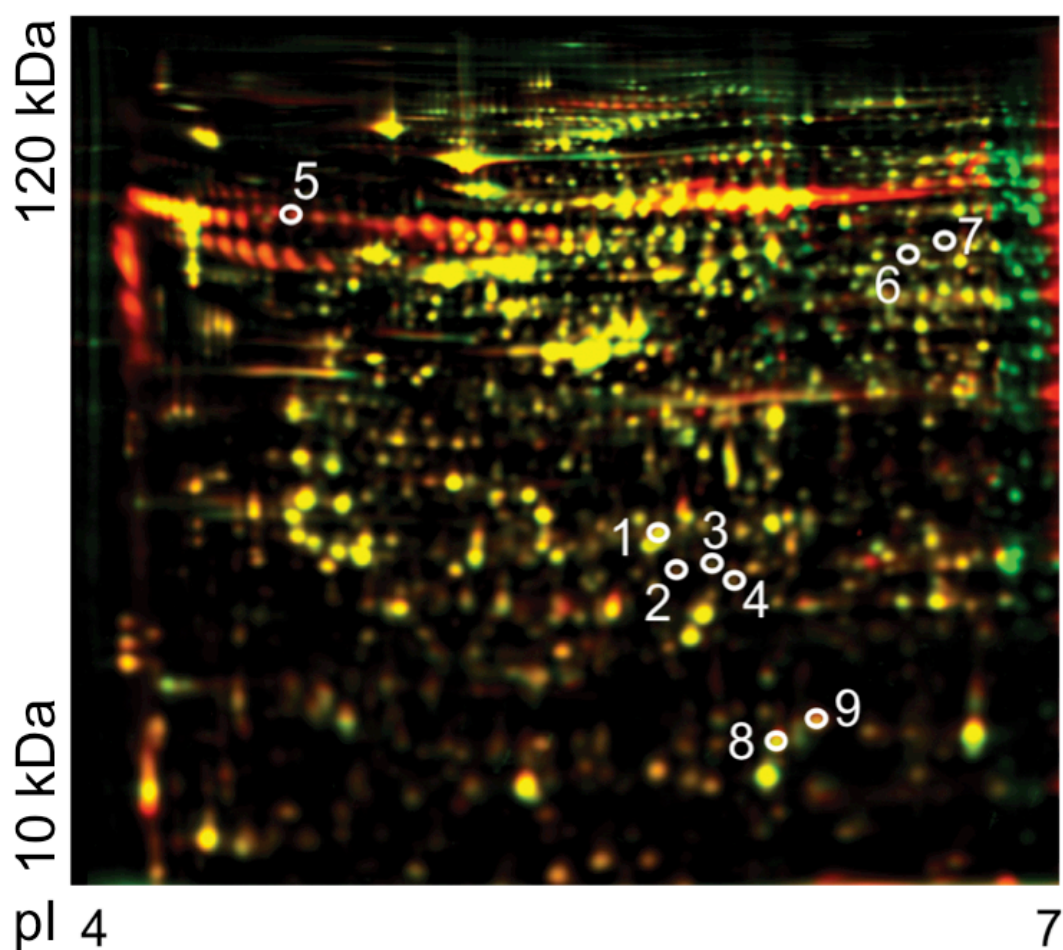


Figure 11: 2D-DIGE analyses of ENTplas treated S9 epithelial cells. Dual view of 120 s ENTplas treated S9 cells compared to untreated control S9 cells at the time point of 48 h after treatment. Green spots represent dominantly expressed proteins in the non-treated control. Red spots represent spots, which are higher expressed in ENTplas treated S9 epithelial cells and yellow protein spots are expressed nearly similarly in controls and ENTplas treated cells. Highlighted protein spots contain examples for posttranslational protein modifications after ENTplas treatment and are enlarged and further explained in **Figure 12**.

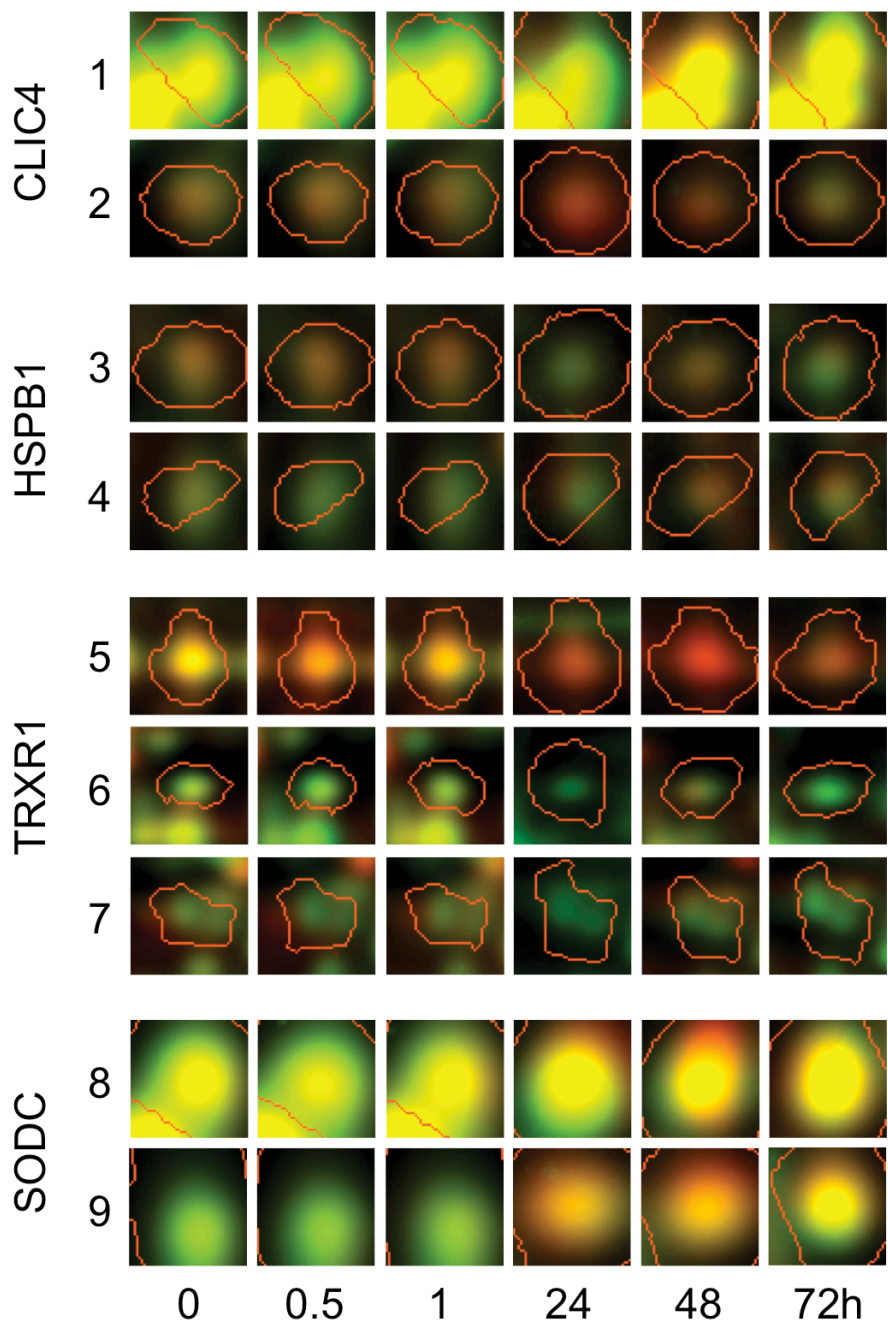


Figure 12: Protein modifications detected after ENTplas treatment. Time course of nine different spots representing modifications of four different proteins of 120 s ENTplas treated S9 epithelial cells compared to the corresponding untreated control at each time point (0 h, 0.5 h, 1 h, 24 h, 48 h and 72 h) after treatment. CLIC4 (chloride intracellular channel protein 4) and HSPB1 (heat shock protein beta-1) show typical multiple spots with characteristic expression profiles of molecular weight related modifications, whereas TRXR1 (thioredoxin-reductase 1) and SODC (superoxide dismutase) show characteristical changes of pI and molecular weight caused by oxidative changes (e.g. cysteine-modifications and methionine oxidation). Posttranslational modifications have been identified by MALDI-MS (e.g. CLIC4: spot_1: AGSDGESIGNCPFSQR (m/z 1680.725) vs. spot_2: AGSDGESIGNC_{3ox}PFSQR (m/z 1728.695).

In order to filter out relevant processes and functions, which are affected by ENTplas treatment, further statistical and bioinformatic methods were used and are described in the following.

8.3. Principal component analysis demonstrates both: experimental quality and the appearance of ENTplas treatment-related effects

PCA reduces dimensionality of data and may visualize the correlations and separations of data subsets (sets of sample replicates or sets of proteins with similar expression [68]). Each sample is described by a 1505 dimensional vector, defined by the 1505 expression values for every detected protein spot. After dimensionality reduction in a 2D chart, principal components describe the highest variances of the data cloud from n-dimensional space. Similar samples, such as technical replicates appear in close sets of data points with equal colour. Different samples appear spatially more distant (see **Figure 13**). The appropriate three-dimensional PCA plot (**Figure S-1**) and all possible projections of the first three principal components (**Figure S-2 A,B,C**) can be found in the supplementary material.

In these figures, equal colour shades represent technical replicates of every condition (controls – green, 120 s ENTplas treated samples – red). With increasing darkness of the colour, the post-interventional observation period increased (light shaded early: 0 h, 0.5 h, 1 h and dark shaded late: 24 h, 48 h, 72 h). The three shown principal components explain 36.46% (PC1), 15.84% (PC2) and 8.88% (PC3), sum = 61.18%, of data variance.

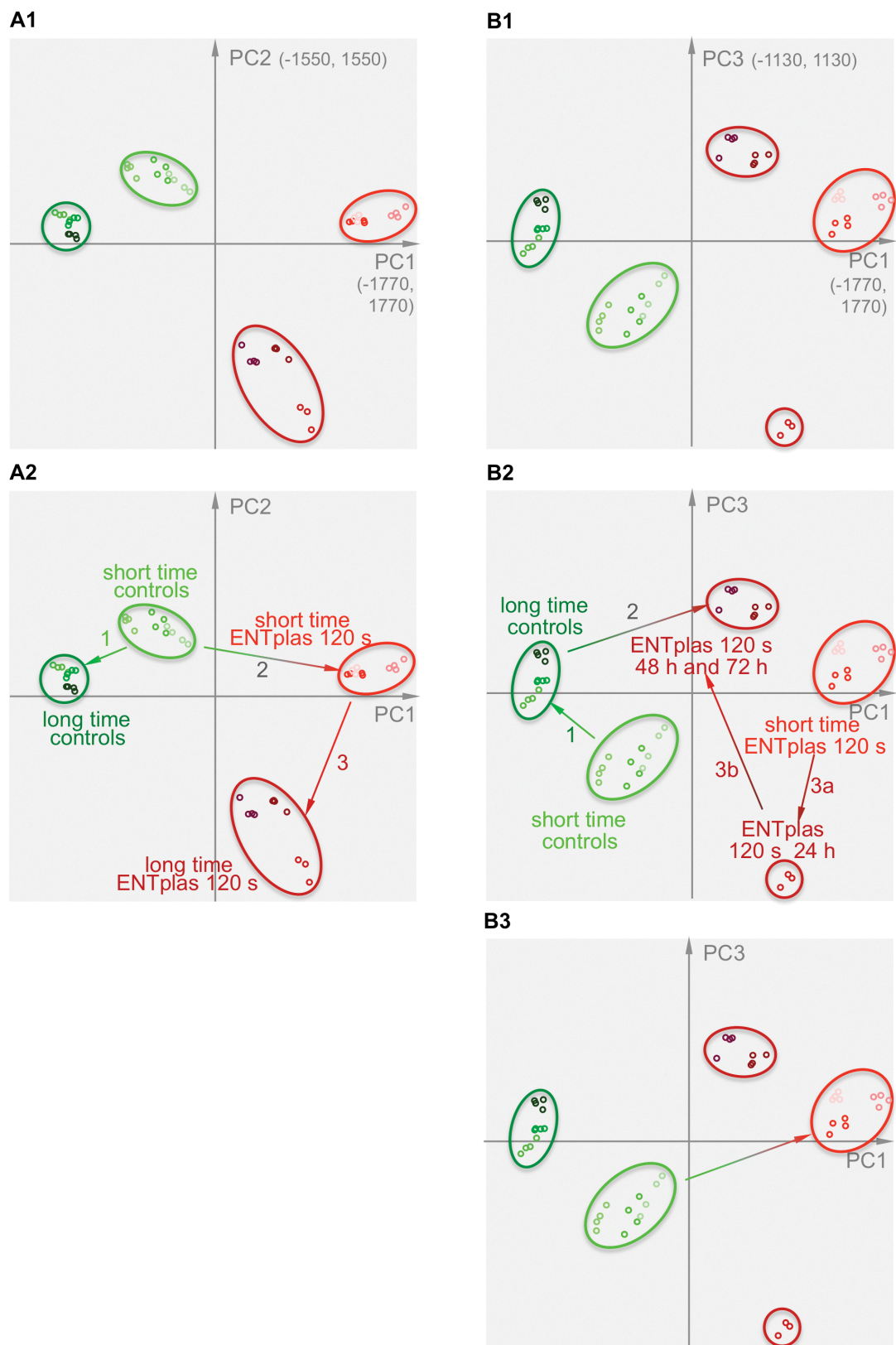


Figure 13: Principal Component Analysis (PCA). 2D-plots of the first three principal components from the protein expression data are displayed, separating all analysed samples. Comparisons between the first and the second principal component (A1, A2) and the comparison between the first and the third principal component (B1-B3) are displayed.

The projection of the first and the second principal component (**Figure 13 A1** and **A2**) shows, that short-time observations (0 h, 0.5 h, 1 h) separate clearly from long-time observations (24 h, 48 h, 72 h) in both untreated controls (arrow 1) and ENTplas treated samples (arrow 3). Untreated controls are clearly separated from ENTplas treated samples (arrow 2, **Figure 13 A2**) and the distance between short and long-time observation is longer for ENTplas samples, than for untreated controls (**Figure 13 A2** and supplemental **Figure S-2 A**). Similar observations can be excerpted from the comparison between the first and the third principal component (**Figure 13 B1-B3**). But the third principal component highlights the pivotal role of the 24 h time point for ENTplas treated samples (arrow 3a and 3b **Figure 13 B2**).

In fact, technical replicates invariably cluster together and thus underscore the adequate technical quality of these experiments. Moreover, the differences between short-time and long-time samples both in controls and ENTplas treated samples represent proliferative differences between these two points of observation. The spatial distance between short-time and long-time ENTplas treated samples is longer than it is between the corresponding controls. This difference in distance may represent the changes in cell status equilibrium observed in the wound-healing model. And at last, the clear offset between controls and non-thermal plasma treated samples represents the effects caused by ENTplas treatment. This underlines, that there are effects by non-thermal plasma treatment and that they interfere with cell status equilibrium and maintenance.

8.4. Statistical comparison and subsequent network analysis of ENTplas treated samples and their corresponding control (GeneSpring®-analysis) give first insights into affected cellular functions and pathways

Protein expression data generated with the Delta2D software were analysed with GeneSpring®. After normalization, subsequent one-way-ANOVA-testing (for parameters see chapter 7.6. Statistical analysis) and fold change filtering (1.5-fold change) of all possible sample pairs, data were further analysed using Ingenuity Pathway Analysis (IPA).

For the short-time observation immediately after ENTplas treatment, 435 spots were significantly changed. 0.5 hours incubation showed 547 significantly changed spots, whereas 1 hour after treatment 446 spots were changed in comparison to the specific control for each time point. The long-time observation at 24 hours incubation after

treatment disclosed 341 spots with fold change greater than 1.5, at 48 hours 344 spots and at 72 hours incubation 277 spots with significantly changed intensity. All results show p-values below $p<0.05$.

Spots, which did not display any difference in intensity over time (0 h to 72 h) or which could not be identified by MALDI-TOF-MS-identification were excluded. Thus, a protein index was established (see **Table S-1**) containing 371 different protein spots for which an at least 1.5-fold change in intensity was observed in at least one time point of the time span from 0 h to 72 h.

The network analysis of this protein index allocated differentially expressed proteins to functional classes and combined expression data with the physiological context (see **Table S-2**).

Early after treatment (first time points after treatment) cell death signalling and oxidative stress response played an important role. Later, cellular reproduction and cellular growth became more prevalent (see **Figure 14-A** and **Figure 14-B**).

A ranking of significantly affected functionally related protein sets showed, that an increase of cell death related proteins dominate the cellular adaptive network immediately after ENTplas treatment. This is followed by a temporary decrease for the following hour and a subsequent increase after 24 h. Functional protein groups related to protein folding and post-translational modifications dominate the intermediate time from 0.5 hours to 24 hours. The long-time effect after 48 h and 72 h is characterized by mutually opposing functional groups: cell death and cellular growth, proliferation and migration in combination with cellular assembly and organization. A plausible explanation for this observation could be, that on the one hand a proportion of cells might be stimulated by ENTplas treatment responding with proliferation, on the other hand some cells might be severely damaged by the acting stressor and activate the cell death signalling pathway.

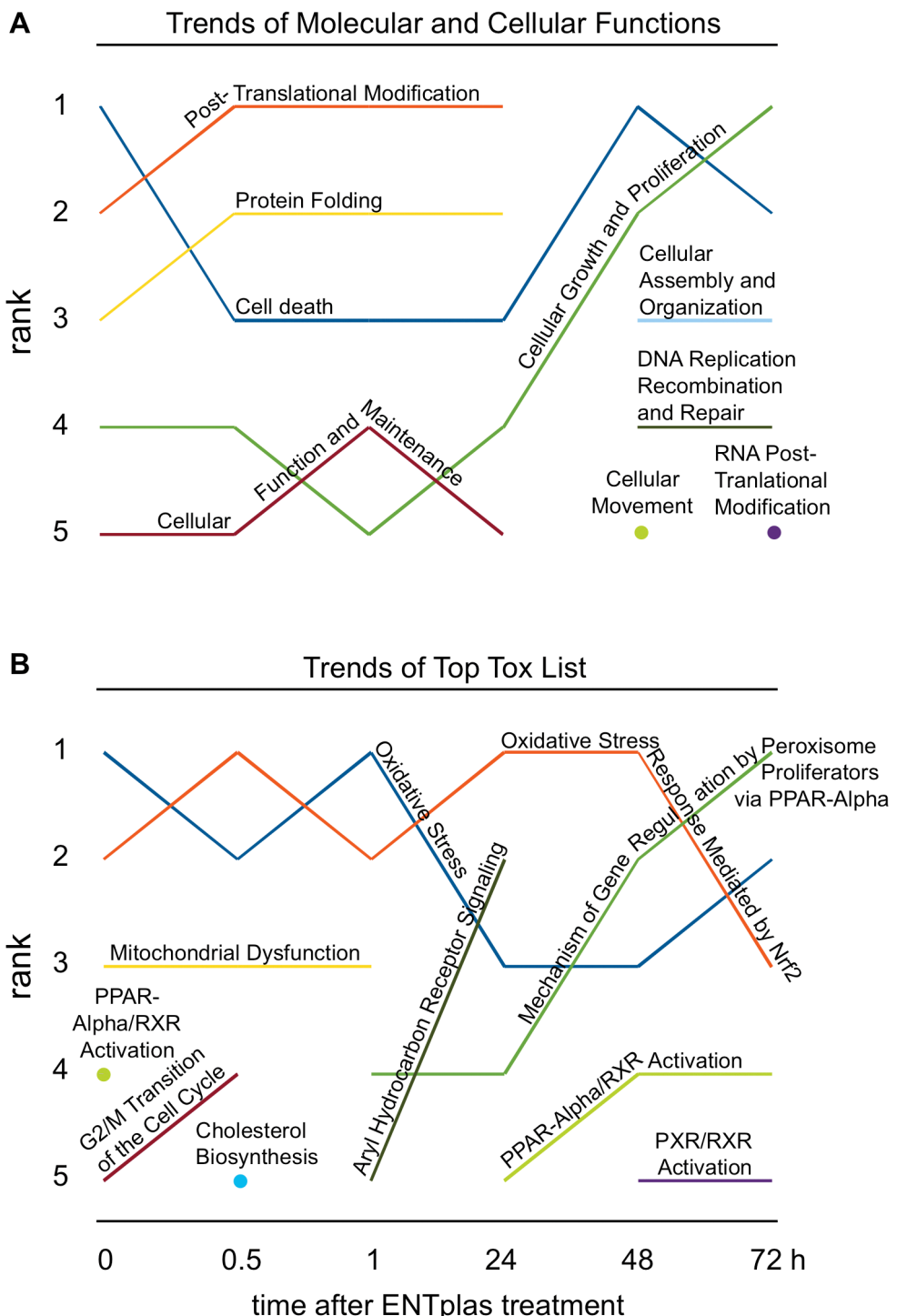


Figure 14: Molecular Function and Toxicity Analysis assessed by IPA (Ingenuity Pathway Analysis). Statistically approved differentially expressed proteins from each time-condition were assigned to networks (Ingenuity Pathway Analysis). Top 5 rankings of molecular and cellular functions (A) and top tox lists (B) were plotted against the time-points after ENTplas treatment. Relevance ranking shows time-dependent developments and importance for cell-status at the specific time-points. Values and colour coding are taken from Table S-2 (supplementary material). All results show a p -value < 0.05 . Detailed information including p -values are shown in supplementary material Table S-2.

Pathways indicating conspicuously oxidative stress and the oxidative stress response mediated by Nrf2 mainly characterize the toxic aspect of ENTplas treatment. Later aryl hydrocarbon receptor signalling and mechanism of gene regulation by peroxisome proliferators via PPAR-Alpha augment the appearance of hazardous compounds. PPAR-Alpha/RXR-activation underlines the probable need for energy supply and was described as a mediator of proliferation induction in the early phase of wound healing [69]. However, in the initially phase, oxidative stress and the response mediated by Nrf2 to this stress, seems to be the major challenge to the ENTplas treated cells. In addition, enhanced G2/M Transition of the cell cycle at early time points (0 h and 0.5 h) and induction of proteins involved in DNA replication, recombination and repair (**Figure 14-A**) at later times (48 h and 72 h) probably also indicate DNA damage. This fact may be considered for risk assessment and future toxicity valuation.

8.5. ENTplas-mediated changes in the proteomic profile displayed by treemaps confirm the appearance of oxidative stress after ENTplas treatment

Voronoi Treemaps were used to intuitively visualize large data sets. Originally used to visualize hierarchical structures of software systems [55], an adapted derivative, previously described by Bernhardt et al. [70] and Otto et al. [67], can serve as a powerful visualization of hierarchically structured protein functional classifications and expression data. In this study KEGG Brite ontology was used and adapted according to the proteins identified in this study. Approximately 1100 identified protein species that corresponded to 450 genes could be allocated to KEGG Brite functional classes. Expression data from Delta2D-analysis were used for expression-related colouring of Treemap cells (see **Figure 15; Movie S-1**). The section “oxidative stress” including oxidative stress related proteins, was extracted from the whole data set (A) and coloured separately for each time point (**Figure 15-B**: 0 h to 72 h; **Movie S-2**). Colourization follows log ratios of normalized expression volumes of ENTplas treated samples divided by the normalized expression volumes of untreated controls. Negative fold changes (fold decrease) are coloured in shades of blue, positive fold changes (fold increase) are coloured in shades of orange. Saturation of orange and blue is reached, when fold change exceeds +5 for orange and -5 for blue (**Movie S-1** and **Movie S-2**).

This visualization protocol shows, that expression patterns changed substantially with the duration of cultivation after ENTplas treatment: Examples are shown in **Figure 15-**

B for members of the proteasome and protein disulphide isomerase, as well as for proteins involved in heat shock response and detoxification of ROS. These results suggest, that ENTplas treatment clearly shows effects on treated cells compared to the untreated controls. The effects and responses to them apparently affect metabolic pathways and lead to changes of proteins, which are related to oxidative stress. Furthermore, the 24 h-time point after ENTplas treatment seems to be crucial for cell status and determination of cell fate, supporting the results previously described from principal component analysis.

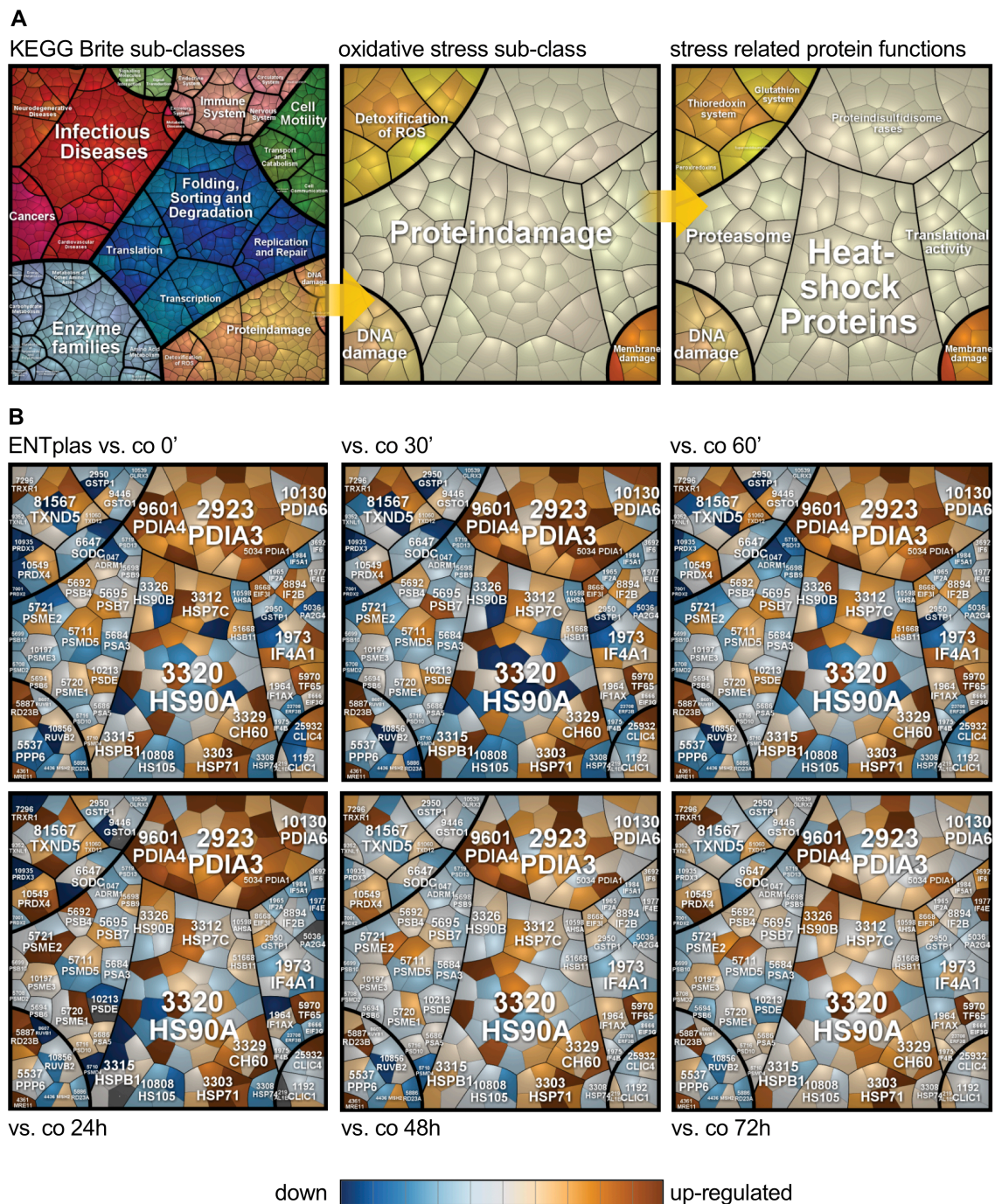


Figure 15: Visualization of large data sets by Voronoi Treemaps. Resulting Treemaps from general analysis of time-related effects of ENTplas treatment in comparison to the corresponding untreated controls in S9 human epithelial cells. Identified proteins were sorted into individualised KEGG-BRITE hierarchy (A). The section “oxidative stress”, containing oxidative stress related proteins from **Fehler! Verweisquelle konnte nicht gefunden werden.**, was extracted from this general hierarchy and displayed for the time course from 0 h up to 72 h (B). Each tile in the structural hierarchies represents one identified protein and was coloured by logarithmic normalized expression values (% volume, normalized by the specific Cy-2-standard) from Delta-2D quantities. The isoluminant divergent colour gradient encodes expression changes: white coloured tiles show a fold change of ‘1’. Blue shaded tiles represent proteins with negative fold change (lower expression in ENTplas treated samples in comparison to the untreated

control) and shades of orange represent proteins with higher fold change than ‘1’. Saturation of blue and orange is reached at an expression level five times higher or lower than the corresponding control.

8.6. Correlation of protein expression patterns displayed by Hierarchical Clustering

In order to describe the differences in the expression profiles between all samples, all data were clustered hierarchically. This was done on the assumption of Euclidean distance metric and average linkage as supported by the TMeV-module of the Delta2D software package. Hierarchical sample clustering [68] illustrates relationships of the overall proteomic profiles of samples (top tree in **Figure 16**, **Figure S-4** on DVD) and spot expression profiles (left tree). The colours of heat map cells represent expression values of all analysed protein spots (total: 1505).

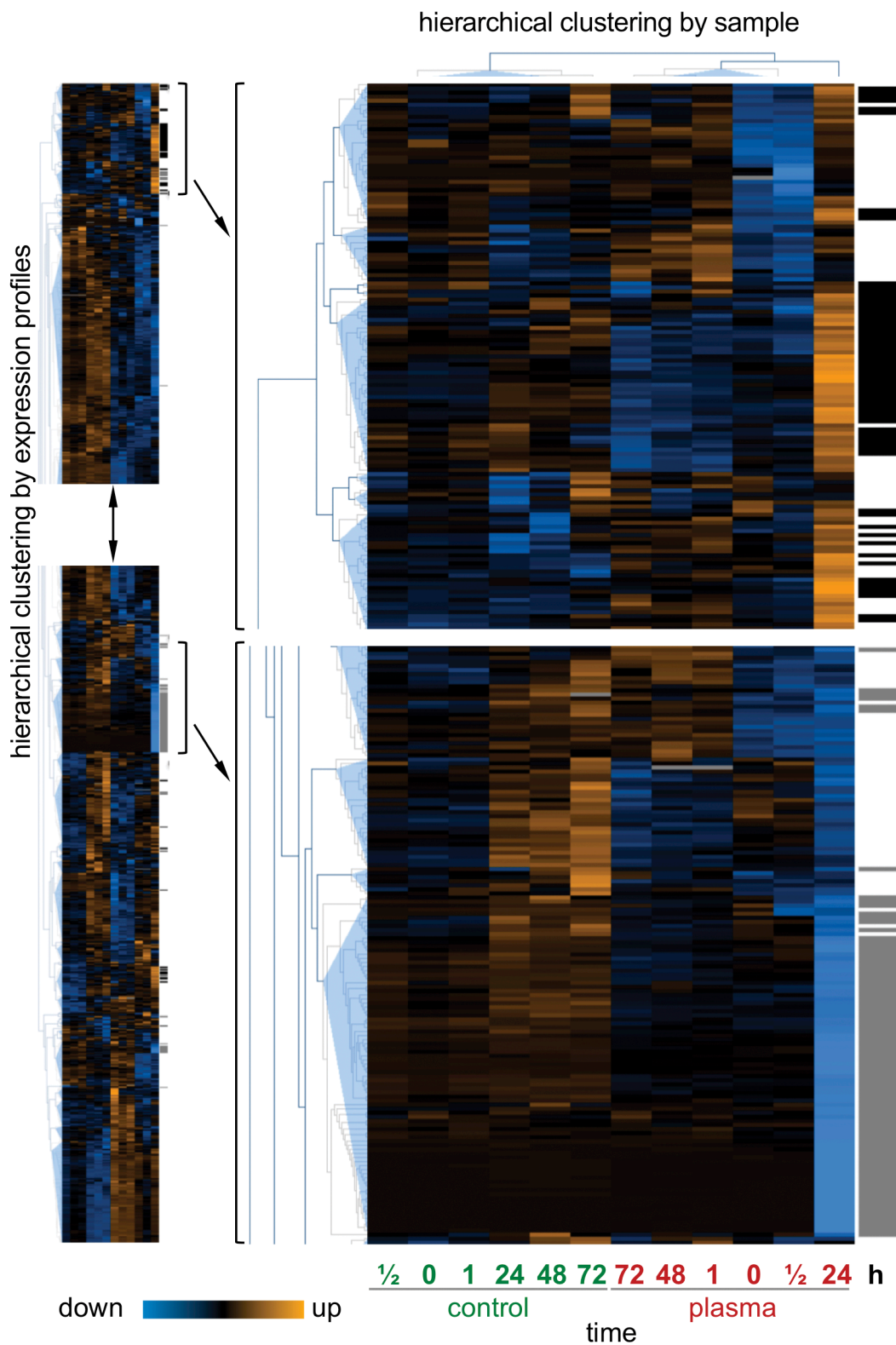


Figure 16: Hierarchical Clustering of detected 2D-DIGE protein spots by sample condition and expression profile. Hierarchically clustered (Euclidean Distance measurement and “average” linkage method) log-transformed expression protein values. 12 samples are shown vertically on the x-axis (sample order is defined on the right side). Spot-expression-values are shown horizontally on the y-axis. High expressions are coloured orange, low expressions are coloured blue and missing

*expressions are coloured grey. Dendograms, both on x- and y-axis, represent the Euclidean Distance between the samples. Hierarchical clusters are subsumed on the third level on the x-axis and on the 24th level on the y-axis. The clusterdendrogram for the samples are roughly grouped in the higher-level clusters, replicated gels merged prior for each sample. The clustering did not use any sample or replicate information. Cluster structure in the rows resulted from grouping of proteins with similar expression profiles (row dendograms are shown on left side). Specific identified proteins from K-means cluster 3 and 4 (see **Figure 17**) are highlighted black (K-means cluster 3) and grey (K-means cluster 4) on the right side of the hierarchical cluster.*

As already shown by PCA analysis, replicates of the same sample cluster together (data not shown – all replicates were grouped in **Figure 16**). Demonstrating the experimental quality. Furthermore, controls and ENTplas treated samples are distinctly separated from each other supporting the idea that ENTplas treatment affects airway S9 epithelial cells. For ENTplas treated samples, the 24 h-incubation replicates separate clearly from all other time points, while 48 h-, and 72 h-incubation replicates approach the controls.

8.7. K-means-Clustering as an assumption-free approach for regulated protein recruitment out of a large data set

In order to find spots, which are similarly expressed over the time of observation, a so-called K-means-clustering was performed using TMeV. This analytical procedure [68] calculates a given number of clusters with different centres. Initialization, which is the definition of k spot centres for clustering, occurs randomly. Therefore, multiple initializations (KMS – k-means supported) may compensate for different outcomes of the clustering approach for a single initialization. After that, every expression profile from the data will be allocated to the best fitting cluster. Thus, spots with similar expression behaviour over time are summarized in spot-lists for each cluster. The time course is shown in a two-dimensional diagram with samples on the x-axis and expression intervals on the y-axis. Spot-ID-lists with appending identifications were exported and analysed by using the IPA software package for network analysis.

According to the observed expression changes, a K-means-clustering with 10 clusters (see **Figure 17** and **S-3**) was calculated by the means of the Euclidean Distance of the genes (=spots). With help of these clusters, effects of plasma-treatment can be detected and described. By this means, several expression profiles can be differentiated as described in the following:

Differences between untreated controls and ENTplas treated samples show a typical offset (see **Figure 17**: Cluster 1, 6, 7, 8, 9 and 10). This supports the results from the principle component analysis and furthermore subsumes proteins, which are responsible for these effects, into more detailed clusters. Cluster 1, 2, 5 and 8 isolate proteins showing long-time incubation effects. Again, the two specific clusters 3 and 4 represent the particular features of the 24 h time point of ENTplas treated samples.

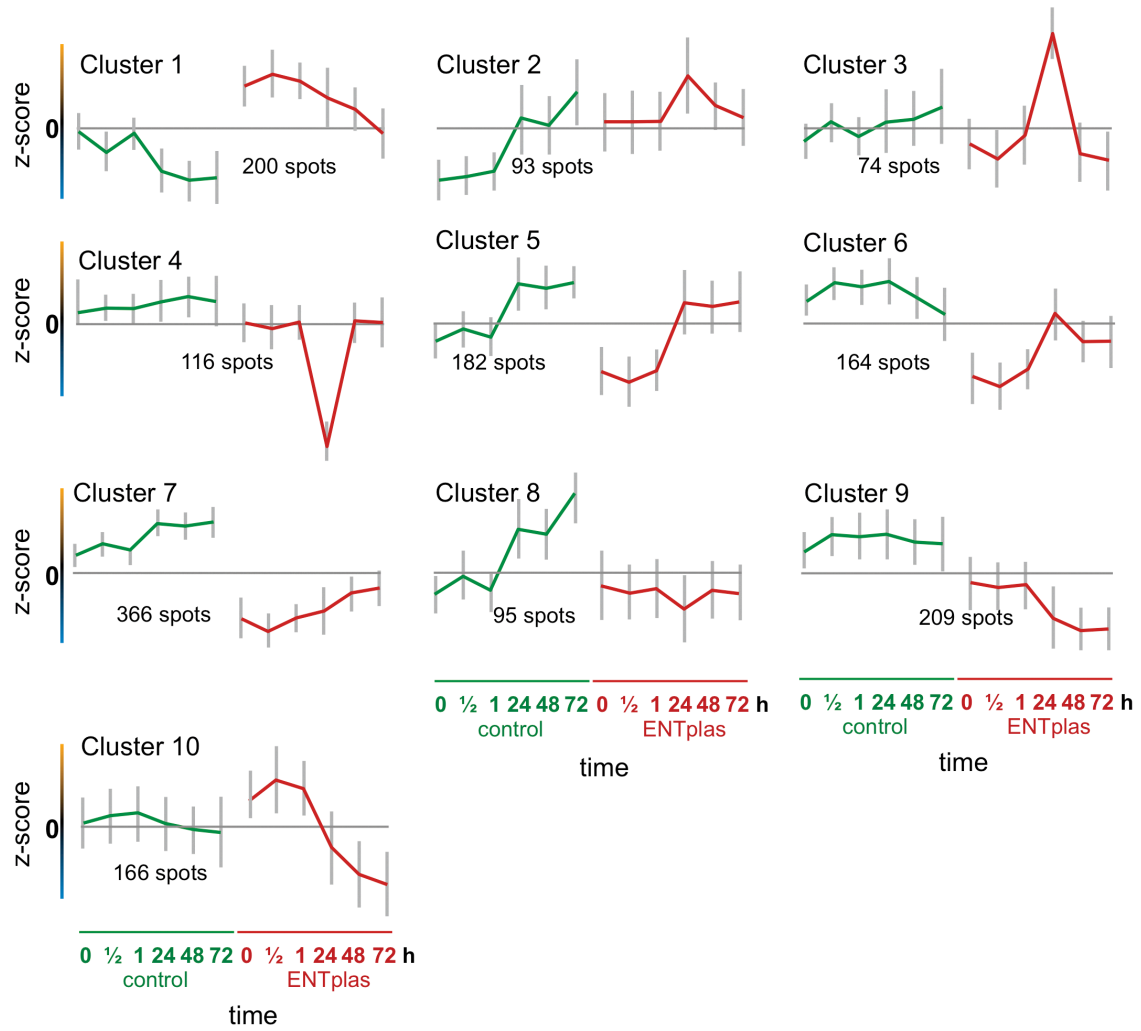


Figure 17: Protein expression profile analysis by K-means clustering. Overview of clusters was computed by TMeV included in Delta2D. Expression profiles from every spot were compared with these given clusters and assorted to the best fitting one. The x-axis shows different groups of samples. The plotting scheme is displayed as a legend below the clusters. From the left to middle, controls in ascending incubation time from 0 h to 72 h are plotted. From the middle to the right, ENTplas treated samples are plotted in ascending incubation time from 0 h to 72 h. On the y-axis, the expression-rate is displayed. Each value is marked with the standard deviation of assorted protein expression values for this specific time point. The horizontal line marks value '0'. Values above that line show higher expression, values below that line lower expression, respectively.

8.8. Network analysis of calculated K-means Cluster using Ingenuity Pathway Analysis (IPA) suggests underlying molecular functions of likely expressed protein subsets

Only identified proteins out of the K-means-clusters were used for IPA network analysis. Resulting networks were visualized and corresponding relationships were summarized. Conclusions can be drawn in combination with the previous K-means-clustering, regarding which pathways are affected and furthermore, how cells react to the treatment. Expression-profiles from K-means-clustering define the assignment of the allocated proteins of those clusters. Thus, combination of both observations is necessary. Summaries of clusters and network-analysis-summary can be found in the supplementary material (**Figure S-3**).

In order to ascertain the focus on the molecular adaptation reactions of epithelial cells to ENTplas treatment, functionally representative clusters are presented:

Clusters 1, 3 and 10 contain proteins, which are up regulated in comparison to the specific control. Networks from Cluster 1 indicate both, the appearance of post-translational modifications, protein folding, gene expression but also cell death, oxidative stress response and DNA Replication, Recombination and Repair. Proteins from this cluster represent both preservation of metabolic capability and cellular stress, including life-threatening stress. Cluster 3 includes proteins, which are specifically up regulated after 24 hours after ENTplas treatment. In contrast, the antagonistic cluster 4 includes proteins, which are specifically repressed after 24 hours after treatment. Protein subsets of clusters 3 and 4 are highlighted in **Figure 16**. At a first glance, the corresponding networks represent similarly affected functions, e.g. post-translational modifications, protein folding and cell-to-cell signalling. However, the toxic aspects differ profoundly. While cluster 3 represents proteins from PPAR-Alpha and RXR-Alpha activation, cell cycle damage checkpoints and gene regulation by peroxisome proliferators, cluster 4 represents predominantly oxidative stress response via Nrf2, cell death, aryl hydrocarbon receptor signalling and hypoxia-inducible factor signalling. This might be an indication that 24 hours after ENTplas treatment cells begin with cellular assembly and that cell death might play a subordinated role as long as cells are able to respond to cellular stress factors. These notions gain support from a comparison of clusters 5 and 7. Although it is showing an offset between controls and ENTplas treated samples, the trend between short-time and long-time response to ENTplas

treatment is interesting: Proteins in the networks from these clusters represent cellular growth and proliferation, post-translational modifications, protein synthesis but also cell death. Interestingly they coincide with the oxidative stress response via Nrf2. Nrf2-signalling plays a key-role. It has to be pointed out that proteins from these clusters show only slight differences between treated samples and corresponding controls, and thus did not appear in analyses presented above, because those were restricted to stringent fold changed differences between untreated controls and their corresponding ENTplas treated samples. However, a trend analysis in-between the treated samples provides additional insight how effects proceed over time. In addition, cluster 10 represents proteins antagonistic to cluster 7.

One can see, that both analytical approaches from chapter 8.4 and this capture result in similar conclusions, but from two different points of view. While the first approach relates to the comparison between ENTplas treated samples and their corresponding control for each time point separately, the second approach is exclusively related to the time-dependent expression profile.

8.9. Immuno Blot analysis of cytosolic Nrf2 expression confirms the involvement of this oxidative stress related regulator

Statistical analyses of the proteomic experiments revealed an important role of oxidative stress response mediated by Nrf2. Unfortunately, Nrf2 itself was not detected with the 2D-DIGE-approach, but only Nrf2-related network-partners. In order to confirm effects of ENTplas treatment on Nrf2 expression in S9 epithelial cells, Immuno Blot analyses were performed, using the same protein extracts of the 2D-DIGE-experiment. For this purpose, antibodies against Nrf2 and Keap1 (see **Figure 18**) were utilized.

Levels of Nrf2 were significantly reduced after ENTplas treatment compared to control samples. For all analysed time points (0 min up to 72 h), bands of lower density were detected in treated samples compared to the corresponding non-treated controls (**Figure 18-A**). Quantitative image analyses confirmed these observations with a p-value of < 0.005 for all time points (**Figure 18-B**).

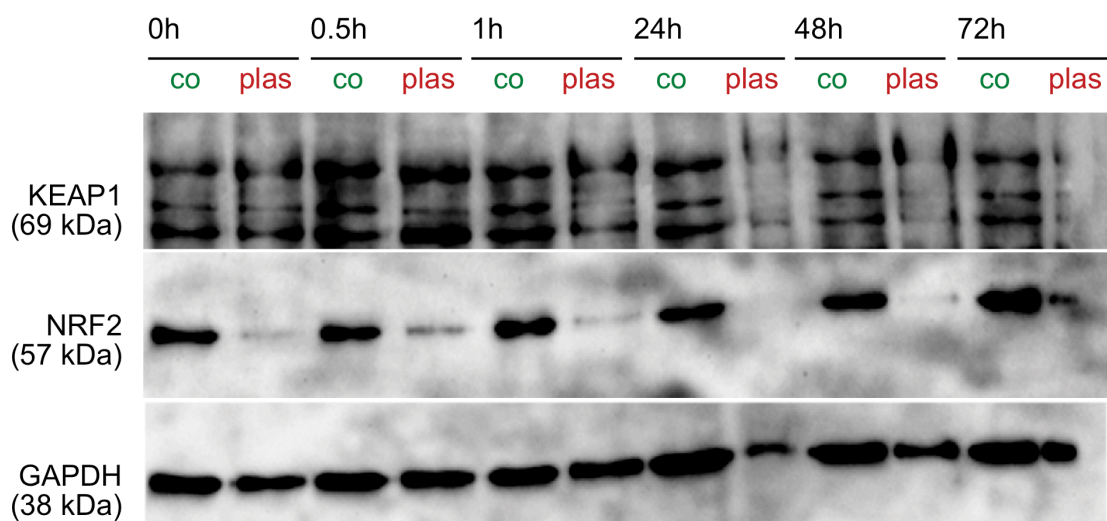
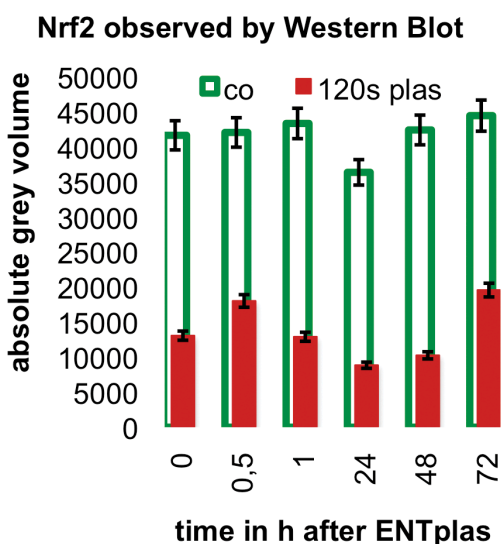
A**B**

Figure 18: Validation of by Immuno Blot analyses of Nrf2 and Keap1 cytosolic concentrations after ENTplas treatment. (A) Cytosolic concentrations of Nrf2 and Keap1 in non-treated control and ENTplas treated S9 epithelial cells are displayed for each time point 0 h up to 72 h after treatment. Immuno Blotting of Nrf2 in S9 epithelial cell extracts shows that Nrf2 disappears after ENTplas treatment while Keap1 undergoes several modifications by ENTplas treatment. The filters were reprobed with an anti-GAPDH mAb to ensure equal loading of the gels. (B) Results from quantitative image analysis of band densities. Statistical testing with students t-test opened statistical significance ($p < 0.005$) between untreated controls and ENTplas treated samples regarding Nrf2 expression for all time points.

Because of the oxidative stress presumably triggered by ENTplas treatment, Nrf2 probably dissociates from the complex formed by Keap1 with Nrf2 and translocates into

the nucleus, where it binds to other proteins and subsequently to the DNA [71], [72]. Therefore, the reduction of cytosolic Nrf2 levels in ENTplas treatment affirms further findings concerning Nrf2 mediated oxidative stress response [73–80].

8.10. Cytosolic concentrations of full length IL-1beta and IL-33 are decreased in S9 epithelial cells after ENTplas treatment, suggesting processes of stimulation and modulation of immune-related cytokines

Immuno Blotting of intracellular cytosolic full-length IL-1 beta and IL-33 reveals a decrease of these pro-interleukins in S9 bronchial epithelial cells 30 minutes and 48 hours after ENTplas treatment in comparison to non-treated control cells (see **Figure 19**). Both interleukins were described as pro-inflammatory cytokines, which furthermore are associated with immunological responses [81], [82]. They are known to be processed under pro-inflammatory conditions via caspase-1 to the particular mature forms, which function as intracellular transcription factors as well as secreted cytokines, which target T-cells and other immune-related targets [83–87].

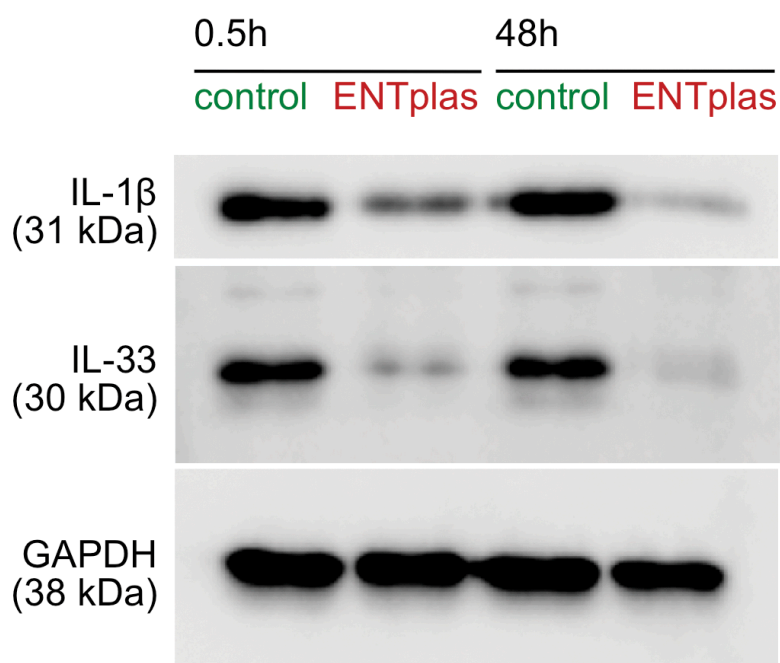


Figure 19: Cytosolic IL-1 beta and IL-33 levels after ENTplas treatment determined by Immuno Blotting. Expression of IL-1 β and IL-33 in non-treated control and ENTplas treated S9 epithelial cells are displayed for the time points 0.5 h and 48 h after treatment. Immuno Blotting of S9 epithelial cell extracts shows that both IL-1 β and IL-33 cytosolic protein amount is decreased dramatically after ENTplas treatment. The filters were reprobed with an anti-GAPDH mAb to ensure equal loading of the gels.

9. Discussion

The effects of non-thermal plasma onto human cells have so far not been extensively studied on protein level. However, such proteomic studies will likely contribute to a better mechanistic understanding of detectable effects, such as, wound healing [15], [17] and apoptosis [3]. Recently it was demonstrated that reactive oxygen species (ROS) appear not only in non-thermal plasma treated cells, but also in the cell culture medium [3], [41].

This thesis provides an overview about how low-temperature plasma treatment affects the protein pattern of human host cells and also illustrates which bio-informatics and statistical techniques may be applied in such analysis. Thus, the thesis presents a workflow for experiments evaluating plasma effects on various tissues for improving care in chronic medical conditions. Wound healing was accelerated at 120 sec plasma exposure in a clinically relevant extent, suggesting a beneficial role in the postoperative period. Proteomic data can help to uncover the molecular mechanisms mediating the observed effects. Furthermore, the application of proteomic approaches in risk assessment will be discussed.

The need for the exploration of the interactions between non-thermal plasma treatment and living cells was recently emphasized [41]. Kalghatgi et al. investigated specific and hypothesis-derived markers for effects like increases in intracellular levels of reactive oxygen species (ROS) or DNA damages. Our proteomic approach complements and extends such a targeted approach. While ROS cannot be observed directly by our method, molecular and metabolic reactions of the cells can indicate the presence of ROS and demonstrate the influence of ROS on cellular structures. Furthermore, it was possible to monitor the strategies of living cells responding to non-thermal plasma stimulation and to define associated biomarkers. These indicators may be subsequently used for risk assessment and quality management of application of non-thermal plasma sources in clinical settings.

Obviously, there are also challenges, which had to be addressed in order to design a practical and reliable method. In addition, specified statistical methods need to be used in order to filter out relevant changes and information. The presented description is a proposal of how to manage these complex issues.

9.1. The influence of non-thermal plasma treatment on wound healing

Non-thermal plasma treatment of S9 epithelial cells in a wound healing model showed diverse effects, which are dependent on the applied dose of plasma. While relatively mild doses of up to 60 seconds show just a small effect on wound healing, a moderate dose of 120 seconds accelerates wound healing. In contrast, higher doses (240 sec and 360 sec) result in significantly impaired wound healing (240 sec) or even to no measurable healing activities (360 sec).

ROS play an important role in non-thermal plasma applications, as shown in the results and as already described by several authors (see above). Although the underlying mechanisms remain still predominantly unclear, a hypothesis based on the new aspect of Nrf2-signalling will be drawn in the following.

Regular wound healing of entire tissues containing multiple layers and different cell types has four phases: first, the initial phase fulfilling haemostasis, second phase establishing an inflammation, the third phase of granulation and at last the fourth phase with remodelling and maturation [88], [89]. This system cannot be applied to the presently used wound model, since only epithelial cells in a cell culture dish were examined. This model lacks of multiple layers, blood vessels, immune cells and different cell types. Hence, the focus is on the aspect of reepithelialisation. Here, cell migration into the wound bed and cell proliferation in the wound surrounding areas are discussed to be the major sources for epithelialisation of the wound [90]. In order to migrate into the wound area, cells need to detach from their underground. This aspect was already examined for keratinocytes. Landsberg et al. [61] were able to show, that non-thermal plasma treatment of HaCaT –cells influences the cell adhesion. The loss of cell adhesion after 30 sec exposure to non-thermal plasma is necessary for subsequent cell migration. Nitric oxide, produced by inflammatory cells in regular wound healing seems to have a great influence on cell migration [91]. It is known, that non-thermal plasma contains distinct amounts of nitric oxides [12], [92], [93]. Thus, non-thermal plasma may contribute to cell migration after alteration of tissue integrity. Additionally, our results outline a higher proliferation activity after non-thermal plasma treatment compared to untreated controls, which highlights the second aspect of reepithelialisation for the wound surrounding areas more in detail.

In order to explain wound-healing support, Nrf2 emerged as a possible key player due to the induction of oxidative stress stimulation by non-thermal plasma application. Every wound shows inflammation accompanied by oxidative stress after a distinct latency time after alteration [94], [95]. Additionally, macrophages can secret hydrogen peroxide for bacterial decontamination [96–98]. Host tissues have to protect themselves from this aggressive environment. Due to the oxidative nature, Nrf2 is a major regulator of stress reaction [78], [79], [99], [100]. Experiments with Nrf2 knockout mice showed prolonged inflammatory phases [101], [102]. Thus, direct activation of Nrf2-pathways by non-thermal plasma treatment may help to control or prevent the inflammatory phase and subsequently reduce time of latency before the cellular phase of wound healing can start. These hypotheses have to be confirmed in further experiments. But the supporting ability of Nrf2 should be addressed, when examining wound healing after non-thermal plasma treatment. Furthermore, the possible contribution of nitric oxides from the applied plasma should be in focus as the cause of various phenomena like angiogenesis and cell migration.

9.2. The role of Nrf2 in ROS-induced intracellular oxidative stress environments after non-thermal plasma treatment

Our results indicate that oxidative stress and the related cellular response play an important role after treatment with non-thermal plasma. Both statistical approaches (time-related and control-related approaches) showed concordantly, that oxidative stress and response to oxidative stress, mediated by Nrf2, are placed in the top 5 rankings of toxicities. Thus, presence of ROS and the resulting oxidative stress / damage can be assumed. Although the mechanisms of oxidative stress cannot be explained in detail, several hints were found among the protein patterns and network analyses, that support already described pathological mechanisms [103], [104]. The present findings include direct modifications and damage of proteins, which were likely caused by the oxidative intracellular environment due to accumulation of reactive oxygen species. The responses to damage, that ROS elicited in cellular organelles and structures, like heat shock protein interactions, DNA repair or apoptosis, also support this notion. **Table 2** summarizes effects, which ENTplas treatment can have on human epithelial cells and combines them with detected and affected proteins of our analyses, especially for the oxidative stress response.

Table 2: Selection of representing markers representing intracellular effects of ENTplas treatment. Damage of proteins, nucleic acids and lipids result in cellular responses, which are exemplarily listed. The last column combines these effects with detected examples from our experiments and analyses, indicating, that oxidative stress occurs after ENTplas treatment in human S9 epithelial cells.

Oxidative stress related effects	Consequences	Immediate effects	Long term responses	Examples from our experiments
Protein damages	Unfolding	• Loose of function • Heat shock protein interaction	Elimination and subsequent new production	Proteasome-related proteins ↑
	Misfolding	• pI-shifts		Translational activity ↑
	De-complexation / dimerization	• Shifts in molecular weight	Refolding and/or Repair	Heat shock proteins ↓ PDIA 1, 3, 4, 6
DNA damages	Single strand scissions			MRE11
	Double strand scissions	• Detection mechanisms	• SOS-repair	PPP6
	Base modifications	• Damage marking	• Apoptosis	MSH2
	Hydrolysed bonds between sugar and base	• Cell cycle arrest	• Cancer-development	KU86 RD23A, RD23B RUVB1, RUVB2
Detoxification of reactive oxygen species (ROS)		Catalase active		(Catalase not found)
	H ₂ O ₂ detoxification	Peroxidases active		PRDX 2, 3, 4, 6
	OH• detoxification	Superoxide dismutase active	• Regeneration of “exhausted” proteins	SODC
	O ₂ [•] detoxification	Thioredoxin-system active	• Appearance of isoforms	TRXR1, TXND5, TXNL5
Membrane modifications	Glutathione-system active			GSTO1, GSTP1, GLRX3
	Membrane oxidation		• Changes in permeability	
	Lipid peroxidation	• Structural changes	• Changes of the membrane potential	AL1B1
	Transporter proteins	• Increased / Decreased protein integration	• Apoptosis	CLIC4

Furthermore, the results from K-means-clustering and the control-related statistical analyses with subsequent network-analyses indicate, that oxidative stress response leads to two diverse responses of cell metabolism. Namely, cellular assembly and proliferation, as well as, cell death and apoptotic activities, which are both associated with different temporal response patterns to non-thermal plasma treatment. While non-thermal plasma treatment shifts the equilibrium between cell death and proliferation in favour of apoptosis and cell death signalling during the first 24 hours after treatment, cellular growth and proliferation on the other side are favoured after 48 hours. These findings suggest, that there exists a mechanism that either drives cells into cell death or mounts adaptive responses allowing survival of low-temperature plasma treatments. These observations may also explain the findings that non-thermal plasma treatment can turn a chronic wound to an acute wound with a better healing probability [18], [105], [106].

Network-analyses can reveal probable key players for such regulatory mechanisms. In this analysis Nrf2 emerged as one leading player in the cellular response to non-thermal plasma treatment. Adding Nrf2 (NFE2L2) to the present list of proteins, which were identified by 2D-DIGE and subsequent MALDI-TOF-MS-identification and performing a subsequent network analysis with IPA links Nrf2 with a selection of proteins, which were altered after non-thermal plasma treatment and were identified by our analyses (see **Figure 20**).

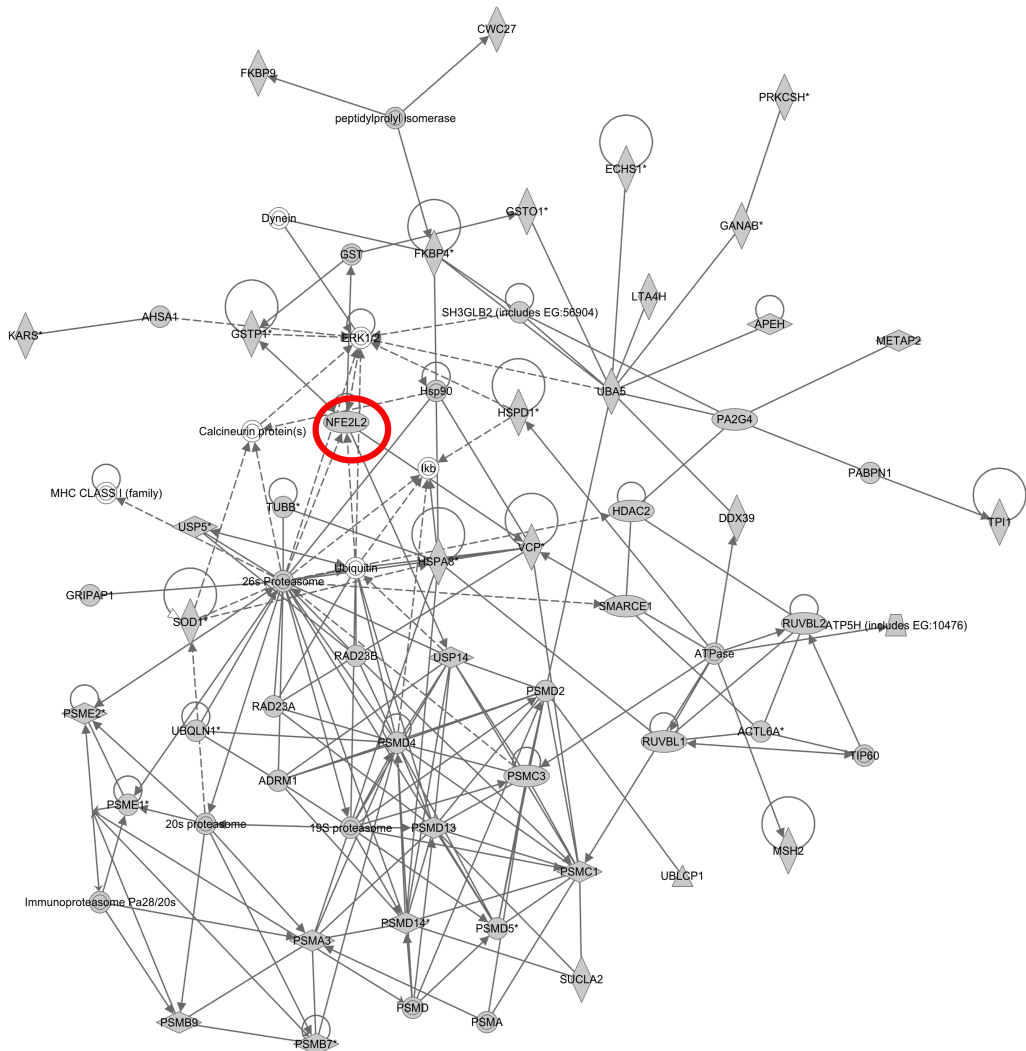


Figure 20: Ingenuity Pathway Analysis network of MALDI-TOF-MS identified proteins from statistical analysis. Direct and indirect relations, described in the literature, between identified and unidentified proteins are displayed. Proteins, which were identified by MALDI-TOF-MS in upper airway epithelial S9 cells, are highlighted in grey. Nrf2 (NFE2L2, red frame) was added due to the identification by the Immuno Blot assay. The resulting network is composed of 57 focus molecules characterized by “post-translational modifications”, “protein folding” and “cancer”. The Score is 87. Molecular and cellular functions show “cell death”, as well as “cellular growth and proliferation” and “cellular function and maintenance”. The Top Tox lists are headed by “Nrf2-mediated oxidative stress response” and “oxidative stress”. The computed network shows, that Nrf2 fits perfectly into previously found network relations and takes a central place in between the displayed relations.

Nuclear factor (erythroid-derived-2)-like 2 (Nrf2) is known as a ubiquitously occurring transcription factor, encoded in the NFE2L2-gene [107]. Under normal conditions Nrf2 is bound to the Keap1 protein in the cytosol of the cell. Keap1 constantly ubiquitinates

Nrf2 in the absence of oxidative agents, which leads to proteasomal degradation of Nrf2 [108], [109]. Increased levels of oxidative or electrophilic agents cause a disruption of cysteine residues in Keap1 and the release of Nrf2 into the cytosol [110], [111]. In this case Keap1 gets ubiquitinated and subsequently degraded by the proteasome. The released Nrf2 is now able to translocate into the nucleus and binds there to the DNA at specific ARE (Antioxidant Response Element)-sites [112]. These ARE-regions are located in the upstream regions of several specific antioxidative genes. Binding of Nrf2 to the ARE-region starts the transcription of the associated downstream genes. Products of these genes like glutathione-S-transferase (GST), heme oxygenase-1 (HO-1) or thioredoxins, possess anti-inflammatory properties (HO-1) [113] and contribute to the control of intracellular oxidative stress [114]. Elevated levels of GST, TRXR1 and others have been found in the 2D-DIGE experiment. Our proposal of Nrf2-activation via non-thermal plasma treatment and the subsequent cascade is summarized in **Figure 21**.

Immuno Blot analysis confirmed the cytosolic decrease of Nrf2 levels in S9 cells after non-thermal plasma treatment. These findings suggest, that Nrf2 plays an important role in oxidative stress response, previously described by several authors [71–73], [75], [77], [78], [80], but also may be a part of regulatory interplays, which can lead to both: cell survival and to cell death. These issues have already been addressed before in different contexts. Oxidative stress, regardless if caused internally or externally, is often linked with ageing and cell death [71], [73], [115]. Proliferation-inducing abilities of Nrf2-signalling, which support the results of dose-dependent, accelerated wound healing effects in ENTplas treated epithelial cells, have also been noted [73], [116], [117]. Nevertheless, these effects need to be studied in more detail.

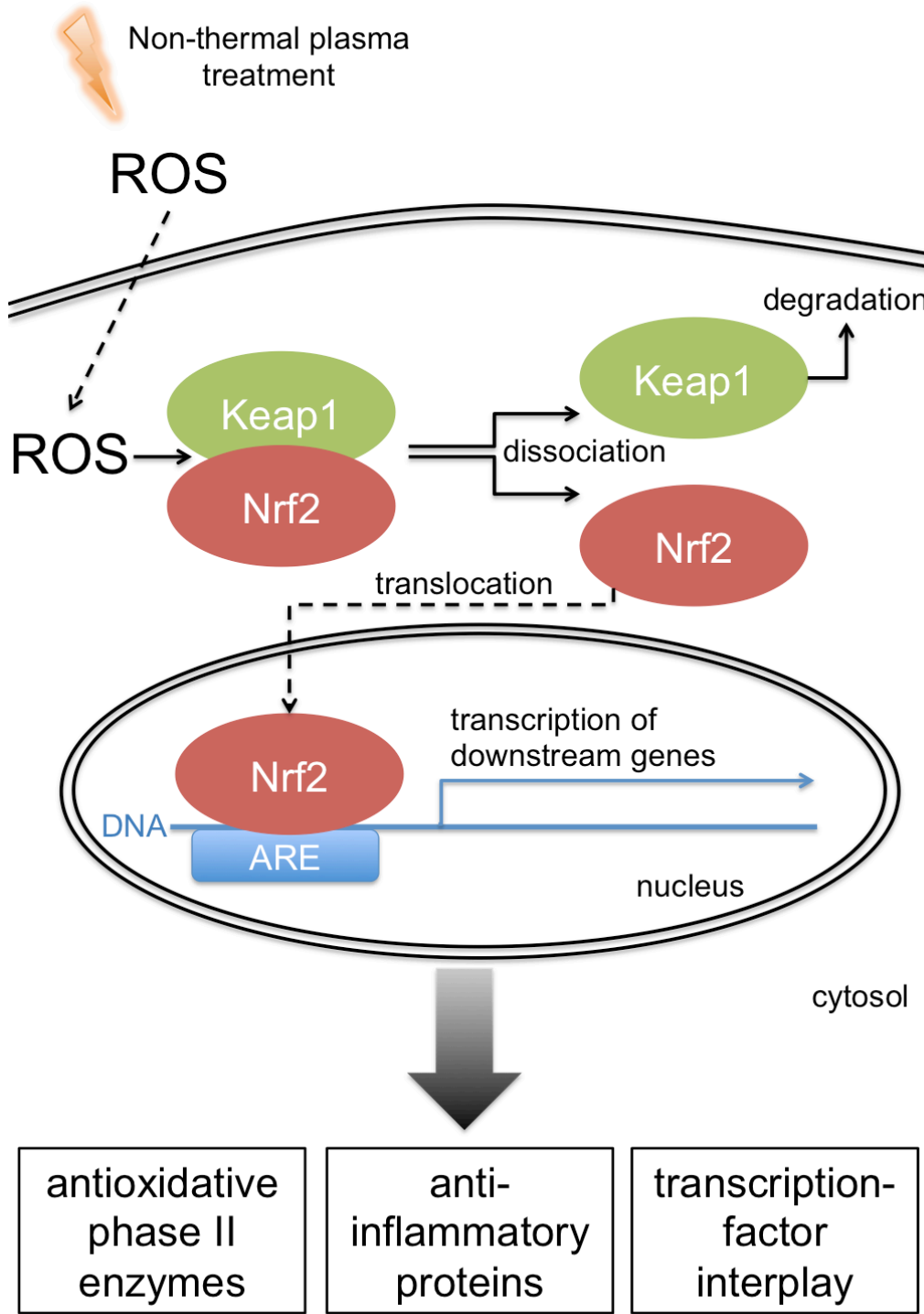


Figure 21: Hypothetical scheme of non-thermal plasma treatment cell stimulation via the Nrf2-pathway. Based on our results, it can be hypothesized, that non-thermal plasma treatment induces oxidative stress with increased amounts of intracellular reactive oxygen (ROS) and nitrogen (not shown here) species. Interactions of ROS with Keap1 lead to the release of Nrf2 into the cytosol and subsequent translocation into the nucleus, where Nrf2 binds to specific ARE-regions and induces transcription of downstream regions containing antioxidative components. Direct and indirect functions and interplays of these Nrf2-related products represent the major oxidative stress response in our experiments.

9.3. Biomarkers for further analyses, risk assessment and plasma-source designing

Network-analyses and time related statistical analyses of expression profiles identified different proteins, which are related to cellular oxidative stress responses (see **Table 2**) and can therefore serve to monitor cellular reactions to this treatment and indicate the cellular stress status. These candidates could be used as possible biomarkers for further studies in order to evaluate effectiveness and toxicities of non-thermal plasma treatments or even for the design of new plasma sources. The hypotheses-free approach leading to these candidates is a clear advantage in biomarker screening.

Furthermore, because of the detection of apparently dose dependent apoptotic activity and DNA [41] of non-thermal plasma treatments, tools for the assessment of the associated risk are necessary before any application in daily medical routine can be envisioned. UV-irradiation related DNA damage is known to be mutagenic and is related to increased occurrence of carcinogenesis. Even if direct damages of the ultraviolet fraction of the non-thermal plasma or of ROS-interactions with the DNA have not been detected, Kalghatgi et al. [41] provided evidence that non-thermal plasma treatment only of the cell culture medium caused an increase in DNA strand scissions in subsequent cell cultivations. This underlines the pivotal role of ROS dependent DNA interactions. For further analyses of additional - so far unknown - side effects, these specific biomarkers must be validated in individual experiments. A proteomic approach monitoring simultaneously over 1000 protein spots can be considered as an in-depth method for characterization of non-thermal plasma-related effects and risks. Even fine adjustments in development of plasma sources and follow-up quality controls can be performed using proteomic approaches. Costs, and complexity of analysis have to be reduced in order to establish a method that is suitable for daily use and routine. Multiple-reaction-monitoring-assays- (MRM) based mass spectrometry for up to 50 target proteins derived from an initial in-depth analysis might be a compromise, fulfilling at least some of the requirements.

9.4. Other potential ENT-specific applications of non-thermal plasma

Wound healing is important for every surgical field and consequently improvements and new applications for the support of healing wounds are of interest. Based on the

presented results, postoperative treatment directly after surgery should be beneficial for wound healing outcome. Another issue is the treatment of chronic wounds. Bender et al. [18] showed, that non-thermal plasma treatment turned a chronic wound on a dog's nose into a healing acute wound. These findings open a large field of possible applications for all fields of surgery. In addition to the support of wound healing, some other applications of non-thermal plasma in the ENT-field are conceivable.

The ability to induce blood clotting with a direct non-thermal plasma treatment is a promising method for minimal invasive and tissue preservative treatment of intraoperative and postoperative bleedings, since non-thermal plasma does not destroy the tissues but induces undirected clotting.

Another aspect is the disinfection respectively decontamination of skin, mucosa and other surfaces. Removing localized growing bacteria for example in the upper airways pre or post surgery or even as a sole treatment is beneficial for wound healing on the one side, but more important it can be a promising treatment of bacteria-related diseases. This is especially true for acute and chronic inflammation as well as diseases, which are related to immune responses to bacterial antigens. *Staphylococcus aureus* and especially MRSA can cause severe infections and furthermore their super antigens are newly associated with chronic diseases like bronchial asthma, nasal polyps and chronic rhino sinusitis [118], [119]. Non-thermal plasma can possibly be used for inactivation or removal of those triggers.

Finally it would be beneficial, if non-thermal plasma treatment can be used for direct modulation of immune responses of the target tissues. First discoveries among lymphocytes regarding sensitivity to non-thermal plasma treatment of different subpopulations and changes in the ratio of T- and B-cells [120] were the reason to perform further experiments with the non-thermal plasma treated airway epithelial cells. Alterations of two different interleukins after non-thermal plasma treatment of epithelial cells have been observed in this thesis and probably indicate the ability of ENTplas treatment to modulate the immune response. Although the preliminary data show the disappearance of IL-33 and IL-1 beta from the cytosol of ENTplas treated S9 epithelial cells, which cannot be explained fully with the present experimental setup, the suggestion of immune system modulation by non-thermal plasma treatment should be the subject for further studies. A therapeutic treatment with non-thermal plasma would be conceivable also for other chronic diseases such as bronchial asthma, chronic rhino-

sinusitis as well as allergic diseases. Besides, experimental set-up enables translation for all various cell lines to extend areas for possible plasma treatment to all parts of chronic medical conditions.

10. References

- [1] T. Gold, “Plasma and Magnetic Fields in the Solar System”, *J Geophys Res*, vol. 64, pp. 1665–1674, 1959.
- [2] H. Conrads and M. Schmidt, “Plasma generation and plasma sources”, *Plasma Sources Sci Technol*, vol. 9, no. 4, pp. 441–454, 2000.
- [3] R. Sensenig, S. Kalghatgi, E. Cerchar, G. Fridman, A. Shereshevsky, B. Torabi, K. P. Arjunan, E. Podolsky, A. Fridman, G. Friedman, J. Azizkhan-Clifford and A. D. Brooks, “Non-thermal Plasma Induces Apoptosis in Melanoma Cells via Production of Intracellular Reactive Oxygen Species”, *Ann Biomed Eng*, 2010.
- [4] J. Heinlin, G. Isbary, W. Stoltz, G. Morfill, M. Landthaler, T. Shimizu, B. Steffes, T. Nosenko, J. Zimmermann and S. Karrer, “Plasma applications in medicine with a special focus on dermatology”, *J Eur Acad Dermatol Venereol*, vol. 25, no. 1, pp. 1–11, 2011.
- [5] M. Laroussi, “Low-Temperature Plasmas for Medicine?”, *IEEE Trans Plasma Sci*, vol. 37, no. 6, pp. 714–725, 2009.
- [6] K.-D. Weltmann, E. Kindel, R. Brandenburg, C. Meyer, R. Bussiahn, C. Wilke and T. von Woedtke, “Atmospheric Pressure Plasma Jet for Medical Therapy: Plasma Parameters and Risk Estimation”, *Contrib Plasm Phys*, vol. 49, pp. 631–640, 2009.
- [7] J. S. Graham, T. W. Gerlach, T. P. Logan, J. P. Bonar, R. J. Fugo, R. B. Lee and M. A. Coatsworth, “Methods of Advanced Wound Management for Care of Combined Traumatic and Chemical Warfare Injuries”, *Eplasty*, vol. 8, p. e34, 2008.
- [8] G. Fridman, G. Friedman, A. Gutsol, A. B. Shekhter, V. N. Vasilets and A. Fridman, “Applied Plasma Medicine”, *Plasma Process Polym*, vol. 5, no. 6, pp. 503–533, 2008.
- [9] J. G. Birmingham, “Mechanisms of bacterial spore deactivation using ambient pressure nonthermal discharges”, *IEEE T Plasma Sci*, vol. 32, no. 4, pp. 1526–1531, 2004.
- [10] G. Fridman, M. Peddinghaus, M. Balasubramanian, H. Ayan, A. Fridman, A. Gutsol, A. Brooks and G. Friedman, “Blood Coagulation and Living Tissue Sterilization by Floating-Electrode Dielectric Barrier Discharge in Air”, *Plasma Chem Plasma P*, vol. 27, no. 1, pp. 113–114, 2006.

-
- [11] S. U. Kalghatgi, G. Fridman, M. Cooper, G. Nagaraj, M. Peddinghaus, M. Balasubramanian, V. N. Vasilets, A. F. Gutsol, A. Fridman and G. Friedman, “Mechanism of Blood Coagulation by Nonthermal Atmospheric Pressure Dielectric Barrier Discharge Plasma”, *IEEE T Plasma Sci*, vol. 35, no. 5, pp. 1559–1566, 2007.
 - [12] A. B. Shekhter, V. A. Serezhenkov, T. G. Rudenko, A. V. Pekshev and A. F. Vanin, “Beneficial effect of gaseous nitric oxide on the healing of skin wounds”, *Nitric Oxide-Biol Ch*, vol. 12, no. 4, pp. 210–219, 2005.
 - [13] E. Kvam, B. Davis, F. Mondello and A. L. Garner, “Non-thermal atmospheric plasma rapidly disinfects multidrug-resistant microbes by inducing cell surface damage”, *Antimicrob Agents Ch*, p. Epub ahead of print, PubMed-ID: 22232292, 2012.
 - [14] M. Laroussi, “Low Temperature Plasma-Based Sterilization: Overview and State-of-the-Art”, *Plasma Processes Polym*, vol. 2, no. 5, pp. 391–400, 2005.
 - [15] Y. Yu, M. Tan, H. Chen, Z. Wu, L. Xu, J. Li, J. Cao, Y. Yang, X. Xiao, X. Lian, X. Lu and Y. Tu, “Non-thermal plasma suppresses bacterial colonization on skin wound and promotes wound healing in mice”, *J Huazhong Univ Sci Technol Med Sci*, vol. 31, no. 3, pp. 390–394, 2011.
 - [16] S. G. Joshi, M. Paff, G. Friedman, G. Fridman, A. Fridman and A. D. Brooks, “Control of methicillin-resistant *Staphylococcus aureus* in planktonic form and biofilms: a biocidal efficacy study of nonthermal dielectric-barrier discharge plasma”, *Am J Infect Control*, vol. 38, no. 4, pp. 293–301, 2010.
 - [17] J. Heinlin, G. Morfill, M. Landthaler, W. Stolz, G. Isbary, J. L. Zimmermann, T. Shimizu and S. Karrer, “Plasma medicine: possible applications in dermatology”, *J Dtsch Dermatol Ges*, vol. 8, no. 12, pp. 968–976, 2010.
 - [18] C. Bender, N.-O. Hübner, K.-D. Weltmann, C. Scharf and A. Kramer, “Tissue tolerable plasma and polihexanide: Are synergistic effects possible to promote healing of chronic wounds? In vivo and in vitro results.”, in *Plasma for bio-decontamination, medicine and food security NATO Chemistry and Biology Serie*, Z. Machala,, K. Hensel and Y. Akishev, Eds. Springer Netherlands, 2012, pp. 321–334.
 - [19] G. B. McCombs and M. L. Darby, “New discoveries and directions for medical, dental and dental hygiene research: low temperature atmospheric pressure plasma”, *Int J Dent Hyg*, vol. 8, no. 1, pp. 10–15, 2010.

- [20] S. Rupf, A. Lehmann, M. Hannig, B. Schäfer, A. Schubert, U. Feldmann and A. Schindler, “Killing of adherent oral microbes by a non-thermal atmospheric plasma jet”, *J Med Microbiol*, vol. 59, no. Pt 2, pp. 206–212, 2010.
- [21] R. E. J. Sladek, S. K. Filoche, C. H. Sissons and E. Stoffels, “Treatment of *Streptococcus mutans* biofilms with a nonthermal atmospheric plasma”, *Lett Appl Microbiol*, vol. 45, no. 3, pp. 318–323, 2007.
- [22] M. G. Kong, G. Kroesen, G. Morfill, T. Nosenko, T. Shimizu, J. Dijk and J. L. Zimmermann, “Plasma medicine: an introductory review”, *New J Phys*, vol. 11, p. 115012, 2009.
- [23] G. E. Morfill, M. G. Kong and J. L. Zimmermann, “Focus on plasma medicine”, *New J. Phys.*, vol. 11, p. 115011, 2009.
- [24] Y. Akishev, M. Grushin, V. Karalnik, N. Trushkin, V. Kholodenko, V. Chugunov, E. Kobzev, N. Zhirkova, I. Irkhina and G. Kireev, “Atmospheric-pressure, nonthermal plasma sterilization of microorganisms in liquids and on surfaces”, *Pure Appl Chem*, vol. 80, no. 9, pp. 1953–1969, 2008.
- [25] F. Rossi, O. Kylian, H. Rauscher, M. Hasiwa and D. Gilliland, “Low pressure plasma discharges for the sterilization and decontamination of surfaces”, *New J Phys*, vol. 11, p. 115017, 2009.
- [26] V. Scholtz, J. Julák, V. Kríha and J. Mosinger, “Decontamination effects of low-temperature plasma generated by corona discharge. Part I: an overview”, *Prague Med Rep*, vol. 108, no. 2, pp. 115–127, 2007.
- [27] V. Scholtz, J. Julák, V. Kríha, J. Mosinger and S. Kopecká, “Decontamination effects of low-temperature plasma generated by corona discharge. Part II: new insights”, *Prague Med Rep*, vol. 108, no. 2, pp. 128–146, 2007.
- [28] M. Moreau, N. Orange and M. G. J. Feuilloye, “Non-thermal plasma technologies: New tools for bio-decontamination”, *Biotechnol Adv*, vol. 26, no. 6, pp. 610–617, 2008.
- [29] M. Laroussi, “Nonthermal decontamination of biological media by atmospheric-pressure plasmas: review, analysis and prospects”, *IEEE Trans. Plasma Sci.*, vol. 30, no. 4, pp. 1409–1415, 2002.
- [30] S. P. Kuo, “Plasma assisted decontamination of bacterial spores”, *Open Biomed Eng J*, vol. 2, pp. 36–42, 2008.
- [31] A. E. Watts, S. L. Fubini, M. Vernier-Singer, C. Golkowski, S. Shin and R. J. Todhunter, “In vitro analysis of nonthermal plasma as a disinfecting agent”, *Am J Vet Res*, vol. 67, no. 12, pp. 2030–2035, 2006.

-
- [32] M. L. Burts, I. Alexeff, E. T. Meek and J. A. McCullers, “Use of atmospheric non-thermal plasma as a disinfectant for objects contaminated with methicillin-resistant *Staphylococcus aureus*”, *Am J Infect Control*, vol. 37, no. 9, pp. 729–733, 2009.
- [33] I. Koban, B. Holtfreter, N.-O. Hübner, R. Matthes, R. Sietmann, E. Kindel, K.-D. Weltmann, A. Welk, A. Kramer and T. Kocher, “Antimicrobial efficacy of non-thermal plasma in comparison to chlorhexidine against dental biofilms on titanium discs in vitro - proof of principle experiment”, *J Clin Periodontol*, vol. 38, no. 10, pp. 956–965, 2011.
- [34] K. Bazaka, M. V. Jacob, R. J. Crawford and E. P. Ivanova, “Plasma-assisted surface modification of organic biopolymers to prevent bacterial attachment”, *Acta Biomater*, vol. 7, no. 5, pp. 2015–2028, 2011.
- [35] R. Morent, N. De Geyter, T. Desmet, P. Dubruel and C. Leys, “Plasma surface modification of biodegradable polymers: a review”, *Plasma Processes Polym*, vol. 8, no. 3, pp. 171–190, 2011.
- [36] R. Förch, A. N. Chifén, A. Bousquet, H. L. Khor, M. Jungblut, L.-Q. Chu, Z. Zhang, I. Osey-Mensah, E.-K. Sinner and W. Knoll, “Recent and Expected Roles of Plasma-Polymerized Films for Biomedical Applications”, *Chem Vapor Depos*, vol. 13, pp. 280–294, 2007.
- [37] P. K. Chu, J. Chen, L. Wang and N. Huang, “Plasma-surface modification of biomaterials”, *Mater Sci Eng R*, vol. 36, no. 5–6, pp. 143–206, 2002.
- [38] G. Daeschlein, T. von Woedtke, E. Kindel, R. Brandenburg, K. Weltmann and M. Jünger, “Antibacterial Activity of an Atmospheric Pressure Plasma Jet Against Relevant Wound Pathogens in vitro on a Simulated Wound Environment”, *Plasma Processes Polym*, vol. 7, no. 3-4, pp. 224–230, 2010.
- [39] S. Kalghatgi, G. Friedman, A. Friedman and A. M. Clyne, “Endothelial cell proliferation is enhanced by low dose non-thermal plasma through fibroblast growth factor-2 release”, *Ann Biomed Eng*, vol. 38, no. 3, pp. 748–757, 2010.
- [40] C.-H. Kim, J. H. Bahn, S.-H. Lee, G.-Y. Kim, S.-I. Jun, K. Lee and S. J. Baek, “Induction of cell growth arrest by atmospheric non-thermal plasma in colorectal cancer cells”, *J Biotechnol*, vol. 150, no. 4, pp. 530–538, 2010.
- [41] S. Kalghatgi, C. M. Kelly, E. Cerchar, B. Torabi, O. Alekseev, A. Friedman, G. Friedman and J. Azizkhan-Clifford, “Effects of non-thermal plasma on Mammalian cells”, *PLoS ONE*, vol. 6, no. 1, p. e16270, 2011.

- [42] M. Laroussi and F. Leipold, “Evaluation of the roles of reactive species, heat, and UV radiation in the inactivation of bacterial cells by air plasmas at atmospheric pressure”, *Int J Mass Spectrom*, vol. 233, no. 1–3, pp. 81–86, 2004.
- [43] S. Ptasińska, B. Bahnev, A. Stypczyńska, M. Bowden, N. J. Mason and N. S. J. Braithwaite, “DNA strand scission induced by a non-thermal atmospheric pressure plasma jet”, *Phys Chem Chem Phys*, vol. 12, no. 28, pp. 7779–7781, 2010.
- [44] K. P. Arjunan, G. Friedman, A. Fridman and A. M. Clyne, “Non-thermal dielectric barrier discharge plasma induces angiogenesis through reactive oxygen species”, *J R Soc Interface*, vol. 9, no. 66, pp. 147–157, 2012.
- [45] P. W. Hellings and J. L. Ceuppens, “Mouse models of global airway allergy: what have we learned and what should we do next?”, *Allergy*, vol. 59, no. 9, pp. 914–919, 2004.
- [46] G. W. Tannock, “More than a smell: the complexity of the normal microflora”, in *Normal microflora: an introduction to microbes inhabiting the human body*, Chapman & Hall, 1995, pp. 3–35.
- [47] D. V. Lim, “Infectious diseases”, in *Microbiology*, WBC/McGraw-Hill, 1998, pp. 449–526.
- [48] P. Marsh, M. V. Martin and M. A. O. Lewis, “The resident oral microflora and orofacial bacterial infections”, in *Oral microbiology*, Churchill-Livingston (Elsevier), 2009, pp. 24–45; 146–160.
- [49] H. Schöfer, N. Brockmeyer, J. Dissemond, I. Effendy, S. Esser, H. K. Geiss, S. Harder, M. Hartmann, U. Jappe, A. Plettenberg, H. Reimann, P. Shah, E. Tschachler and T. A. Wichelhaus, “Staphylococcal infections of the skin and mucous membranes. Guideline of the German Dermatologic Society, Study Group of Dermatologic Infectiology”, *J Dtsch Dermatol Ges*, vol. 3, no. 9, pp. 726–734, 2005.
- [50] E. Tschachler, N. Brockmeyer, I. Effendy, H. K. Geiss, S. Harder, M. Hartmann, U. Jappe, A. Plettenberg, H. Rasokat, H. Reimann, P. Shah, M. Stückler, T. A. Wichelhaus and H. Schöfer, “Streptococcal infections of the skin and mucous membranes”, *J Dtsch Dermatol Ges*, vol. 5, no. 6, pp. 527–532, 2007.
- [51] C. Roth, A. G. Beule, A. Kramer, W. Hosemann, T. Kohlmann and C. Scharf, “Response analysis of stimulating efficacy of polihexanide in an in vitro wound model with respiratory ciliary epithelial cells”, *Skin Pharmacol Physiol*, vol. 23 Suppl, pp. 35–40, 2010.

-
- [52] J. Dissemond, V. Gerber, A. Kramer, G. Riepe, R. Strohal, A. Vasel-Biergans and T. Eberlein, “A practice-oriented recommendation for treatment of critically colonised and locally infected wounds using polihexanide”, *J Tissue Viability*, vol. 19, no. 3, pp. 106–115, 2010.
- [53] T. Winter, J. Winter, M. Polak, K. Kusch, U. Mäder, R. Sietmann, J. Ehlbeck, S. van Hijum, K.-D. Weltmann, M. Hecker and H. Kusch, “Characterization of the global impact of low temperature gas plasma on vegetative microorganisms”, *Proteomics*, vol. 11, no. 17, pp. 3518–3530, 2011.
- [54] R. Westermeier, T. Naven and H.-R. Höpker, “Proteomics Technology and Mass Spectrometry”, in *Proteomics in Practice: A Guide to Successful Experimental Design*, Second, Completely Revised ed., Wiley-VCH Verlag GmbH & Co. KGaA, 2008, pp. 19–150; 215–272.
- [55] D. B. Friedman, S. Hoving and R. Westermeier, “Isoelectric focusing and two-dimensional gel electrophoresis”, *Meth Enzymol*, vol. 463, pp. 515–540, 2009.
- [56] H. Junker, S. Venz, U. Zimmermann, A. Thiele, C. Scharf and R. Walther, “Stage-related alterations in renal cell carcinoma--comprehensive quantitative analysis by 2D-DIGE and protein network analysis”, *PLoS ONE*, vol. 6, no. 7, p. e21867, 2011.
- [57] A. Farajzadeh Deroee, J. Oweinah, M. Naraghi, W. Hosemann, B. Athari, U. Völker and C. Scharf, “Regression of polypoid nasal mucosa after systemic corticosteroid therapy: a proteomics study”, *Am J Rhinol Allergy*, vol. 23, no. 5, pp. 480–485, 2009.
- [58] T. R. Flotte, S. A. Afione, R. Solow, M. L. Drumm, D. Markakis, W. B. Guggino, P. L. Zeitlin and B. J. Carter, “Expression of the cystic fibrosis transmembrane conductance regulator from a novel adeno-associated virus promoter”, *J Biol Chem*, vol. 268, no. 5, pp. 3781–3790, 1993.
- [59] P. L. Zeitlin, L. Lu, J. Rhim, G. Cutting, G. Stetten, K. A. Kieffer, R. Craig and W. B. Guggino, “A cystic fibrosis bronchial epithelial cell line: immortalization by adeno-12-SV40 infection”, *Am J Respir Cell Mol Biol*, vol. 4, no. 4, pp. 313–319, 1991.
- [60] A. G. Beule, T. Athanasiadis, J. Field, W. Hosemann, P.-J. Wormald and L. W. Tan, “Effects of simulated bleeding in an in vitro nasal fibroblast wound healing model”, *Am J Rhinol Allergy*, vol. 24, no. 3, pp. 186–191, 2010.
- [61] K. Landsberg, C. Scharf, K. Darm, K. Wende, G. Daeschlein, E. Kindel, K.-D. Weltmann and T. von Woedtke, “Use of Proteomics to Investigate Plasma-Cell Interactions”, *Plasma Med*, vol. 1, no. 1, pp. 55–63, 2011.

- [62] M. M. Bradford, “A rapid and sensitive method for the quantitation of microgram quantities of protein utilizing the principle of protein-dye binding”, *Anal Biochem*, vol. 72, pp. 248–254, 1976.
- [63] T. Thiele, L. Steil, S. Gebhard, C. Scharf, E. Hammer, M. Brigulla, N. Lubenow, K. J. Clemetson, U. Völker and A. Greinacher, “Profiling of alterations in platelet proteins during storage of platelet concentrates”, *Transfusion*, vol. 47, no. 7, pp. 1221–1233, 2007.
- [64] S. Luhn, M. Berth, M. Hecker and J. Bernhardt, “Using standard positions and image fusion to create proteome maps from collections of two-dimensional gel electrophoresis images”, *Proteomics*, vol. 3, no. 7, pp. 1117–1127, 2003.
- [65] C. Eymann, A. Dreisbach, D. Albrecht, J. Bernhardt, D. Becher, S. Gentner, L. T. Tam, K. Büttner, G. Buurman, C. Scharf, S. Venz, U. Völker and M. Hecker, “A comprehensive proteome map of growing *Bacillus subtilis* cells”, *Proteomics*, vol. 4, no. 10, pp. 2849–2876, 2004.
- [66] P. D. Thomas, “PANTHER: a browsable database of gene products organized by biological function, using curated protein family and subfamily classification”, *Nucleic Acids Res*, vol. 31, pp. 334–341, 2003.
- [67] A. Otto, J. Bernhardt, H. Meyer, M. Schaffer, F.-A. Herbst, J. Siebourg, U. Mäder, M. Lalk, M. Hecker and D. Becher, “Systems-wide temporal proteomic profiling in glucose-starved *Bacillus subtilis*”, *Nat Commun*, vol. 1, p. 137, 2010.
- [68] M. Berth, F. M. Moser, M. Kolbe and J. Bernhardt, “The state of the art in the analysis of two-dimensional gel electrophoresis images”, *Appl Microbiol Biotechnol*, vol. 76, no. 6, pp. 1223–1243, 2007.
- [69] L. Michalik, B. Desvergne, N. S. Tan, S. Basu-Modak, P. Escher, J. Rieusset, J. M. Peters, G. Kaya, F. J. Gonzalez, J. Zakany, D. Metzger, P. Chambon, D. Duboule and W. Wahli, “Impaired skin wound healing in peroxisome proliferator-activated receptor (PPAR)alpha and (PPAR)beta mutant mice”, *J Cell Biol*, vol. 154, no. 4, pp. 799–814, 2001.
- [70] J. Bernhardt, S. Funke, M. Hecker and J. Siebourg, “Visualizing Gene Expression Data via Voronoi Treemaps”, in *IEEE*, 2009, pp. 233–241.
- [71] T. M. Stępkowski and M. K. Kruszewski, “Molecular cross-talk between the NRF2/KEAP1 signaling pathway, autophagy, and apoptosis”, *Free Radical Bio Med*, vol. 50, no. 9, pp. 1186–1195, 2011.

-
- [72] K. Taguchi, H. Motohashi and M. Yamamoto, “Molecular mechanisms of the Keap1-Nrf2 pathway in stress response and cancer evolution”, *Genes Cells*, vol. 16, no. 2, pp. 123–140, 2011.
- [73] L. Baird and A. T. Dinkova-Kostova, “The cytoprotective role of the Keap1-Nrf2 pathway”, *Arch Toxicol*, vol. 85, no. 4, pp. 241–272, 2011.
- [74] T. A. Beyer, U. Auf dem Keller, S. Braun, M. Schäfer and S. Werner, “Roles and mechanisms of action of the Nrf2 transcription factor in skin morphogenesis, wound repair and skin cancer”, *Cell Death Differ*, vol. 14, no. 7, pp. 1250–1254, 2007.
- [75] S. Braun, C. Hanselmann, M. G. Gassmann, U. auf dem Keller, C. Born-Berclaz, K. Chan, Y. W. Kan and S. Werner, “Nrf2 transcription factor, a novel target of keratinocyte growth factor action which regulates gene expression and inflammation in the healing skin wound”, *Mol Cell Biol*, vol. 22, no. 15, pp. 5492–5505, 2002.
- [76] C. J. Harvey, R. K. Thimmulappa, A. Singh, D. J. Blake, G. Ling, N. Wakabayashi, J. Fujii, A. Myers and S. Biswal, “Nrf2-regulated glutathione recycling independent of biosynthesis is critical for cell survival during oxidative stress”, *Free Radical Bio Med*, vol. 46, no. 4, pp. 443–453, 2009.
- [77] S. F. Leiser and R. A. Miller, “Nrf2 Signaling, a Mechanism for Cellular Stress Resistance in Long-Lived Mice”, *Mol Cell Biol*, vol. 30, no. 3, pp. 871–884, 2009.
- [78] K. N. Lewis, J. Mele, J. D. Hayes and R. Buffenstein, “Nrf2, a Guardian of Healthspan and Gatekeeper of Species Longevity”, *Integr Comp Biol*, vol. 50, no. 5, pp. 829–843, 2010.
- [79] J. Maher and M. Yamamoto, “The rise of antioxidant signaling—the evolution and hormetic actions of Nrf2”, *Toxicol Appl Pharmacol*, vol. 244, no. 1, pp. 4–15, 2010.
- [80] L. Marrot, C. Jones, P. Perez and J.-R. Meunier, “The significance of Nrf2 pathway in (photo)-oxidative stress response in melanocytes and keratinocytes of the human epidermis”, *Pigm Cell Res*, vol. 21, no. 1, pp. 79–88, 2007.
- [81] K. Y. Arai, M. Ono, C. Kudo, A. Fujioka, R. Okamura, Y. Nomura and T. Nishiyama, “IL-1 β stimulates activin betaA mRNA expression in human skin fibroblasts through the MAPK pathways, the nuclear factor-kappaB pathway, and prostaglandin E2”, *Endocrinology*, vol. 152, no. 10, pp. 3779–3790, 2011.

- [82] A. M. Küchler, J. Pollheimer, J. Balogh, J. Sponheim, L. Manley, D. R. Sorensen, P. M. De Angelis, H. Scott, and G. Haraldsen, “Nuclear interleukin-33 is generally expressed in resting endothelium but rapidly lost upon angiogenic or proinflammatory activation”, *Am J Pathol*, vol. 173, no. 4, pp. 1229–1242, 2008.
- [83] A. M. Miller, “Role of IL-33 in inflammation and disease”, *J Inflamm*, vol. 8, p. 22, 2011.
- [84] P. Kunes, Z. Holubcová, M. Kolácková and J. Krejsek, “The counter-regulation of atherogenesis: a role for interleukin-33”, *Acta Medica (Hradec Kralove)*, vol. 53, no. 3, pp. 125–129, 2010.
- [85] S. Ali, A. Mohs, M. Thomas, J. Klare, R. Ross, M. L. Schmitz and M. U. Martin, “The dual function cytokine IL-33 interacts with the transcription factor NF-κB to dampen NF-κB-stimulated gene transcription”, *J Immunol*, vol. 187, no. 4, pp. 1609–1616, 2011.
- [86] V. L. Rozlomiy and A. G. Markov, “Effect of interleukin-1 β on the expression of tight junction proteins in the culture of HaCaT keratinocytes”, *Bull Exp Biol Med*, vol. 149, no. 3, pp. 280–283, 2010.
- [87] L. D. Church, G. P. Cook and M. F. McDermott, “Primer: inflammasomes and interleukin 1 β in inflammatory disorders”, *Nat Clin Pract Rheumatol*, vol. 4, pp. 34–42, 2008.
- [88] A. K. Deodhar and R. E. Rana, “Surgical physiology of wound healing: a review”, *J Postgrad Med*, vol. 43, no. 2, pp. 52–56, 1997.
- [89] K. S. Midwood, L. V. Williams and J. E. Schwarzauer, “Tissue repair and the dynamics of the extracellular matrix”, *Int J Biochem Cell Biol*, vol. 36, no. 6, pp. 1031–1037, 2004.
- [90] M. M. Santoro and G. Gaudino, “Cellular and molecular facets of keratinocyte reepithelialization during wound healing”, *Exp Cell Res*, vol. 304, no. 1, pp. 274–286, 2005.
- [91] M. B. Witte and A. Barbul, “Role of nitric oxide in wound repair”, *Am J Surg*, vol. 183, no. 4, pp. 406–412, 2002.
- [92] A. V. Pipa, T. Bindemann, R. Foest, E. Kindel, J. Röpcke and K.-D. Weltmann, “Absolute production rate measurements of nitric oxide by an atmospheric pressure plasma jet (APPJ)”, *J Phys D Appl Phys*, vol. 41, no. 19, p. 194011, 2008.
- [93] A. V. Pipa, S. Reuter, R. Foest and K.-D. Weltmann, “Controlling the NO production of an atmospheric pressure plasma jet”, *J Phys D Appl Phys*, vol. 45, no. 8, p. 085201, 2012.

-
- [94] R. A. Clark, “Basics of cutaneous wound repair”, *J Dermatol Surg Oncol*, vol. 19, no. 8, pp. 693–706, 1993.
 - [95] C. C. Johnstone and A. Farley, “The physiological basics of wound healing”, *Nurs Stand*, vol. 19, no. 43, pp. 59–65, 2005.
 - [96] M. Rojkind, J.-A. Domínguez-Rosales, N. Nieto and P. Greenwel, “Role of hydrogen peroxide and oxidative stress in healing responses”, *Cell Mol Life Sci*, vol. 59, no. 11, pp. 1872–1891, 2002.
 - [97] S. Schreml, M. Landthaler, M. Schäferling and P. Babilas, “A new star on the H₂O₂rizon of wound healing?”, *Exp Dermatol*, vol. 20, no. 3, pp. 229–231, 2011.
 - [98] A. Soneja, M. Drews and T. Malinski, “Role of nitric oxide, nitrooxidative and oxidative stress in wound healing”, *Pharmacol Rep*, vol. 57 Suppl, pp. 108–119, 2005.
 - [99] J. Kim, Y.-N. Cha and Y.-J. Surh, “A protective role of nuclear factor-erythroid 2-related factor-2 (Nrf2) in inflammatory disorders”, *Mutat Res-Fund Mol M*, vol. 690, no. 1–2, pp. 12–23, 2010.
 - [100] H. Motohashi and M. Yamamoto, “Nrf2–Keap1 defines a physiologically important stress response mechanism”, *Trends Mol Med*, vol. 10, no. 11, pp. 549–557, 2004.
 - [101] U. auf dem Keller, M. Huber, T. A. Beyer, A. Kümin, C. Siemes, S. Braun, P. Bugnon, V. Mitropoulos, D. A. Johnson, J. A. Johnson, D. Hohl and S. Werner, “Nrf transcription factors in keratinocytes are essential for skin tumor prevention but not for wound healing”, *Mol Cell Biol*, vol. 26, no. 10, pp. 3773–3784, 2006.
 - [102] T. A. Beyer, U. auf dem Keller, S. Braun, M. Schafer and S. Werner, “Roles and mechanisms of action of the Nrf2 transcription factor in skin morphogenesis, wound repair and skin cancer”, *Cell Death Differ*, vol. 14, no. 7, pp. 1250–1254, 2007.
 - [103] C. M. Bergamini, S. Gambetti, A. Dondi and C. Cervellati, “Oxygen, Reactive Oxygen Species and Tissue Damage”, *Curr Pharm Des*, vol. 10, no. 14, pp. 1611–1626, 2004.
 - [104] S. Toyokuni, “Reactive oxygen species-induced molecular damage and its application in pathology”, *Pathol Int*, vol. 49, no. 2, pp. 91–102, 1999.
 - [105] T. Nosenko, T. Shimizu and G. E. Morfill, “Designing plasmas for chronic wound disinfection”, *New J Phys*, vol. 11, p. 115013, 2009.

- [106] G. Isbary, G. Morfill, H. U. Schmidt, M. Georgi, K. Ramrath, J. Heinlin, S. Karrer, M. Landthaler, T. Shimizu, B. Steffes, W. Bunk, R. Monetti, J. L. Zimmermann, R. Pompl and W. Stolz, “A first prospective randomized controlled trial to decrease bacterial load using cold atmospheric argon plasma on chronic wounds in patients”, *Brit J Dermatol*, vol. 163, no. 1, pp. 78–82, 2010.
- [107] P. Moi, “Isolation of NF-E2-Related Factor 2 (Nrf2), a NF-E2-Like Basic Leucine Zipper Transcriptional Activator that Binds to the Tandem NF-E2/AP1 Repeat of the beta-Globin Locus Control Region”, *P Nat Acad Sci*, vol. 91, no. 21, pp. 9926–9930, 1994.
- [108] A. Kobayashi, M.-I. Kang, H. Okawa, M. Ohtsuji, Y. Zenke, T. Chiba, K. Igarashi and M. Yamamoto, “Oxidative Stress Sensor Keap1 Functions as an Adaptor for Cul3-Based E3 Ligase To Regulate Proteasomal Degradation of Nrf2”, *Mol Cell Biol*, vol. 24, no. 16, pp. 7130–7139, 2004.
- [109] A. Giudice, C. Arra and M. C. Turco, “Review of molecular mechanisms involved in the activation of the Nrf2-ARE signaling pathway by chemopreventive agents”, *Methods Mol Biol*, vol. 647, pp. 37–74, 2010.
- [110] K. R. Sekhar, G. Rachakonda and M. L. Freeman, “Cysteine-based regulation of the CUL3 adaptor protein Keap1”, *Toxicol Appl Pharmacol*, vol. 244, no. 1, pp. 21–26, 2010.
- [111] T. Yamamoto, T. Suzuki, A. Kobayashi, J. Wakabayashi, J. Maher, H. Motohashi and M. Yamamoto, “Physiological significance of reactive cysteine residues of Keap1 in determining Nrf2 activity”, *Mol Cell Biol*, vol. 28, no. 8, pp. 2758–2770, 2008.
- [112] K. Itoh, T. Chiba, S. Takahashi, T. Ishii, K. Igarashi, Y. Katoh, T. Oyake, N. Hayashi, K. Satoh, I. Hatayama, M. Yamamoto and Y. Nabeshima, “An Nrf2/small Maf heterodimer mediates the induction of phase II detoxifying enzyme genes through antioxidant response elements”, *Biochem Biophys Res Commun*, vol. 236, no. 2, pp. 313–322, 1997.
- [113] N. C. Macgarvey, H. B. Suliman, R. R. Bartz, P. Fu, C. M. Withers, K. E. Welty-Wolf and C. A. Piantadosi, “Activation of Mitochondrial Biogenesis by HO-1-mediated Nrf2 Induction Rescues Mice from Lethal *S. Aureus* Sepsis”, *Am J Resp Crit Care*, p. Epub ahead of print PubMed-ID: 22312014, 2012.
- [114] M. Koháryová and M. Kolárová, “Oxidative stress and thioredoxin system”, *Gen Physiol Biophys*, vol. 27, no. 2, pp. 71–84, 2008.
- [115] A. Bokov, A. Chaudhuri and A. Richardson, “The role of oxidative damage and stress in aging”, *Mech Ageing Dev*, vol. 125, no. 10–11, pp. 811–826, 2004.

-
- [116] N. Wakabayashi, S. Shin, S. L. Slocum, E. S. Agoston, J. Wakabayashi, M.-K. Kwak, V. Misra, S. Biswal, M. Yamamoto and T. W. Kensler, “Regulation of Notch1 signaling by Nrf2: implications for tissue regeneration”, *Sci Signal*, vol. 3, no. 130, p. ra52, 2010.
 - [117] S. Homma, Y. Ishii, Y. Morishima, T. Yamadori, Y. Matsuno, N. Haraguchi, N. Kikuchi, H. Satoh, T. Sakamoto, N. Hizawa, K. Itoh and M. Yamamoto, “Nrf2 Enhances Cell Proliferation and Resistance to Anticancer Drugs in Human Lung Cancer”, *Clin Cancer Res*, vol. 15, no. 10, pp. 3423–3432, 2009.
 - [118] C. Bachert, N. Zhang, G. Holtappels, L. De Lobel, P. van Cauwenberge, S. Liu, P. Lin, J. Bousquet and K. Van Steen, “Presence of IL-5 protein and IgE antibodies to staphylococcal enterotoxins in nasal polyps is associated with comorbid asthma”, *J Allergy Clin Immunol*, vol. 126, no. 5, pp. 962–968, 968.e1–6, 2010.
 - [119] C. Bachert, S. E. M. Claeys, P. Tomassen, T. van Zele and N. Zhang, “Rhinosinusitis and asthma: a link for asthma severity”, *Curr Allergy Asthma Rep*, vol. 10, no. 3, pp. 194–201, 2010.
 - [120] B. Haertel, F. Volkmann, T. von Woedtke and U. Lindequist, “Differential sensitivity of lymphocyte subpopulations to non-thermal atmospheric-pressure plasma”, *Immunobiology*, p. Epub ahead of print, PubMed-ID: 22130036, 2011.

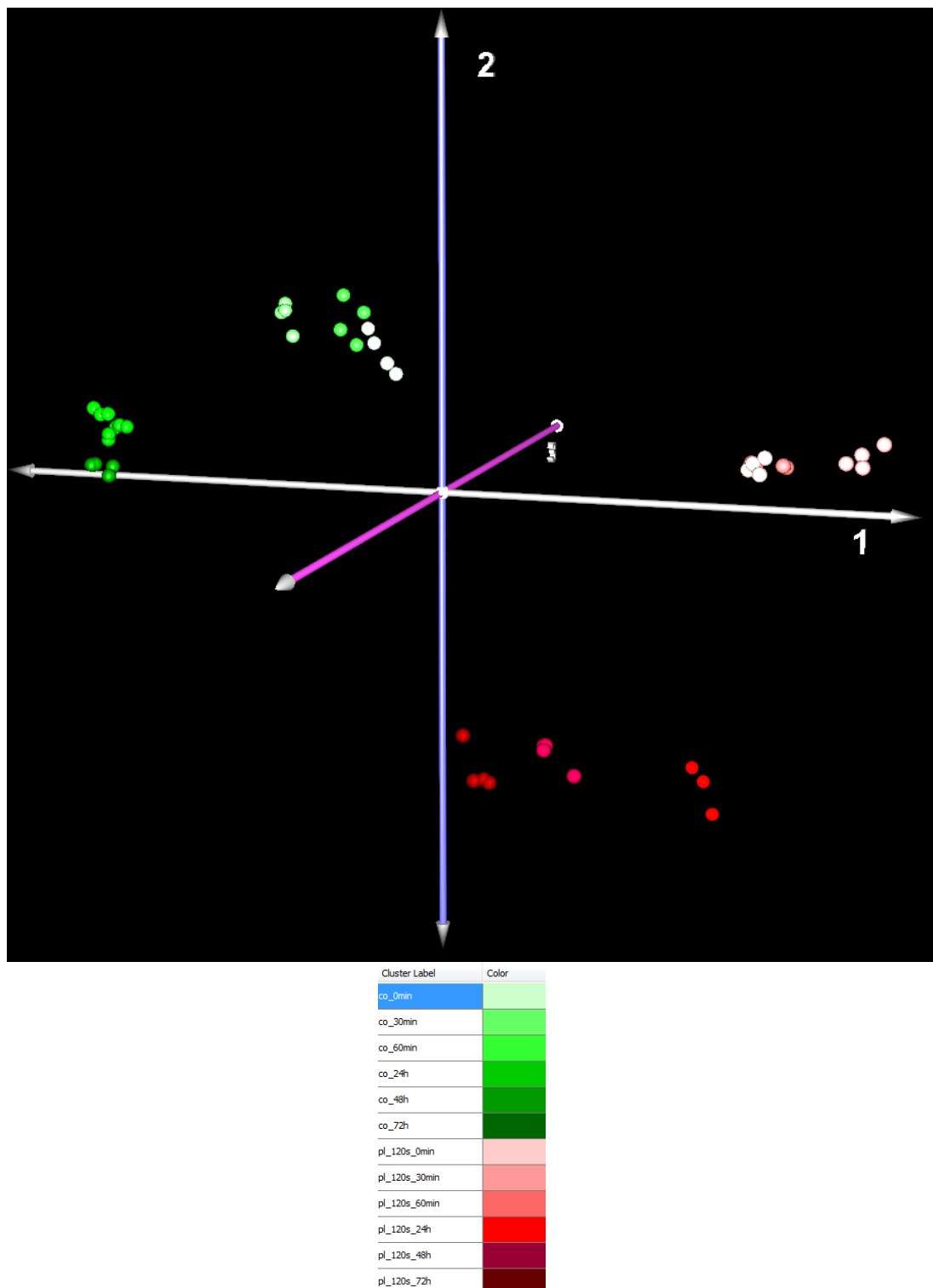
11. Appendix

Supplemental material	ii
1. Figure S-1	ii
2. Figure S-2	iv
3. Figure S-3	viii
4. Figure S-4 (see DVD).....	xxiv
5. Table S-1.....	xxv
6. Table S-2.....	lviii
7. Movie S-1 (see DVD)	lx
8. Movie S-2 (see DVD)	lxi
Danksagung.....	lxiii

Supplemental material

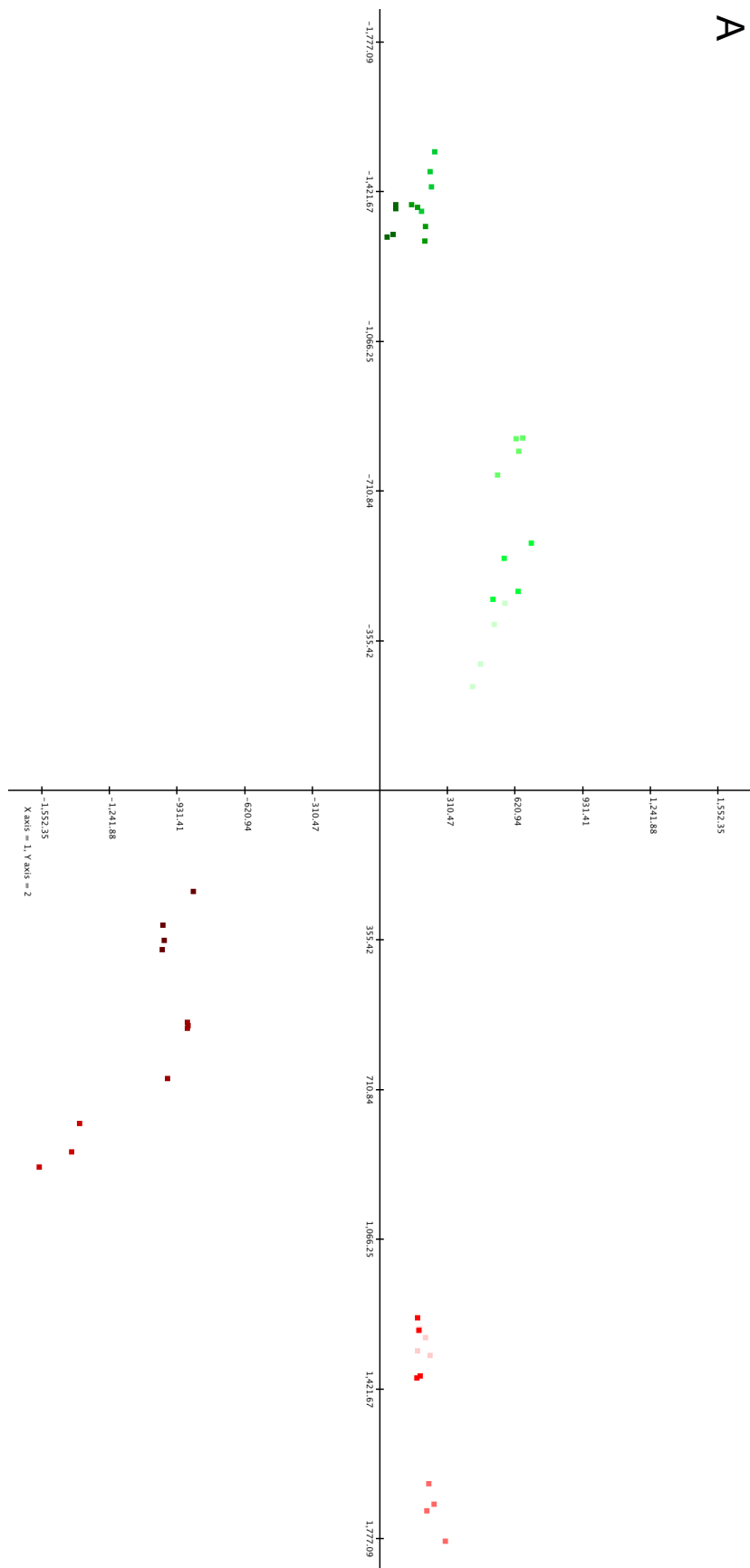
1. Figure S-1

Three-dimensional Principal Component Analysis. 3D-plot of the first three principal components of Principal Component Analysis (PCA) from the protein expression data separates all analysed samples. Each dot represents one sample with its technical replicates. Controls are coloured green, ENTplas treated samples are coloured red. Lightest shaded dots represent samples analysed immediately after treatment (0 h). The darker the dots become, the later the samples were analysed (0.5 h up to 72 h). Differential expression between untreated controls and ENTplas treated samples and between short-time and long-time effects were interesting for interpretation. The resulting model indicates a general effect of ENTplas treatment to the cells at each analysed time point. Furthermore, differences between short-time and long-time incubation can be observed.

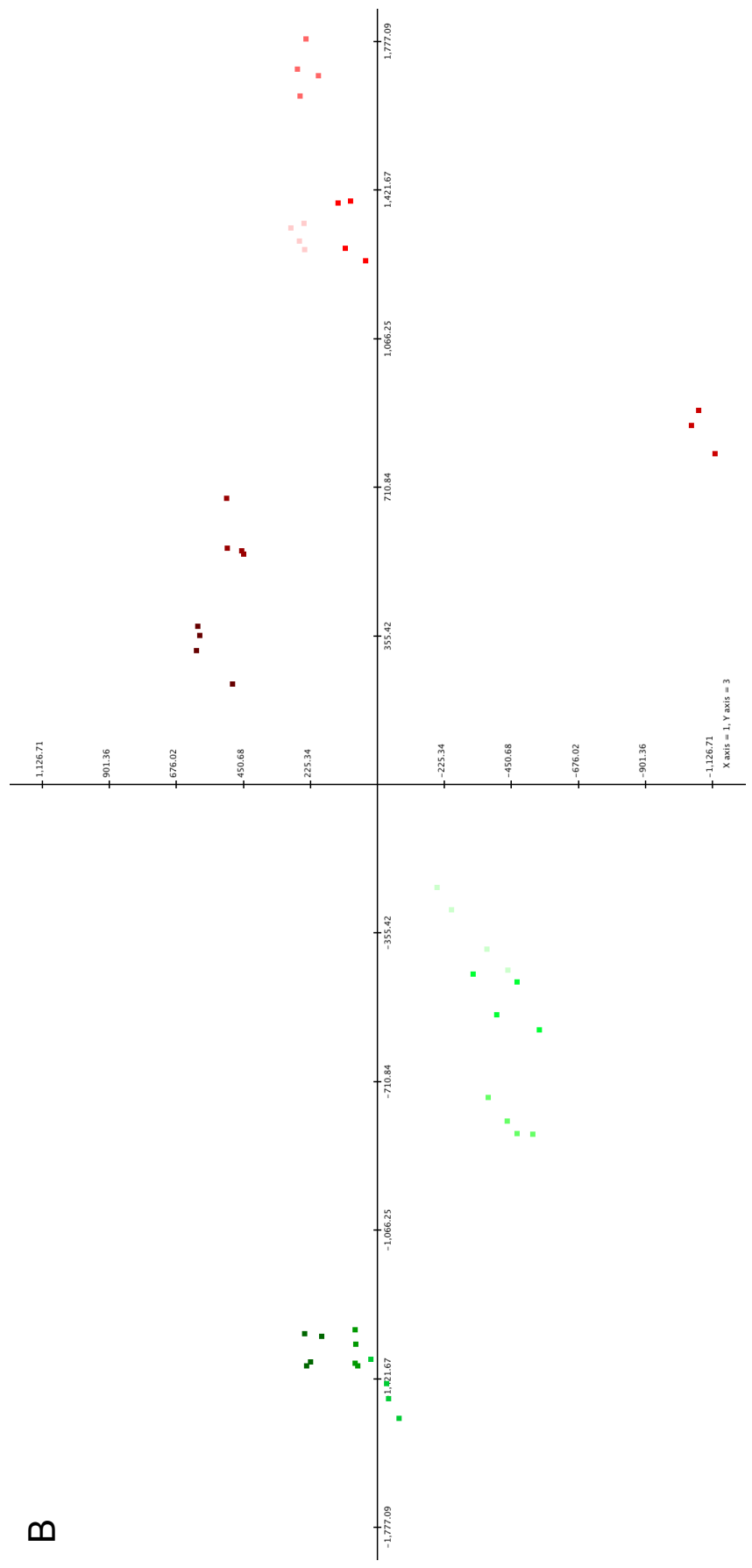


2. Figure S-2

Two-dimensional plotting of the first three principal components of PCA. 2D-plots of the first three principal components of PCA from the protein expression data separate all analysed samples. Values conform to these, from **Figure 13**. Due to three-dimensional model pictured two-dimensionally, all three possibilities in comparison were displayed separately. **(A)** Shows the comparison between the first (x-axis) and the second (y-axis) principal component. **(B)** Comparison between the first (x-axis) and the third (y-axis) principal component and **(C)** second (x-axis) and third (y-axis) component compared. Separation between controls and ENTplas-treated samples and separation between short-time and long-time observation are detectable.

A**V**

B

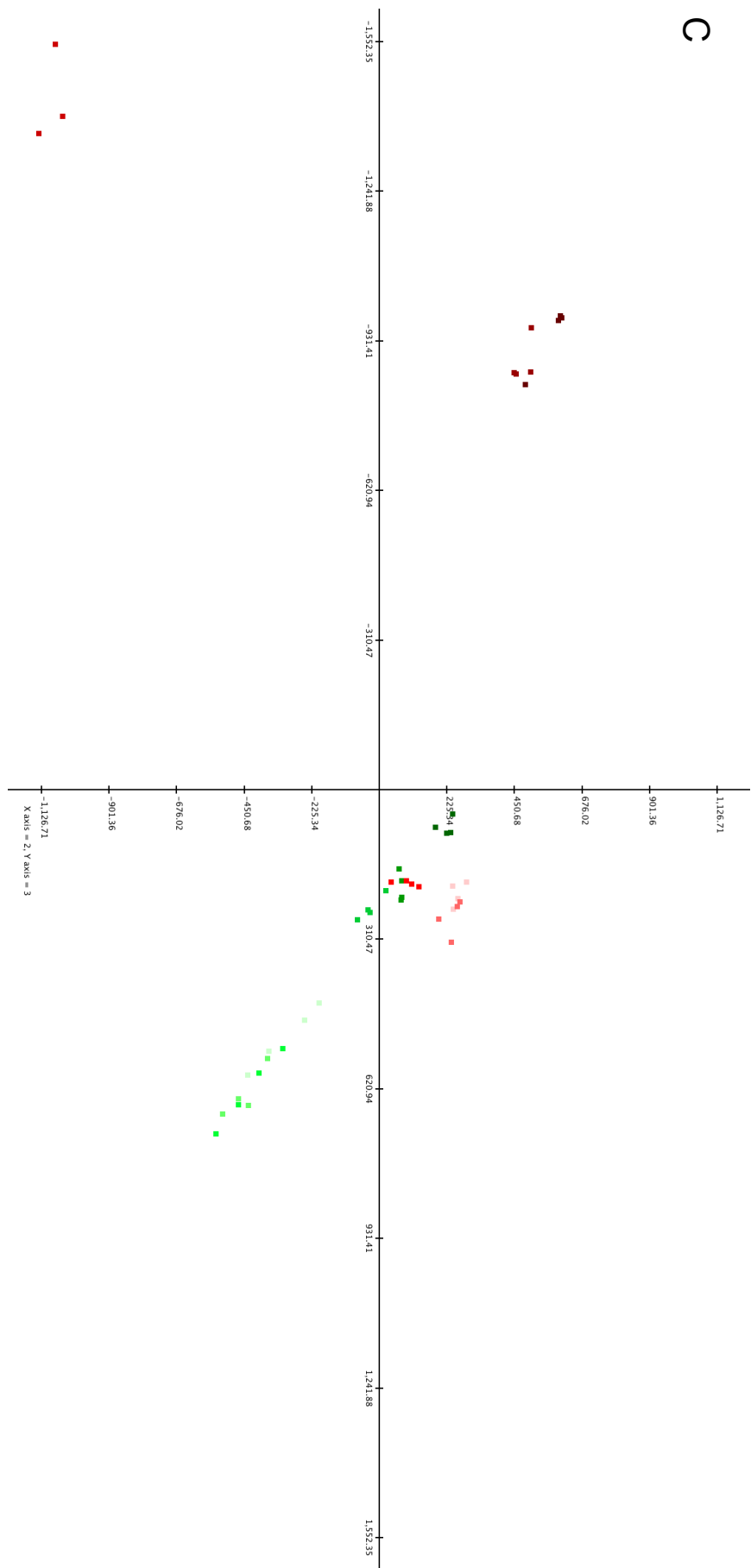


X=1st principal component
Y=3rd principal component

vi

C

X=2nd principal component
Y=3rd principal component



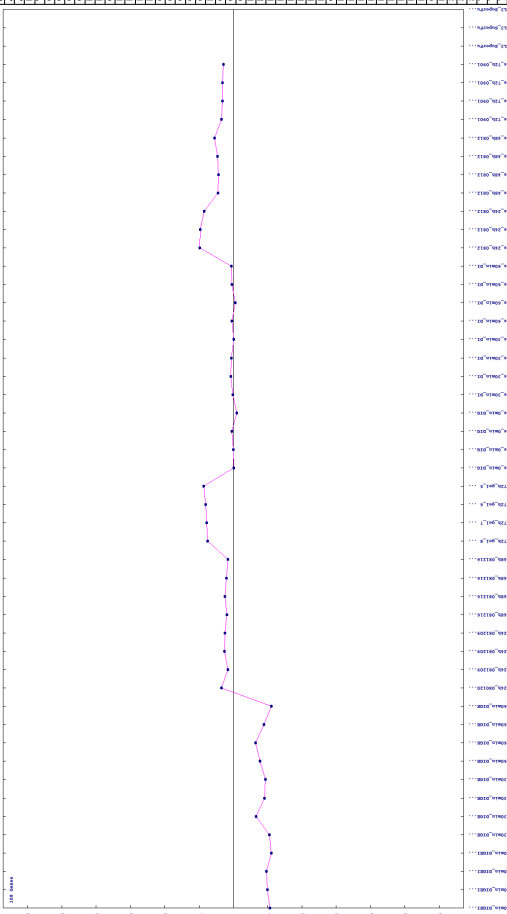
3. Figure S-3

Merged results from K-means Clustering and Ingenuity Pathway Analysis. Summary of clusters from K-means-clustering with resulting expression-profiles from all analysed spots are combined with the corresponding results from subsequent network analyses using IPA and the table of K-means cluster assorted proteins: ten different K-means clusters were computed by TMeV. Expression profiles from all 1505 protein spots were compared with these given clusters and spots were subsequently assorted to the best fitting computed expression profile cluster. The x-axis shows different quadruples of samples (including technical replicates – indicated by subscript numbers). From the left to middle, controls are plotted in ascending incubation time from 0 h to 72 h. From the middle to the right, ENTplas-treated samples are plotted in ascending incubation time from 0 h to 72 h. On the y-axis, the expression-rate is displayed. The horizontal line marks value '0'. Values above that line show higher expression, values below that line lower expression, respectively. In addition, summary results from network-analysis using Ingenuity Pathway Analysis (IPA) are displayed. Spot-lists of identified proteins from the K-means clustering were analysed separately for each cluster. Direct and indirect relationships were considered. Resulting networks, molecular and cellular functions, as well as top tox lists are displayed. Corresponding spot-lists are displayed separately. Protein names and information were appended via Ingenuity Pathway Analysis-software package, whereas proteins, resulting in multiple spots on the 2D-PAGE, are noted with a "D". This overview combines statistical results with their corresponding biological relevance.

Cluster 1

Total 162 spots, 92 proteins identified out of 59 spots

Cluster 2



Molecular and Cellular Functions		pvvalue/Molecules	Top Tok Lists
1.	Post-Translational Modification	5.83E-08 – 1.53E-02 / 10	1.
2.	Protein Folding	5.83E-08 – 1.05E-06 / 6	
3.	Cellular Function and Maintenance	5.91E-05 – 4.91E-02 / 6	2.
4.	Protein Degradation	7.24E-05 – 7.24E-05 / 2	3.
5.	Protein Synthesis	1.88E-04 – 3.08E-02 / 9	

Top Tax Lists	p-valueRatio
Decrease Permeability Transition of Mitochondria and Mitochondrial Membrane	1.36e-02 / 1.15 (0.2)
1.	
Hypoxia-Inducible Factor Signaling	1.56e-02 / 2.70 (0.029)
2.	
NFKB-mediated Oxidative Stress Response	1.83e-02 / 3.20 (0.015)
3.	
Increase Bradykinin	2.17e-02 / 1.8 (0.125)
4.	
Liver Necrosis/Cell Death	6.32e-02 / 21.56 (0.13)
5.	

Molecular and Cellular Functions	
	Percentage
1. Post-Translational Modification	5%
2. Protein Folding	1%
3. Cellular Function and Maintenance	5%
4. Protein Degradation	4%
5. Protein Synthesis	7%
	1%

Top Tox List	Molecules	p-valueRatio
	Decrease Permeability	1.36E-02 / 1.5 (0.2)
1.	Formation of Mitochondria and Mitochondrial Membrane	
2.	Hypoxia-inducible Factor Signalling	1.56E-02 / 270 (0.029)
3.	RF2-mediated Oxidative Stress Response	1.83E-02 / 3205 (0.015)
	Increase Cardiacia	2.17E-02 / 1.8 (0.04)
	Increase Cytosol	2.17E-02 / 1.8 (0.04)

	P-value/Ratio
base Permeability on of and trial one	1.36E-02 / 1/5 (2)
p-inducible Signaling Pathways Mediated by Stress	1.56E-02 / 2/70 (0.29)
base Cardiac Function	1.83E-02 / 3/205 (0.15)
base Bradycardia	2.17E-02 / 1/8

area s
nsitid
echo
echo
mbran
oxia
tor S
=2-m
lativ
pon
ease

Top Tax Lists	De Tran Mit Men
	1.
Top Molecules	-08 - -02 / 10
	-08 - -06 / 16
	-05 - -02 / 16
	-05 - -05 / 12
	-04 - -02 / 19
	-03 - -01 / 19

valu
83E
53E
83E
05E
91E
91E
24E
24E
88E
05E

Protein Quality Control and Cellular Functions	
1.	Post-Translational Modification
2.	Protein Folding
3.	Cellular Function and Maintenance
4.	Protein Degradation
5.	Protein Synthesis

Ecu 1 2 3 4 Ecu

Molecule	Score	Functions
Translational	56	Protein Translation, Folding, Function Maintenance
Cytoskeleton	18	F, Cytoskeletal Assembly, Morphology
Cell Cycle		cycle, Cancer.

ork
st-Tr
dific
tein
llula
d Ma
ncer
velo
mor
|| Cy

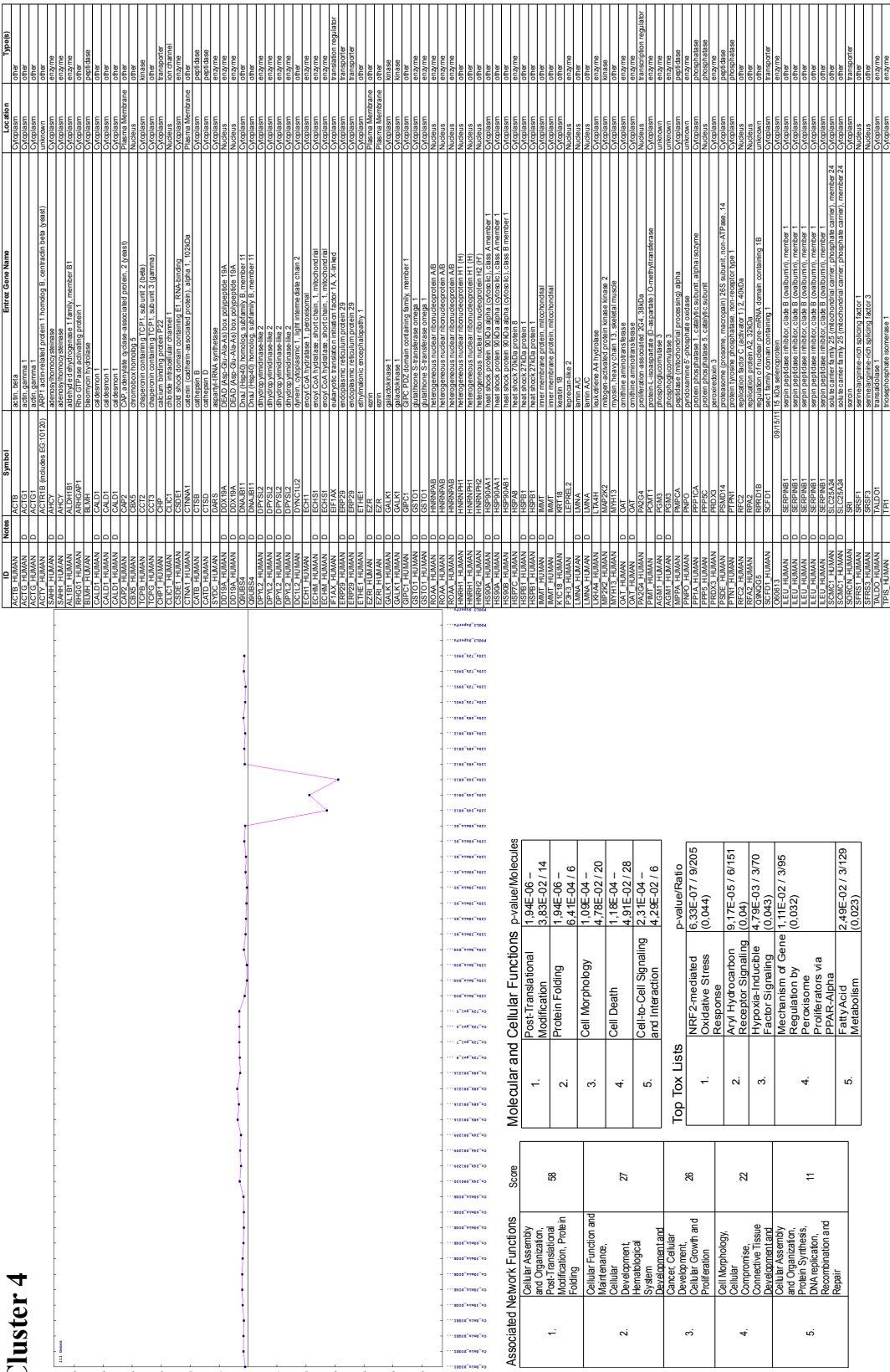
Associated Networks	Po Mc Pre Co an Ca De Tu Ce
	1. 2.

Total 108 genes, 57 proteins identified out of 40 spots

Cluster 3

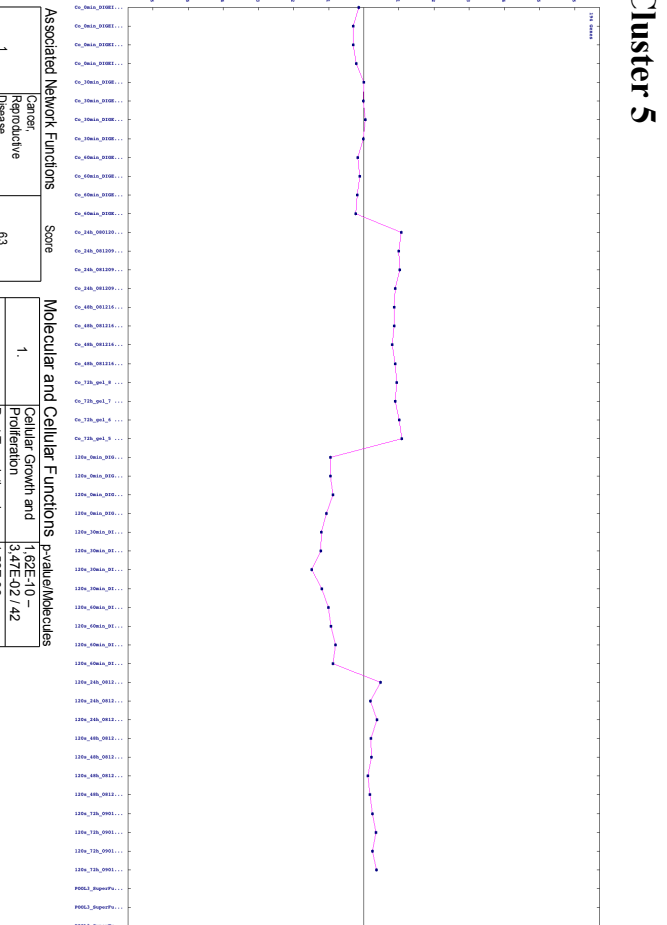
Total 63 genes, 75 proteins identified out of 41 spots

Cluster 4



Total 111 genes, 108 proteins identified out of 61 spots

Cluster 5



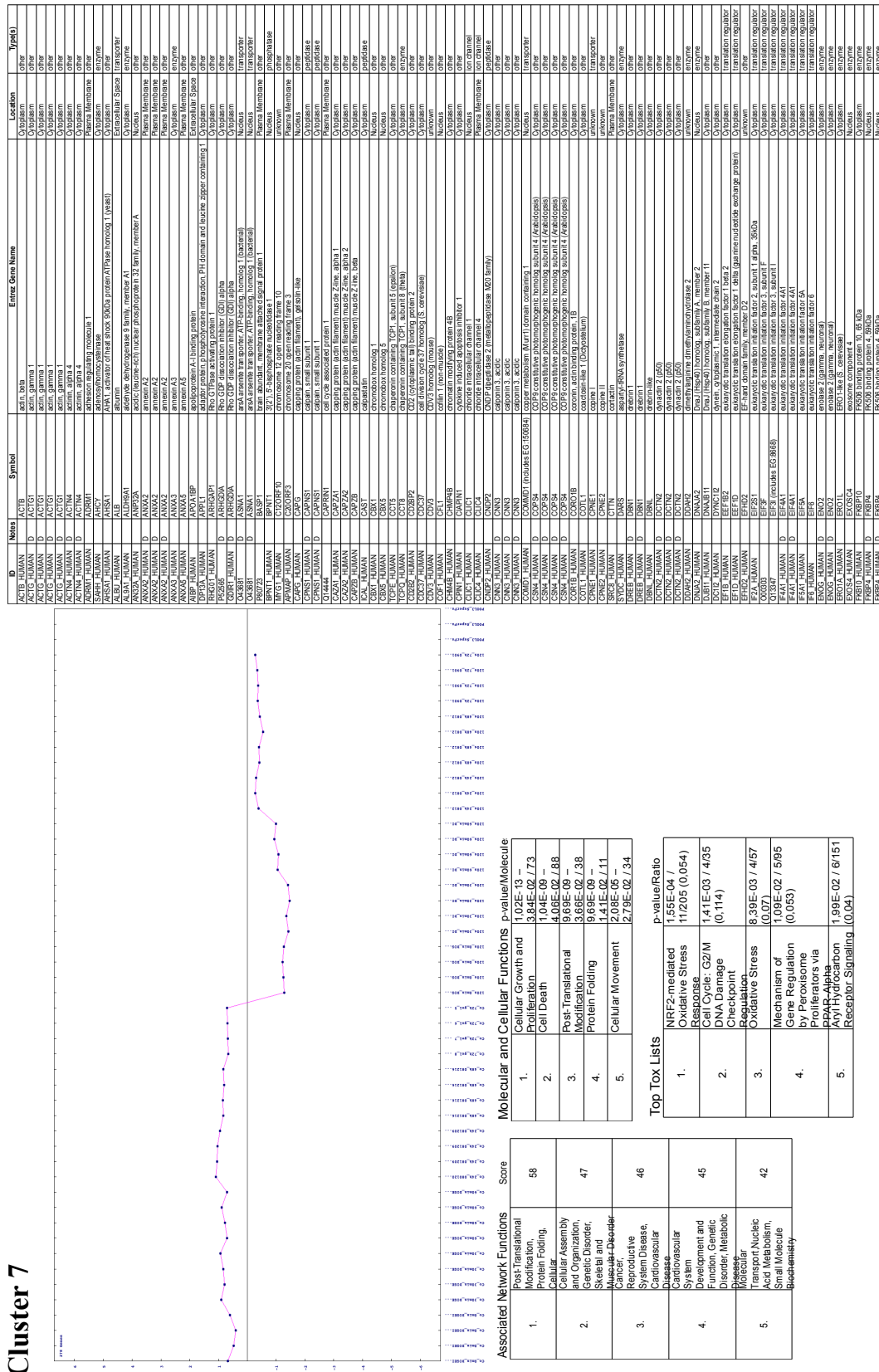
Total 194 genes, 120 proteins identified out of 70 spots

Continued from Cluster 4

Cluster 6

	ID	Name	Symbol	Entrez Gene Name	Location	Type(s)
1.	ACTB_HUMAN	Actin, Tissue Type	ACTB	actin, beta	17q21.31	Cytoskeleton
2.	AKT1_HUMAN	AKT1	AKT1	AKT1, Serine/threonine kinase 1	12q13.11	Cytoskeleton
3.	ANXA2_HUMAN	Anxa2	ANXA2	annexin A2	1q21.3	Chains, Membrane
4.	ATM_HUMAN	Atm	ATM	ataxia telangiectasia mutated protein	11q23.1	Cytoskeleton
5.	CALD_HUMAN	Caldesmon	CALD	caldesmon	Other	
6.	CDX2_HUMAN	Cdx2	CDX2	homeobox protein Cdx-2	12q13.11	Cytoskeleton
7.	CHKA_HUMAN	Chka	CHKA	cholinesterase, alpha 3	12q13.11	Cytoskeleton
8.	CHKB_HUMAN	Chkb	CHKB	cholinesterase, beta	12q13.11	Cytoskeleton
9.	CLSPN_HUMAN	Clspn	CLSPN	clspn	Other	
10.	COL1A1_HUMAN	Col1a1	COL1A1	collagen, type I, alpha 1	17q21.31	Cytoskeleton
11.	COL1A2_HUMAN	Col1a2	COL1A2	collagen, type I, alpha 2	17q21.31	Cytoskeleton
12.	COL5A1_HUMAN	Col5a1	COL5A1	collagen, type V, alpha 1	17q21.31	Cytoskeleton
13.	COL5A2_HUMAN	Col5a2	COL5A2	collagen, type V, alpha 2	17q21.31	Cytoskeleton
14.	COL6A1_HUMAN	Col6a1	COL6A1	collagen, type VI, alpha 1	17q21.31	Cytoskeleton
15.	COL6A2_HUMAN	Col6a2	COL6A2	collagen, type VI, alpha 2	17q21.31	Cytoskeleton
16.	COL6A3_HUMAN	Col6a3	COL6A3	collagen, type VI, alpha 3	17q21.31	Cytoskeleton
17.	COL6A4_HUMAN	Col6a4	COL6A4	collagen, type VI, alpha 4	17q21.31	Cytoskeleton
18.	COL6A5_HUMAN	Col6a5	COL6A5	collagen, type VI, alpha 5	17q21.31	Cytoskeleton
19.	COL6A6_HUMAN	Col6a6	COL6A6	collagen, type VI, alpha 6	17q21.31	Cytoskeleton
20.	COL6A7_HUMAN	Col6a7	COL6A7	collagen, type VI, alpha 7	17q21.31	Cytoskeleton
21.	COL6A8_HUMAN	Col6a8	COL6A8	collagen, type VI, alpha 8	17q21.31	Cytoskeleton
22.	COL6A9_HUMAN	Col6a9	COL6A9	collagen, type VI, alpha 9	17q21.31	Cytoskeleton
23.	COL6A10_HUMAN	Col6a10	COL6A10	collagen, type VI, alpha 10	17q21.31	Cytoskeleton
24.	COL6A11_HUMAN	Col6a11	COL6A11	collagen, type VI, alpha 11	17q21.31	Cytoskeleton
25.	COL6A12_HUMAN	Col6a12	COL6A12	collagen, type VI, alpha 12	17q21.31	Cytoskeleton
26.	COL6A13_HUMAN	Col6a13	COL6A13	collagen, type VI, alpha 13	17q21.31	Cytoskeleton
27.	COL6A14_HUMAN	Col6a14	COL6A14	collagen, type VI, alpha 14	17q21.31	Cytoskeleton
28.	COL6A15_HUMAN	Col6a15	COL6A15	collagen, type VI, alpha 15	17q21.31	Cytoskeleton
29.	COL6A16_HUMAN	Col6a16	COL6A16	collagen, type VI, alpha 16	17q21.31	Cytoskeleton
30.	COL6A17_HUMAN	Col6a17	COL6A17	collagen, type VI, alpha 17	17q21.31	Cytoskeleton
31.	COL6A18_HUMAN	Col6a18	COL6A18	collagen, type VI, alpha 18	17q21.31	Cytoskeleton
32.	COL6A19_HUMAN	Col6a19	COL6A19	collagen, type VI, alpha 19	17q21.31	Cytoskeleton
33.	COL6A20_HUMAN	Col6a20	COL6A20	collagen, type VI, alpha 20	17q21.31	Cytoskeleton
34.	COL6A21_HUMAN	Col6a21	COL6A21	collagen, type VI, alpha 21	17q21.31	Cytoskeleton
35.	COL6A22_HUMAN	Col6a22	COL6A22	collagen, type VI, alpha 22	17q21.31	Cytoskeleton
36.	COL6A23_HUMAN	Col6a23	COL6A23	collagen, type VI, alpha 23	17q21.31	Cytoskeleton
37.	COL6A24_HUMAN	Col6a24	COL6A24	collagen, type VI, alpha 24	17q21.31	Cytoskeleton
38.	COL6A25_HUMAN	Col6a25	COL6A25	collagen, type VI, alpha 25	17q21.31	Cytoskeleton
39.	COL6A26_HUMAN	Col6a26	COL6A26	collagen, type VI, alpha 26	17q21.31	Cytoskeleton
40.	COL6A27_HUMAN	Col6a27	COL6A27	collagen, type VI, alpha 27	17q21.31	Cytoskeleton
41.	COL6A28_HUMAN	Col6a28	COL6A28	collagen, type VI, alpha 28	17q21.31	Cytoskeleton
42.	COL6A29_HUMAN	Col6a29	COL6A29	collagen, type VI, alpha 29	17q21.31	Cytoskeleton
43.	COL6A30_HUMAN	Col6a30	COL6A30	collagen, type VI, alpha 30	17q21.31	Cytoskeleton
44.	COL6A31_HUMAN	Col6a31	COL6A31	collagen, type VI, alpha 31	17q21.31	Cytoskeleton
45.	COL6A32_HUMAN	Col6a32	COL6A32	collagen, type VI, alpha 32	17q21.31	Cytoskeleton
46.	COL6A33_HUMAN	Col6a33	COL6A33	collagen, type VI, alpha 33	17q21.31	Cytoskeleton
47.	COL6A34_HUMAN	Col6a34	COL6A34	collagen, type VI, alpha 34	17q21.31	Cytoskeleton
48.	COL6A35_HUMAN	Col6a35	COL6A35	collagen, type VI, alpha 35	17q21.31	Cytoskeleton
49.	COL6A36_HUMAN	Col6a36	COL6A36	collagen, type VI, alpha 36	17q21.31	Cytoskeleton
50.	COL6A37_HUMAN	Col6a37	COL6A37	collagen, type VI, alpha 37	17q21.31	Cytoskeleton
51.	COL6A38_HUMAN	Col6a38	COL6A38	collagen, type VI, alpha 38	17q21.31	Cytoskeleton
52.	COL6A39_HUMAN	Col6a39	COL6A39	collagen, type VI, alpha 39	17q21.31	Cytoskeleton
53.	COL6A40_HUMAN	Col6a40	COL6A40	collagen, type VI, alpha 40	17q21.31	Cytoskeleton
54.	COL6A41_HUMAN	Col6a41	COL6A41	collagen, type VI, alpha 41	17q21.31	Cytoskeleton
55.	COL6A42_HUMAN	Col6a42	COL6A42	collagen, type VI, alpha 42	17q21.31	Cytoskeleton
56.	COL6A43_HUMAN	Col6a43	COL6A43	collagen, type VI, alpha 43	17q21.31	Cytoskeleton
57.	COL6A44_HUMAN	Col6a44	COL6A44	collagen, type VI, alpha 44	17q21.31	Cytoskeleton
58.	COL6A45_HUMAN	Col6a45	COL6A45	collagen, type VI, alpha 45	17q21.31	Cytoskeleton
59.	COL6A46_HUMAN	Col6a46	COL6A46	collagen, type VI, alpha 46	17q21.31	Cytoskeleton
60.	COL6A47_HUMAN	Col6a47	COL6A47	collagen, type VI, alpha 47	17q21.31	Cytoskeleton
61.	COL6A48_HUMAN	Col6a48	COL6A48	collagen, type VI, alpha 48	17q21.31	Cytoskeleton
62.	COL6A49_HUMAN	Col6a49	COL6A49	collagen, type VI, alpha 49	17q21.31	Cytoskeleton
63.	COL6A50_HUMAN	Col6a50	COL6A50	collagen, type VI, alpha 50	17q21.31	Cytoskeleton
64.	COL6A51_HUMAN	Col6a51	COL6A51	collagen, type VI, alpha 51	17q21.31	Cytoskeleton
65.	COL6A52_HUMAN	Col6a52	COL6A52	collagen, type VI, alpha 52	17q21.31	Cytoskeleton
66.	COL6A53_HUMAN	Col6a53	COL6A53	collagen, type VI, alpha 53	17q21.31	Cytoskeleton
67.	COL6A54_HUMAN	Col6a54	COL6A54	collagen, type VI, alpha 54	17q21.31	Cytoskeleton
68.	COL6A55_HUMAN	Col6a55	COL6A55	collagen, type VI, alpha 55	17q21.31	Cytoskeleton
69.	COL6A56_HUMAN	Col6a56	COL6A56	collagen, type VI, alpha 56	17q21.31	Cytoskeleton
70.	COL6A57_HUMAN	Col6a57	COL6A57	collagen, type VI, alpha 57	17q21.31	Cytoskeleton
71.	COL6A58_HUMAN	Col6a58	COL6A58	collagen, type VI, alpha 58	17q21.31	Cytoskeleton
72.	COL6A59_HUMAN	Col6a59	COL6A59	collagen, type VI, alpha 59	17q21.31	Cytoskeleton
73.	COL6A60_HUMAN	Col6a60	COL6A60	collagen, type VI, alpha 60	17q21.31	Cytoskeleton
74.	COL6A61_HUMAN	Col6a61	COL6A61	collagen, type VI, alpha 61	17q21.31	Cytoskeleton
75.	COL6A62_HUMAN	Col6a62	COL6A62	collagen, type VI, alpha 62	17q21.31	Cytoskeleton
76.	COL6A63_HUMAN	Col6a63	COL6A63	collagen, type VI, alpha 63	17q21.31	Cytoskeleton
77.	COL6A64_HUMAN	Col6a64	COL6A64	collagen, type VI, alpha 64	17q21.31	Cytoskeleton
78.	COL6A65_HUMAN	Col6a65	COL6A65	collagen, type VI, alpha 65	17q21.31	Cytoskeleton
79.	COL6A66_HUMAN	Col6a66	COL6A66	collagen, type VI, alpha 66	17q21.31	Cytoskeleton
80.	COL6A67_HUMAN	Col6a67	COL6A67	collagen, type VI, alpha 67	17q21.31	Cytoskeleton
81.	COL6A68_HUMAN	Col6a68	COL6A68	collagen, type VI, alpha 68	17q21.31	Cytoskeleton
82.	COL6A69_HUMAN	Col6a69	COL6A69	collagen, type VI, alpha 69	17q21.31	Cytoskeleton
83.	COL6A70_HUMAN	Col6a70	COL6A70	collagen, type VI, alpha 70	17q21.31	Cytoskeleton
84.	COL6A71_HUMAN	Col6a71	COL6A71	collagen, type VI, alpha 71	17q21.31	Cytoskeleton
85.	COL6A72_HUMAN	Col6a72	COL6A72	collagen, type VI, alpha 72	17q21.31	Cytoskeleton
86.	COL6A73_HUMAN	Col6a73	COL6A73	collagen, type VI, alpha 73	17q21.31	Cytoskeleton
87.	COL6A74_HUMAN	Col6a74	COL6A74	collagen, type VI, alpha 74	17q21.31	Cytoskeleton
88.	COL6A75_HUMAN	Col6a75	COL6A75	collagen, type VI, alpha 75	17q21.31	Cytoskeleton
89.	COL6A76_HUMAN	Col6a76	COL6A76	collagen, type VI, alpha 76	17q21.31	Cytoskeleton
90.	COL6A77_HUMAN	Col6a77	COL6A77	collagen, type VI, alpha 77	17q21.31	Cytoskeleton
91.	COL6A78_HUMAN	Col6a78	COL6A78	collagen, type VI, alpha 78	17q21.31	Cytoskeleton
92.	COL6A79_HUMAN	Col6a79	COL6A79	collagen, type VI, alpha 79	17q21.31	Cytoskeleton
93.	COL6A80_HUMAN	Col6a80	COL6A80	collagen, type VI, alpha 80	17q21.31	Cytoskeleton
94.	COL6A81_HUMAN	Col6a81	COL6A81	collagen, type VI, alpha 81	17q21.31	Cytoskeleton
95.	COL6A82_HUMAN	Col6a82	COL6A82	collagen, type VI, alpha 82	17q21.31	Cytoskeleton
96.	COL6A83_HUMAN	Col6a83	COL6A83	collagen, type VI, alpha 83	17q21.31	Cytoskeleton
97.	COL6A84_HUMAN	Col6a84	COL6A84	collagen, type VI, alpha 84	17q21.31	Cytoskeleton
98.	COL6A85_HUMAN	Col6a85	COL6A85	collagen, type VI, alpha 85	17q21.31	Cytoskeleton
99.	COL6A86_HUMAN	Col6a86	COL6A86	collagen, type VI, alpha 86	17q21.31	Cytoskeleton
100.	COL6A87_HUMAN	Col6a87	COL6A87	collagen, type VI, alpha 87	17q21.31	Cytoskeleton
101.	COL6A88_HUMAN	Col6a88	COL6A88	collagen, type VI, alpha 88	17q21.31	Cytoskeleton
102.	COL6A89_HUMAN	Col6a89	COL6A89	collagen, type VI, alpha 89	17q21.31	Cytoskeleton
103.	COL6A90_HUMAN	Col6a90	COL6A90	collagen, type VI, alpha 90	17q21.31	Cytoskeleton
104.	COL6A91_HUMAN	Col6a91	COL6A91	collagen, type VI, alpha 91	17q21.31	Cytoskeleton
105.	COL6A92_HUMAN	Col6a92	COL6A92	collagen, type VI, alpha 92	17q21.31	Cytoskeleton
106.	COL6A93_HUMAN	Col6a93	COL6A93	collagen, type VI, alpha 93	17q21.31	Cytoskeleton
107.	COL6A94_HUMAN	Col6a94	COL6A94	collagen, type VI, alpha 94	17q21.31	Cytoskeleton
108.	COL6A95_HUMAN	Col6a95	COL6A95	collagen, type VI, alpha 95	17q21.31	Cytoskeleton
109.	COL6A96_HUMAN	Col6a96	COL6A96	collagen, type VI, alpha 96	17q21.31	Cytoskeleton
110.	COL6A97_HUMAN	Col6a97	COL6A97	collagen, type VI, alpha 97	17q21.31	Cytoskeleton
111.	COL6A98_HUMAN	Col6a98	COL6A98	collagen, type VI, alpha 98	17q21.31	Cytoskeleton
112.	COL6A99_HUMAN	Col6a99	COL6A99	collagen, type VI, alpha 99	17q21.31	Cytoskeleton
113.	COL6A100_HUMAN	Col6a100	COL6A100	collagen, type VI, alpha 100	17q21.31	Cytoskeleton
114.	COL6A101_HUMAN	Col6a101	COL6A101	collagen, type VI, alpha 101	17q21.31	Cytoskeleton
115.	COL6A102_HUMAN	Col6a102	COL6A102	collagen, type VI, alpha 102	17q21.31	Cytoskeleton
116.	COL6A103_HUMAN	Col6a103	COL6A103	collagen, type VI, alpha 103	17q21.31	Cytoskeleton
117.	COL6A104_HUMAN	Col6a104	COL6A104	collagen, type VI, alpha 104	17q21.31	Cytoskeleton
118.	COL6A105_HUMAN	Col6a105	COL6A105	collagen, type VI, alpha 105	17q21.31	Cytoskeleton
119.	COL6A106_HUMAN	Col6a106	COL6A106	collagen, type VI, alpha 106	17q21.31	Cytoskeleton
120.	COL6A107_HUMAN	Col6a107	COL6A107	collagen, type VI, alpha 107	17q21.31	Cytoskeleton
121.	COL6A108_HUMAN	Col6a108	COL6A108	collagen, type VI, alpha 108	17q21.31	Cytoskeleton
122.	COL6A109_HUMAN	Col6a109	COL6A109	collagen, type VI, alpha 109	17q21.31	Cytoskeleton
123.	COL6A110_HUMAN	Col6a110	COL6A110	collagen, type VI, alpha 110	17q21.31	Cytoskeleton
124.	COL6A111_HUMAN	Col6a111	COL6A111	collagen, type VI, alpha 111	17q21.31	Cytoskeleton
125.	COL6A112_HUMAN	Col6a112	COL6A112	collagen, type VI, alpha 112	17q21.31	Cytoskeleton
126.	COL6A113_HUMAN	Col6a113	COL6A113	collagen, type VI, alpha 113	17q21.31	Cytoskeleton
127.	COL6A114_HUMAN	Col6a114	COL6A114	collagen, type VI, alpha 114	17q21.31	Cytoskeleton
128.	COL6A115_HUMAN	Col6a115	COL6A115	collagen, type VI, alpha 115	17q21.31	Cytoskeleton
129.	COL6A116_HUMAN	Col6a116	COL6A116	collagen, type VI, alpha 116	17q21.31	Cytoskeleton
130.	COL6A117_HUMAN	Col6a117	COL6A117	collagen, type VI, alpha 117	17q21.31	Cytoskeleton
131.	COL6A118_HUMAN	Col6a118	COL6A118	collagen, type VI, alpha 118	17q21.31	Cytoskeleton
132.	COL6A119_HUMAN	Col6a119	COL6A119	collagen, type VI, alpha 119	17q21.31	Cytoskeleton
133.	COL6A120_HUMAN	Col6a120	COL6A120	collagen, type VI, alpha 120	17q21.31	Cytoskeleton
134.	COL6A121_HUMAN	Col6a121	COL6A121	collagen, type VI, alpha 121	17q21.31	Cytoskeleton
135.	COL6A122_HUMAN	Col6a122	COL6A122	collagen, type VI, alpha 122	17q21.31	Cytoskeleton
136.	COL6A123_HUMAN	Col6a123	COL6A123	collagen, type VI, alpha 123	17q21.31	Cytoskeleton
137.	COL6A124_HUMAN	Col6a124	COL6A124	collagen, type VI, alpha 124	17q21.31	Cytoskeleton
138.	COL6A125_HUMAN					

Cluster 7



Total 278 genes, 337 proteins identified out of 187 spots

Continued from Cluster 7

Continued from Cluster 7

Cluster 8

Total 224 genes, 180 proteins identified out of 120 spots

Continued from Cluster 8

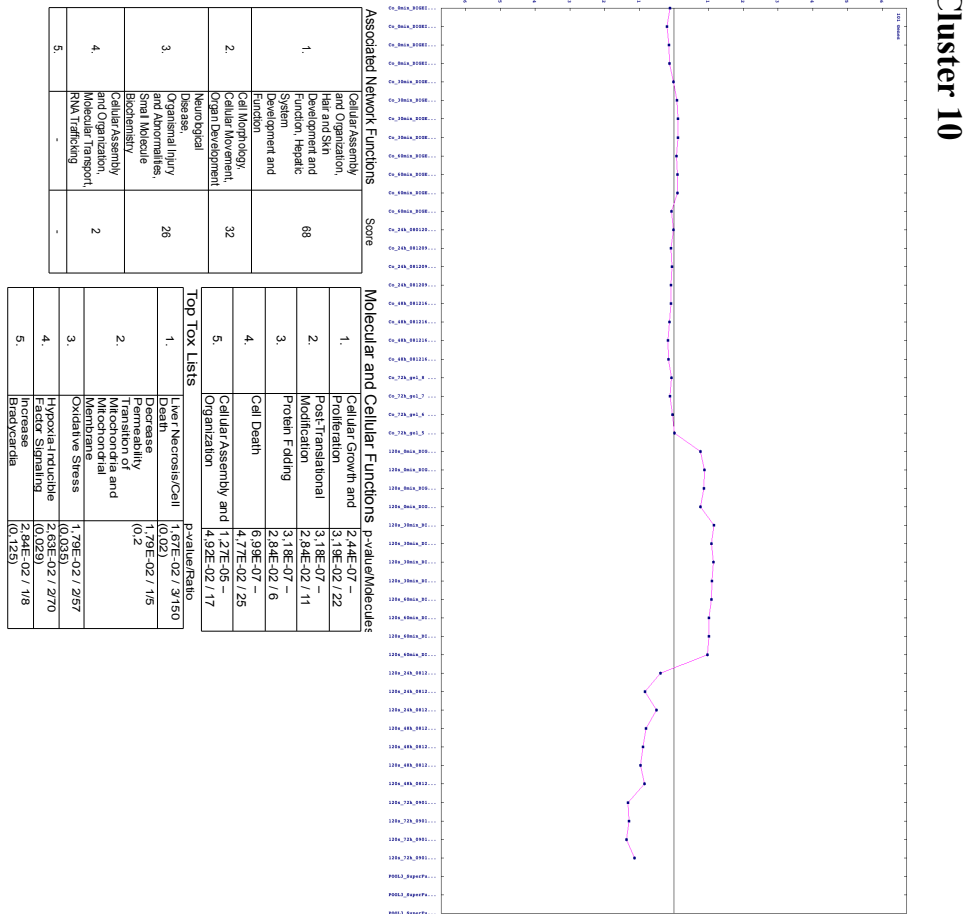
Cluster 9

Cluster 9					
Associated Network Functions	Score	Molecular and Cellular Functions	p-value	Molecule	Gene Name
Cancer, Reproductive, System Disease, Cell/Molecular	55	Cellular Growth and Proliferation, Cellular Assembly and Organization, Cell Death, Cell Death, Genetic	1. 3.9E-05; 2. 7.8E-05 – 7.0E-05; 3. 4.75E-02 / 3.8E-02; 4. 1.42E-04 – 4.83E-02 / 1.55; 5. 4.69E-04 – 4.09E-02 / 4	1. NFKB1; 2. NFKB1-mediated Signaling; 3. Amyloid Precursor Protein Signaling; 4. PPAR Alpha/RXR- Alpha Activation; 5. Glutathione Depletion, Phase II Reactions.	NFKB1; NFKB1-mediated Signaling; Amyloid Precursor Protein Signaling; PPAR Alpha/RXR- Alpha Activation; Glutathione Depletion, Phase II Reactions.
Development, Drug Metabolism, Lipid Metabolism, Cell/Molecular	25	Post-translational Modification, Small Molecule Biology	1. Hypoxia-inducible Factor Signaling; 2. NFKB1-mediated Signaling; 3. Amyloid Precursor Protein Signaling; 4. PPAR Alpha/RXR- Alpha Activation; 5. Glutathione Depletion, Phase II Reactions.	Hypoxia-inducible Factor Signaling; NFKB1-mediated Signaling; Amyloid Precursor Protein Signaling; PPAR Alpha/RXR- Alpha Activation; Glutathione Depletion, Phase II Reactions.	
Development, Drug Metabolism, Cell/Molecular	20	Cellular Growth and Proliferation, Cell Death	1. 3.99E-03 / 5/151; 2. 3.02E-03 / 6/205; 3. 0.033; 4. 1.07E-01 / 3/65; 5. 1.36E-01 / 1/21 (0.048)	1. NFKB1-mediated Signaling; 2. Amyloid Precursor Protein Signaling; 3. Amyloid Precursor Protein Signaling; 4. PPAR Alpha/RXR- Alpha Activation; 5. Glutathione Depletion, Phase II Reactions.	NFKB1-mediated Signaling; Amyloid Precursor Protein Signaling; Amyloid Precursor Protein Signaling; PPAR Alpha/RXR- Alpha Activation; Glutathione Depletion, Phase II Reactions.
Top Tox LISTS	37	P-value/Ratio			
1. Hypoxia-inducible Factor Signaling	1.4E-03 / 4/70	P-value/Ratio			
2. NFKB1-mediated Signaling	3.02E-03 / 6/205	P-value/Ratio			
3. Amyloid Precursor Protein Signaling	3.99E-03 / 5/151	P-value/Ratio			
4. PPAR Alpha/RXR- Alpha Activation	1.07E-01 / 3/65	P-value/Ratio			
5. Glutathione Depletion, Phase II Reactions	1.36E-01 / 1/21 (0.048)	P-value/Ratio			
Post-translational Modification, Small Molecule Biology	11	P-value/Ratio			
1. NFKB1; 2. NFKB1-mediated Signaling; 3. Amyloid Precursor Protein Signaling; 4. PPAR Alpha/RXR- Alpha Activation; 5. Glutathione Depletion, Phase II Reactions.	1. NFKB1; 2. NFKB1-mediated Signaling; 3. Amyloid Precursor Protein Signaling; 4. PPAR Alpha/RXR- Alpha Activation; 5. Glutathione Depletion, Phase II Reactions.	P-value/Ratio			
2. NFKB1-mediated Signaling	3.02E-03 / 6/205	P-value/Ratio			
3. Amyloid Precursor Protein Signaling	3.99E-03 / 5/151	P-value/Ratio			
4. PPAR Alpha/RXR- Alpha Activation	1.07E-01 / 3/65	P-value/Ratio			
5. Glutathione Depletion, Phase II Reactions	1.36E-01 / 1/21 (0.048)	P-value/Ratio			

Total 173 genes, 146 proteins identified out of 86 spots

Continued from Cluster 9

Cluster 10



卷之三

Total 101 genes, 71 proteins identified out of 42 spots

4. Figure S-4 (see DVD)

Hierarchical Clustering by all samples and treatment conditions. Hierarchically clustered (Euclidean Distance measurement and “average” linkage method) log-transformed expression protein values. 12 samples (6 controls 0.5 h to 72 h and 6 ENTplas treated samples 0.5 h to 72 h) are shown vertically on the x-axis (sample order is defined in the top tree). Spot-expression-values for all 1505 detected protein spots are shown horizontally on the y-axis. High expressions are coloured yellow, low expressions are coloured blue and missing expressions are coloured grey. This statistical technique visualizes similarities and differences of different samples (vertically) and protein spots (horizontally). Dendrograms, both on x- and y-axis, represent the Euclidean Distance between the samples. Hierarchical clusters are subsumed on the third level on the x-axis and on the 24th level on the y-axis. Specific identified proteins from K-means cluster 3 and 4 (see **Figure 17**) are highlighted red (K-means cluster 3) and blue (K-means cluster 4) on the right side of the hierarchical cluster. They show each similar expression profiles and were therefore assigned to the same clusters.

5. Table S-1

Established master list from GeneSpring® analyses. This master list contains all significant altered protein spots of the DIGE-experiment. Only proteins, that showed at least a fold change greater than 1.5 for one time point and moreover were identified by MALDI-TOF-MS, were included. The fold change was statistically calculated in a multiple step procedure. After normalisation of every sample spot to the corresponding internal standard (this enables comparison between different gels) followed the calculation of the medians of all four replicates of each sample. Finally, medians of the treated samples were divided by the medians of the controls. Protein identification from MALDI-TOF-MS and information were appended via Ingenuity Pathway Analysis-software package. Multiple identifications of the same protein spot were split up into each unique identification (ID XY-1, ID XY-2) and subsequently combined with the spot-specific expression values.

LZ-ID	KZ-ID	0min	30min	60min	24h	48h	72h	Protein *	Symbol in IPA	Entrez Gene Name	Location	Type(s)	
ID1449-1	ID985-1	-1,583	-1,585	-1,360	-1,226	-1,164	-1,190	1433B	YWHAB	tyrosine 3-monoxygenase/tryptophan 5-monoxygenase activation protein, beta polypeptide	Cytoplasm	other	
ID1373-2	ID74214-2	-1,400	-1,668	-1,390	2,154	1,020	1,015	1433E	YWHAE	tyrosine 3-monoxygenase/tryptophan 5-monoxygenase activation protein, epsilon polypeptide	Cytoplasm	other	
ID1449-2	ID985-2	-1,583	-1,585	-1,360	-1,226	-1,164	-1,190	1433G	D	YWHAG	tyrosine 3-monoxygenase/tryptophan 5-monoxygenase activation protein, gamma polypeptide	Cytoplasm	other
ID1425	ID986	-1,564	-1,558	-1,462	-1,191	-1,189	-1,071	1433G	D	YWHAG	tyrosine 3-monoxygenase/tryptophan 5-monoxygenase activation protein, gamma polypeptide	Cytoplasm	other
ID1429-1	ID991-1	-1,781	-1,668	-1,498	-1,454	-1,325	-1,219	1433T	(includes EG: 10971)	YWHAQ	tyrosine 3-monoxygenase/tryptophan 5-monoxygenase activation protein, theta polypeptide	Cytoplasm	other
ID348681-2	ID964-2	1,233	1,243	1,323	1,606	1,108	1,127	1433Z	D	YWHAZ	tyrosine 3-monoxygenase/tryptophan 5-monoxygenase activation protein, zeta polypeptide	Cytoplasm	enzyme
ID1429-2	ID991-2	-1,781	-1,668	-1,498	-1,454	-1,325	-1,219	1433Z	D	YWHAZ	tyrosine 3-monoxygenase/tryptophan 5-monoxygenase activation protein, zeta polypeptide	Cytoplasm	enzyme
ID768-2	ID508-2	1,888	2,288	1,981	4,371	4,553	3,410	2AAA	D	PPP2R1A	protein phosphatase 2, regulatory subunit A, alpha	Cytoplasm	phosphatase
ID801	ID517	1,188	1,516	1,247	1,623	1,704	1,549	2AAA	D	PPP2R1A	protein phosphatase 2, regulatory subunit A, alpha	Cytoplasm	phosphatase
ID828-3	ID566-3	1,799	2,398	2,061	3,217	3,072	2,468	2AAA	D	PPP2R1A	protein phosphatase 2, regulatory subunit A, alpha	Cytoplasm	phosphatase
ID767-1	ID501-1	1,942	2,566	2,128	4,545	4,749	3,764	2AAB	PPP2R1B	protein phosphatase 2, regulatory subunit A, beta	unknown	phosphatase	
ID1358-2	ID946-2	-1,327	-1,211	-1,119	-1,739	-1,585	-1,613	3HIDH	D	HIBADH	3-hydroxyisobutyrate dehydrogenase	Cytoplasm	enzyme
ID1399-1	ID973-1	-1,522	-1,606	-1,380	-1,164	-1,023	-1,055	3HIDH	D	HIBADH	3-hydroxyisobutyrate dehydrogenase	Cytoplasm	enzyme
ID1433-2	ID998-2	-1,004	1,049	1,044	1,733	1,184	1,177	6PGL	PGLS	6-phosphogluconolactonase	Cytoplasm	enzyme	
ID1372-5	ID957-5	-1,396	-1,506	-1,330	-1,447	-1,159	-1,066	TPM3L					
ID362224-2	ID157676-2	1,137	1,473	1,517	1,260	-1,197	-1,056	ACL6A	D	ACTL6A	actin-like 6A	Nucleus	other

* doubles: duplicates (same identification but different spots) are marked with a "D"

LZ-ID	KZ-ID	0min	30min	60min	24h	48h	72h	Protein *	Symbol in IPA	Entrez Gene Name	Location	Type(s)	
ID992-2	ID158562-2	1,317	1,249	1,326	-1,640	-1,591	-1,555	ACL6A D	ACTL6A	actin-like 6A	Nucleus	other	
ID651	ID412	-1,523	-1,108	-1,284	-1,489	-1,214	-1,246	ACPH	APEH	N-acylaminoacyl-peptide hydrolase	Cytoplasm	peptidase	
ID1058-3	ID746-3	-1,328	-1,428	-1,093	-1,921	-1,982	-1,711	ACTB	ACTB	actin, beta	Cytoplasm	other	
ID1073-2	ID748-2	1,894	1,777	1,681	1,156	-1,132	-1,061	ACTB	ACTB	actin, beta	Cytoplasm	other	
ID1078-4	ID749-4	-1,015	1,071	1,005	-1,529	-1,464	-1,283	ACTB	ACTB	actin, beta	Cytoplasm	other	
ID1080-3	ID772-3	-1,182	-1,165	-1,364	-1,450	-1,527	-1,322	ACTB	ACTB	actin, beta	Cytoplasm	other	
ID1064-2	ID775-2	1,102	1,150	1,157	-1,152	1,348	1,527	ACTB	ACTB	actin, beta	Cytoplasm	other	
ID360270-2	ID82531-2	-2,238	-4,907	-2,505	1,086	-1,380	-1,493	ACTB	ACTB	actin, beta	Cytoplasm	other	
ID478-1	ID1020-1	1,183	1,548	1,334	3,117	1,567	1,532	ACTG	ACTG	actin, gamma 1	Cytoplasm	other	
ID1027-2	ID729-2	1,124	1,136	1,168	1,618	1,211	1,370	ACTG	ACTG	actin, gamma 1	Cytoplasm	other	
ID1037-2	ID734-2	1,166	1,022	1,229	1,550	1,222	1,305	ACTG	ACTG	actin, gamma 1	Cytoplasm	other	
ID1055-1	ID745-1	1,434	1,868	2,008	3,559	2,018	1,392	ACTG	ACTG	actin, gamma 1	Cytoplasm	other	
ID1058-4	ID746-4	-1,328	-1,428	-1,093	-1,921	-1,982	-1,711	ACTG	ACTG	actin, gamma 1	Cytoplasm	other	
ID1073-1	ID748-1	1,894	1,777	1,681	1,156	-1,132	-1,061	ACTG	ACTG	actin, gamma 1	Cytoplasm	other	
ID1067	ID761	1,101	1,118	1,068	-1,751	1,324	1,570	ACTG	ACTG	actin, gamma 1	Cytoplasm	other	
ID1080-1	ID772-1	-1,182	-1,165	-1,364	-1,450	-1,527	-1,322	ACTG	ACTG	actin, gamma 1	Cytoplasm	other	
ID1064-1	ID775-1	1,102	1,150	1,157	-1,152	1,348	1,527	ACTG	ACTG	actin, gamma 1	Cytoplasm	other	
ID1077-2	ID776-2	-1,752	-1,618	-1,426	-1,147	-1,287	-1,200	ACTG	ACTG	actin, gamma 1	Cytoplasm	other	
ID1119-2	ID807-2	1,448	1,405	1,448	2,291	1,463	1,355	ACTG	ACTG	actin, gamma 1	Cytoplasm	other	
ID1104	ID811	1,002	1,025	1,011	-1,999	1,400	1,594	ACTG	ACTG	actin, gamma 1	Cytoplasm	other	
ID360270-1	ID82531-1	-2,238	-4,907	-2,505	1,086	-1,380	-1,493	ACTG	ACTG	actin, gamma 1	Cytoplasm	other	
ID8247	ID1689989	-1,760	-1,924	-1,997	-2,381	-1,510	-1,473	ACTN4	ACTN4	actinin, alpha 4	Cytoplasm	other	
ID507-1	ID289-1	-1,784	-1,926	-1,857	-2,078	-1,654	-1,475	ACTN4	ACTN4	actinin, alpha 4	Cytoplasm	other	
ID518-1	ID319-1	-1,545	-1,672	-1,631	-1,898	-1,529	-1,317	ACTN4	ACTN4	actinin, alpha 4	Cytoplasm	other	
ID517	ID404189	-1,260	-1,301	-1,429	-1,563	-1,346	-1,155	ACTN4	ACTN4	actinin, alpha 4	Cytoplasm	other	
ID31063-3	ID8294-3	-1,980	-1,592	-1,597	-4,548	-1,465	-1,337	ACTY	(includes EG: 10120)	ACTR1B	ARPI actin-related protein 1 homolog	unknown	other

* doubles: duplicates (same identification but different spots) are marked with a "D"

LZ-ID	KZ-ID	0min	30min	60min	24h	48h	72h	Protein *	Symbol in IPA	Entrez Gene Name	Location	Type(s)	
ID1052-2	ID321899-2	-2,208	-1,741	-1,987	-1,464	-1,214	-1,204	ADRM1	ADRM1	adhesion regulating molecule 1	Plasma Membrane	other	
ID697-2	ID32180-2	1,395	1,302	1,200	1,928	2,741	2,515	AGM1	PGM3	phosphoglucomutase 3	unknown	enzyme	
ID490428-2	ID37371-2	1,616	1,506	1,434	-4,032	1,041	1,101	AGM1	PGM3	phosphoglucomutase 3	unknown	enzyme	
ID467907	ID527	1,633	2,052	1,795	-1,337	1,009	1,018	AGM1	PGM3	phosphoglucomutase 3	unknown	enzyme	
ID1077-1	ID776-1	-1,752	-1,618	-1,426	-1,147	-1,287	-1,200	AHSA1	AHSA1	AHA1, activator of heat shock 90kDa protein ATPase homolog 1 (yeast)	Cytoplasm	other	
ID894	ID650	-1,100	-1,218	-1,033	-3,299	-1,041	1,066	AL1B1	ALDH1B1	aldehyde dehydrogenase 1 family, member B1	Cytoplasm	enzyme	
ID939	ID679	-1,308	-1,162	-1,134	-1,754	-1,307	-1,211	AL9A1	ALDH9A1	aldehyde dehydrogenase 9 family, member A1	Cytoplasm	enzyme	
ID384077-2	ID525-2	1,479	1,835	1,524	-1,160	1,053	1,046	AMPM2	METAP2	methionyl aminopeptidase 2	Cytoplasm	peptidase	
ID1240-2	ID899-2	-1,617	-1,631	-1,547	-1,195	-1,149	-1,126	ANXA2	ANXA2	annexin A2	Plasma Membrane	other	
ID825-2	ID576-2	1,373	1,803	1,549	2,220	2,095	1,735	ANXA3	ANXA3	annexin A3	Cytoplasm	enzyme	
ID213992	ID177191	-1,640	-1,335	-1,283	-1,517	-1,340	-1,336	ANXA5	D	ANXA5	annexin A5	Plasma Membrane	
ID1345-1	ID926-1	2,250	2,388	2,197	2,275	1,848	1,635	ANXA5	D	ANXA5	annexin A5	Plasma Membrane	
ID445851-2	ID515333-2	1,052	-1,549	-1,213	-1,186	-1,163	-1,159	APMAP	C20ORF3	chromosome 20 open reading frame 3	Plasma Membrane	other	
ID965	ID711	-1,546	-1,719	-1,492	-2,102	-1,666	-1,469	ARP3	D	ACTR3	ARP3 actin-related protein 3 homolog (yeast)	Plasma Membrane	other
ID1078-2	ID749-2	-1,015	1,071	1,005	-1,529	-1,464	-1,283	ARP3	D	ACTR3	ARP3 actin-related protein 3 homolog (yeast)	Plasma Membrane	other
ID1046-1	ID83121-1	12,137	9,453	7,307	1,021	-1,083	-1,075	ARP3	D	ACTR3	ARP3 actin-related protein 3 homolog (yeast)	Plasma Membrane	other
ID1121-2	ID791-2	-2,318	-1,878	-1,737	-1,679	-1,415	-1,224	ARSA1					
ID1152	ID810	-1,711	-2,007	-1,508	-1,328	-1,065	-1,068	ARSA1					
ID1560-1	ID1071-1	1,576	1,301	1,622	1,517	1,163	1,161	ATP5H	(includes EG: 10476)	ATP5H	ATP synthase, H ⁺ transporting, mitochondrial Fo complex, subunit d	Cytoplasm	transporter

* doubles: duplicates (same identification but different spots) are marked with a “D“

LZ-ID	KZ-ID	0min	30min	60min	24h	48h	72h	Protein *	Symbol in IPA	Entrez Gene Name	Location	Type(s)	
ID3737	ID1705345	1,220	1,149	1,415	2,323	1,414	1,478	ATPB	D	ATPSB	ATP synthase, H ⁺ transporting, mitochondrial F1 complex, beta polypeptide	Cytoplasm	transporter
ID9272	ID6772	1,489	1,479	1,623	1,430	1,112	1,076	ATPB	D	ATPSB	ATP synthase, H ⁺ transporting, mitochondrial F1 complex, beta polypeptide	Cytoplasm	transporter
ID936	ID6669	-1,671	-2,377	-1,828	-1,454	-1,322	-1,251	BASP					
ID1596-1	ID1088-1	1,049	-1,307	-1,279	-1,903	-1,861	-1,936	BID	BID	BH3 interacting domain death agonist	Cytoplasm	other	
ID1183-1	ID841-1	-1,630	-1,537	-1,458	-1,593	-1,097	-1,009	BIEA	BLVRA	biliverdin reductase A	Cytoplasm	enzyme	
ID934-4	ID684-4	-1,335	-1,433	-1,399	-3,437	-1,460	-1,241	BLMH	BLMH	bleomycin hydrolase	Cytoplasm	peptidase	
ID644-4	ID372-4	1,041	-1,155	-1,003	1,589	-1,207	-1,006	CALDI	D	CALDI	caldesmon 1	Cytoplasm	other
ID625-2	ID385-2	-1,210	-1,270	-1,159	4,079	-1,183	-1,075	CALDI	D	CALDI	caldesmon 1	Cytoplasm	other
ID488759	ID39059	-1,314	-1,355	-1,068	-3,679	-1,782	-1,409	CALDI	D	CALDI	caldesmon 1	Cytoplasm	other
ID2174	ID406280	1,144	1,204	1,207	1,647	1,532	1,435	CALR	D	CALR	calreticulin	Cytoplasm	transcription regulator
ID50273-2	ID432714-2	3,264	2,811	3,212	1,702	2,033	1,547	CALR	D	CALR	calreticulin	Cytoplasm	transcription regulator
ID745-1	ID451-1	2,087	2,005	2,023	4,005	3,963	3,006	CALR	D	CALR	calreticulin	Cytoplasm	transcription regulator
ID53317	ID383210	1,213	1,219	1,245	1,590	1,101	1,238	CALU	D	CALU	calumenin	Cytoplasm	other
ID1027-1	ID729-1	1,124	1,136	1,168	1,618	1,211	1,370	CALU	D	CALU	calumenin	Cytoplasm	other
ID1037-1	ID734-1	1,166	1,022	1,229	1,550	1,222	1,305	CALU	D	CALU	calumenin	Cytoplasm	other
ID479360	ID6983	1,299	1,204	1,358	-2,024	1,074	1,214	CAP2	CAP2	CAP, adenylate cyclase-associated protein, 2 (yeast)	Plasma Membrane	other	
ID496907	ID20733	-1,146	-1,373	-1,510	-1,844	-1,496	-1,570	CAPG	D	CAPG	capping protein (actin filament), gelsolin-like	Nucleus	other
ID1128-2	ID790-2	-1,304	-1,416	-1,400	-1,561	-1,229	-1,050	CAPG	D	CAPG	capping protein (actin filament), gelsolin-like	Nucleus	other
ID1512	ID1033	1,905	2,498	2,143	2,349	1,821	1,447	CATB	CTSB	cathepsin B	Cytoplasm	peptidase	
ID693-2	ID431-2	1,585	1,420	1,406	1,712	2,194	2,250	CBR4	CBR4	carboxyl reductase 4	unknown	enzyme	
ID1560-2	ID1071-2	1,576	1,301	1,622	1,517	1,163	1,161	CBX5		chromobox homolog 5	Nucleus	other	

* doubles: duplicates (same identification but different spots) are marked with a "D"

LZ-ID	KZ-ID	0min	30min	60min	24h	48h	72h	Protein *	Symbol in IPA	Entrez Gene Name	Location	Type(s)
ID1399-3	ID973-3	-1,522	-1,606	-1,380	-1,164	-1,023	-1,055	CDV3	CDV3 homolog (mouse)	unknown	other	
ID827	ID560	1,287	1,296	1,566	1,624	1,535	1,525	CH60	D	HSPD1	Cytoplasm	enzyme
ID826-1	ID572-1	1,581	1,577	1,776	1,543	1,383	1,242	CH60	D	HSPD1	Cytoplasm	enzyme
ID1378	ID958	-1,960	-1,575	-1,252	-1,255	-1,107	CLIC1	CLIC1	chloride intracellular channel 1	Nucleus	ion channel	
ID1478-3	ID1020-3	1,183	1,548	1,334	3,117	1,567	1,532	CLIC4	D	CLIC4	chloride intracellular channel 4	Plasma Membrane
ID1409-2	ID982-2	-2,012	-1,783	-1,654	-1,369	-1,201	-1,068	CLIC4	D	CLIC4	chloride intracellular channel 4	Plasma Membrane
ID923-2	ID632-2	-1,452	-1,444	-1,575	-1,561	-1,538	-1,304	CNDP2	D	CNDP2	CNDP dipeptidase 2 (metallopeptidase M20 family)	Cytoplasm
ID918-2	ID636-2	1,108	-1,176	-1,419	-1,743	-1,442	-1,329	CNDP2	D	CNDP2	CNDP dipeptidase 2 (metallopeptidase M20 family)	Cytoplasm
ID1154-1	ID803-1	-1,398	-1,498	-1,463	-1,664	-1,239	-1,183	CNN3		Calponin 3, acidic	Cytoplasm	other
ID1641	ID1110	-2,355	-2,265	-1,807	-1,619	-2,050	-1,778	COF1		cofilin 1 (non-muscle)	Nucleus	other
ID1632-2	ID1099-2	-1,657	-1,393	-1,298	-1,084	-1,190	-1,033	COMMD1	(includes EG: 150684)	copper metabolism (Murr1) domain containing 1	Nucleus	transporter
ID693-1	ID431-1	1,585	1,420	1,406	1,712	2,194	2,250	COR1B	D	CORO1B	coronin, actin binding protein, 1B	Cytoplasm
ID384077-4	ID525-4	1,479	1,835	1,524	-1,160	1,053	1,046	COR1B	D	CORO1B	coronin, actin binding protein, 1B	Cytoplasm
ID235608	ID90567	1,768	1,653	1,661	1,624	1,968	1,719	COR1B	D	CORO1B	coronin, actin binding protein, 1B	Cytoplasm
ID1769	ID1167	-1,784	-1,745	-1,444	-1,045	-1,217	1,023	COTL1		COTL1	coactosin-like 1 (Dictyostelium)	Cytoplasm
ID1167-4	ID831-4	-1,483	-1,567	-1,492	-1,458	-1,296	-1,155	CPN1		CIAPIN1	cytokine induced apoptosis inhibitor 1	Cytoplasm
ID384077-3	ID525-3	1,479	1,835	1,524	-1,160	1,053	1,046	CPNE1	D	CPNE1	copine I	other
ID791	ID550	1,212	1,340	1,210	-1,565	-1,195	-1,204	CPNE1	D	CPNE1	copine I	transporter
ID812-2	ID577-2	1,117	1,137	1,214	1,038	-1,180	-1,155	CPNE1	D	CPNE1	copine I	transporter
ID808-2	ID585-2	1,312	1,504	1,384	1,100	1,191	1,112	CPNE1	D	CPNE1	copine I	transporter
ID405373-3	ID635677-3	1,780	1,608	1,634	1,039	1,080	1,169	CPNE1	D	CPNE1	copine I	transporter
ID808-1	ID585-1	1,312	1,504	1,384	1,100	1,191	1,112	CPNE3		CPNE3	copine III	Cytoplasm kinase

* doubles: duplicates (same identification but different spots) are marked with a “D“

LZ-ID	KZ-ID	0min	30min	60min	24h	48h	72h	Protein *	Symbol in IPA	Entrez Gene Name	Location	Type(s)
ID1401-1	ID996-1	-1,644	-1,432	-1,290	-1,364	-1,407	-1,312	CPNS1	CAPNS1	calpain, small subunit 1	Cytoplasm	peptidase
ID1502	ID1028	1,767	2,204	1,887	2,123	1,394	1,158	CRK	CRK	v-crk sarcoma virus CT10 oncogene homolog (avian)	Cytoplasm	other
ID565	ID39497	-1,276	-1,322	-1,194	-5,082	-2,180	-2,362	CSDE1	CSDE1	cold shock domain containing El, RNA-binding	Cytoplasm	enzyme
ID1077-3	ID776-3	-1,752	-1,618	-1,426	-1,147	-1,287	-1,200	CSN4	COPS4	COP9 constitutive photomorphogenic homolog subunit 4 (Arabidopsis)	Cytoplasm	other
ID1282-2	ID893-2	1,025	1,154	-1,000	-2,111	-1,597	-1,478	CSN6	COPS6	COP9 constitutive photomorphogenic homolog subunit 6 (Arabidopsis)	Nucleus	other
ID26959	ID55589	-1,553	-1,568	-1,746	-3,528	-3,983	-2,111	CTNA1	CTNNA1	catenin (cadherin-associated protein), alpha 1, 102kDa	Plasma Membrane	other
ID650	ID403	-1,197	-1,272	-1,280	-2,011	-1,791	-1,675	DCH12	DYNC112	dynein, cytoplasmic 1, intermediate chain 2	Cytoplasm	other
ID586647-1	ID7535-1	-1,030	-1,050	-1,073	-2,819	-1,225	-1,120	DC1L2	DYNC1IL2	dynein, cytoplasmic 1, light intermediate chain 2	Cytoplasm	other
ID380472	ID642266	1,490	1,418	1,367	3,970	4,553	3,126	DCTN1	DCTN1	dynactin 1	Cytoplasm	other
ID302775-1	ID1691858-1	-1,345	-1,539	-1,425	-1,370	-1,263	-1,186	DCTN2	DCTN2	dynactin 2 (p50)	Cytoplasm	other
ID893-1	ID633-1	-1,315	-1,304	-1,290	-3,680	-1,248	-1,060	DD19A	D	DEAD (Asp-Glu-Ala-As) box polypeptide 19A	Nucleus	enzyme
ID902-1	ID651-1	-1,072	-1,110	-1,060	-2,550	-1,537	-1,427	DD19A	D	DEAD (Asp-Glu-Ala-As) box polypeptide 19A	Nucleus	enzyme
ID1188-1	ID853-1	1,433	1,566	1,321	-1,108	-1,009	1,149	DDAHI	DDAHI	dimethylarginine dimethylaminohydrolase 1	Cytoplasm	enzyme
ID943-3	ID678-3	-1,025	1,069	-1,347	-1,797	-1,261	-1,341	DDX39	DDX39	DEAD (Asp-Glu-Ala-Asp) box polypeptide 39	Nucleus	enzyme
ID445851-1	ID515333-1	1,052	-1,549	-1,213	-1,186	-1,163	-1,159	DNJA2	DNJA2	DnaJ (Hsp40) homolog, subfamily A, member 2	Nucleus	enzyme
ID559-2	ID357-2	-1,505	-2,088	-1,781	-1,565	-1,488	-1,410	DP13A	APPL1	adaptor protein, phosphotyrosine interaction, PH domain and leucine zipper containing 1	Cytoplasm	other
ID122740	ID1585410	1,056	1,326	1,514	4,956	1,375	2,214	DP13B	APPL2	adaptor protein, phosphotyrosine interaction, PH domain and leucine zipper containing 2	Cytoplasm	other

*doubles: duplicates (same identification but different spots) are marked with a "D"

LZ-ID	KZ-ID	0min	30min	60min	24h	48h	72h	Protein *	Symbol in IPA	Entrez Gene Name	Location	Type(s)	
ID13335	ID155877	1,183	1,161	1,610	-2,390	-1,322	-1,213	DPOD2	D	POLD2	polymerase (DNA directed), delta 2, regulatory subunit 50kDa	Nucleus	enzyme
ID410	ID95006	-1,165	-1,392	-2,009	-3,419	-2,804	-2,118	DPOD2	D	POLD2	polymerase (DNA directed), delta 2, regulatory subunit 50kDa	Nucleus	enzyme
ID644-1	ID372-1	1,041	-1,155	-1,003	1,589	-1,207	-1,006	DPYL2	D	DPYSL2	dihydropyrimidinase-like 2	Cytoplasm	enzyme
ID673-2	ID442-2	-1,649	-1,404	-1,539	2,963	-1,158	1,041	DPYL2	D	DPYSL2	dihydropyrimidinase-like 2	Cytoplasm	enzyme
ID755	ID492	2,009	2,133	1,953	4,151	4,155	3,130	DPYL2	D	DPYSL2	dihydropyrimidinase-like 2	Cytoplasm	enzyme
ID778-1	ID528-1	-1,182	-1,231	-1,196	-5,922	-1,185	-1,085	DPYL2	D	DPYSL2	dihydropyrimidinase-like 2	Cytoplasm	enzyme
ID35820	ID551	1,317	1,606	1,340	-2,379	3,040	2,113	DPYL2	D	DPYSL2	dihydropyrimidinase-like 2	Cytoplasm	enzyme
ID435	ID240	-1,254	-1,373	-1,324	-2,012	-1,400	-1,365	DREB	D	DBNI	dreb1	Cytoplasm	other
ID428-2	ID241-2	-1,336	-1,613	-1,409	-1,790	-1,410	-1,334	DREB	D	DBNI	dreb1	Cytoplasm	other
ID1352-1	ID932-1	1,149	1,201	1,247	-3,179	1,116	-1,049	ECH1	ECH1	enoyl CoA hydratase 1, peroxisomal	Cytoplasm	enzyme	
ID1453-2	ID1013-2	-1,162	-1,254	-1,006	-10,673	-1,079	-1,128	ECHM	D	ECHS1	enoyl CoA hydratase, short chain, 1, mitochondrial	Cytoplasm	enzyme
ID1473	ID1021	-1,206	-1,135	-1,082	-2,975	1,182	1,104	ECHM	D	ECHS1	enoyl CoA hydratase, short chain, 1, mitochondrial	Cytoplasm	enzyme
ID610	ID373	1,127	1,105	-1,103	-2,259	-1,236	-1,102	EFG1					
ID1355-2	ID940-2	-1,503	-1,408	-1,245	-1,168	-1,218	-1,169	EFHD2		EFHD2	EF-hand domain family, member D2	unknown	other
ID1128-1	ID790-1	-1,304	-1,416	-1,400	-1,561	-1,229	-1,050	EI2BL					
ID1078-1	ID749-1	-1,015	1,071	1,005	-1,529	-1,464	-1,283	EIF3G	D	EIF3G	eukaryotic translation initiation factor 3, subunit G	Cytoplasm	translation regulator
ID1188-2	ID853-2	1,433	1,566	1,321	-1,108	-1,009	1,149	EIF3I		EIF3I (includes EG_8668)	eukaryotic translation initiation factor 3, subunit I	Cytoplasm	translation regulator
ID1015	ID718	2,396	2,585	2,200	4,212	4,091	3,125	ENOA		ENO1	enolase 1, (alpha)	Cytoplasm	transcription regulator
ID15652	ID340984	-1,780	-1,658	-1,407	-1,354	-1,200	-1,201	ENO2	D	ENO2	enolase 2 (gamma, neuronal)	Cytoplasm	enzyme
ID917-3	ID642-3	-1,667	-1,456	-1,369	-1,594	-1,204	-1,182	ENO2	D	ENO2	enolase 2 (gamma, neuronal)	Cytoplasm	enzyme
ID953-1	ID690-1	1,055	1,077	1,043	-1,660	-1,371	-1,466	ENO2	D	ENO2	enolase 2 (gamma, neuronal)	Cytoplasm	enzyme
ID1001	ID721	-1,709	-1,436	-1,347	-1,564	-1,187	-1,126	ENO2	D	ENO2	enolase 2 (gamma, neuronal)	Cytoplasm	enzyme

* doubles: duplicates (same identification but different spots) are marked with a “D“

LZ-ID	KZ-ID	0min	30min	60min	24h	48h	72h	Protein *	Symbol in IPA	Entrez Gene Name	Location	Type(s)	
ID105671-2	ID236729-2	-1,230	1,089	-1,270	1,713	1,139	1,254	ENPL	D	HSP90B1	heat shock protein 90kDa beta (Grp94), member 1	Cytoplasm	other
ID132924	ID285159	1,784	1,705	2,242	-1,217	-1,275	-1,256	ENPL	D	HSP90B1	heat shock protein 90kDa beta (Grp94), member 1	Cytoplasm	other
ID462	ID311	1,113	1,200	-1,077	1,541	1,339	1,266	ENPL	D	HSP90B1	heat shock protein 90kDa beta (Grp94), member 1	Cytoplasm	other
ID622-3	ID400-3	-1,653	-1,807	-1,627	-1,755	-1,425	-1,261	ERF3B		GSPT2	G1 to S phase transition 2	Cytoplasm	translation regulator
ID518-2	ID319-2	-1,545	-1,672	-1,631	-1,898	-1,529	-1,317	ERO1A		ERO1L	ERO1-like (<i>S. cerevisiae</i>)	Cytoplasm	enzyme
ID1463-1	ID1014-1	-1,566	-1,283	-1,287	-3,216	-1,085	-1,105	ERP29	D	ERP29	endoplasmic reticulum protein 29	Cytoplasm	transporter
ID1408-2	ID987-2	1,099	1,081	1,209	-4,552	-1,056	-1,117	ERP29	D	ERP29	endoplasmic reticulum protein 29	Cytoplasm	transporter
ID1433-3	ID998-3	-1,004	1,049	1,044	1,733	1,184	1,177	ERP29	D	ERP29	endoplasmic reticulum protein 29	Cytoplasm	transporter
ID1463-3	ID1014-3	-1,566	-1,283	-1,287	-3,216	-1,085	-1,105	ETHE1		ETHE1	ethylmalonic encephalopathy 1	Cytoplasm	other
ID644-3	ID372-3	1,041	-1,155	-1,003	1,589	-1,207	-1,006	EZR1	D	EZR	ezrin	Plasma Membrane	other
ID625-1	ID385-1	-1,210	-1,270	-1,159	4,079	-1,183	-1,075	EZR1	D	EZR	ezrin	Plasma Membrane	other
ID627-3	ID401-3	1,278	1,241	1,305	1,599	1,818	1,574	FETA		AFP	alpha-fetoprotein	Extracellular Space	transporter
ID843-2	ID549-2	-1,444	-1,597	-1,492	-1,309	-1,372	-1,253	FKBP4	D	FKBP4	FK506 binding protein 4, 59kDa	Nucleus	enzyme
ID871	ID608	-1,504	-1,557	-1,403	-1,253	-1,142	-1,072	FKBP4	D	FKBP4	FK506 binding protein 4, 59kDa	Nucleus	enzyme
ID878-1	ID620-1	-1,404	-1,539	-1,373	-1,261	-1,211	-1,155	FKBP4	D	FKBP4	FK506 binding protein 4, 59kDa	Nucleus	enzyme
ID405373-2	ID635677-2	1,780	1,608	1,634	1,039	1,080	1,169	FKBP4	D	FKBP4	FK506 binding protein 4, 59kDa	Nucleus	enzyme
ID692	ID438	1,641	1,555	1,829	-1,027	-1,199	-1,343	FKBP9		FK506 binding protein 9, 63 kDa	Cytoplasm	enzyme	
ID11137-1	ID799-1	1,163	1,168	1,128	-3,538	-1,361	-1,242	GALK1		GALK1	galactokinase 1	Cytoplasm	kinase
ID309937-2	ID1646-2	-1,316	1,116	-1,182	-2,228	-2,363	-1,739	GANAB	D	GANAB	glucosidase, alpha; neutral AB	Cytoplasm	enzyme
ID510-1	ID298-1	-1,326	-1,220	-1,302	-2,388	-1,646	-1,500	GANAB	D	GANAB	glucosidase, alpha; neutral AB	Cytoplasm	enzyme
ID508-2	ID333-2	-1,647	-1,719	-1,787	-1,396	-1,459	-1,611	GANAB	D	GANAB	glucosidase, alpha; neutral AB	Cytoplasm	enzyme
ID4596	ID451761	-1,976	-1,574	-1,726	-1,849	-1,614	-1,315	GANAB	D	GANAB	glucosidase, alpha; neutral AB	Cytoplasm	enzyme

*doubles: duplicates (same identification but different spots) are marked with a "D"

LZ-ID	KZ-ID	0min	30min	60min	24h	48h	72h	Protein *	Symbol in IPA	Entrez Gene Name	Location	Type(s)
ID1282-4	ID893-4	1,025	1,154	-1,000	-2,111	-1,597	-1,478	GBB1	D	GNB1	guanine nucleotide binding protein (G protein), beta polypeptide 1	Plasma Membrane
ID1291-2	ID910-2	-1,679	-1,364	-1,299	-1,203	-1,278	-1,144	GBB1	D	GNB1	guanine nucleotide binding protein (G protein), beta polypeptide 1	Plasma Membrane
ID1282-3	ID893-3	1,025	1,154	-1,000	-2,111	-1,597	-1,478	GBB2	D	GNB2	guanine nucleotide binding protein (G protein), beta polypeptide 2	Plasma Membrane
ID1291-3	ID910-3	-1,679	-1,364	-1,299	-1,203	-1,278	-1,144	GBB2	D	GNB2	guanine nucleotide binding protein (G protein), beta polypeptide 2	Plasma Membrane
ID828-1	ID566-1	1,799	2,398	2,061	3,217	3,072	2,468	GDIA	D	GDII	GDP dissociation inhibitor 1	Cytoplasm
ID825-1	ID576-1	1,373	1,803	1,549	2,220	2,095	1,735	GDIA	D	GDII	GDP dissociation inhibitor 1	other
ID940	ID695	-2,055	-1,993	-1,830	-1,735	-1,516	-1,334	GDIB	D	GDII	GDP dissociation inhibitor 2	Cytoplasm
ID584-1	ID368-1	-1,062	-1,038	-1,113	-2,256	-1,077	-1,129	GEELS	D	GSN	gelsolin	Extracellular Space
ID585-2	ID370-2	-1,203	-1,175	-1,241	-2,337	-1,398	-1,360	GEELS	D	GSN	gelsolin	Extracellular Space
ID17482	ID467249	1,251	1,390	1,332	3,265	2,862	2,125	GEELS	D	GSN	gelsolin	Extracellular Space
ID1166	ID20411	-1,093	-1,349	-1,248	-3,121	-1,041	1,106	GIPC1		GIPC1	GIPC PDZ domain containing family, member 1	Cytoplasm
ID1167-1	ID831-1	-1,483	-1,567	-1,492	-1,458	-1,296	-1,155	GLRX3	D	GLRX3	glutaredoxin 3	Cytoplasm
ID535	ID282	1,093	1,077	1,173	1,512	1,086	1,008	GLU2B	D	PRKCSH	protein kinase C substrate 80K-H	Cytoplasm
ID2111	ID381253	1,224	1,197	1,328	1,566	1,255	1,319	GLU2B	D	PRKCSH	protein kinase C substrate 80K-H	Cytoplasm
ID309937-1	ID1646-1	-1,316	1,116	-1,182	-2,228	-2,363	-1,739	GRAP1		GRIP1	associated protein 1	Plasma Membrane
ID681-1	ID448-1	1,145	1,086	1,050	1,593	1,355	1,439	GRP75	D	HSPA9	heat shock 70kDa protein 9 (mortalin)	Cytoplasm
ID710-3	ID485-3	1,735	1,726	1,632	1,535	1,400	1,340	GRP75	D	HSPA9	heat shock 70kDa protein 9 (mortalin)	Cytoplasm
ID943-1	ID678-1	-1,025	1,069	-1,347	-1,797	-1,261	-1,341	GSHB	D	GSS	glutathione synthetase	Cytoplasm
ID960	ID703	-1,517	-1,444	-1,394	-1,268	-1,065	1,002	GSHB	D	GSS	glutathione synthetase	Cytoplasm
ID1393	ID965	-1,328	1,041	-1,070	-6,662	-1,011	1,139	GSTO1	D	GSTO1	glutathione S-transferase omega 1	Cytoplasm
ID422947-1	ID974-1	-1,126	-1,228	-1,174	-1,414	-1,661	-1,495	GSTO1	D	GSTO1	glutathione S-transferase omega 1	Cytoplasm
ID1408-1	ID987-1	1,099	1,081	1,209	-4,552	-1,056	-1,117	GSTO1	D	GSTO1	glutathione S-transferase omega 1	Cytoplasm

* doubles: duplicates (same identification but different spots) are marked with a “D“

LZ-ID	KZ-ID	0min	30min	60min	24h	48h	72h	Protein *	Symbol in IPA	Entrez Gene Name	Location	Type(s)	
ID1516	ID1035	-1,603	-1,307	-1,268	-1,313	-1,173	-1,059	GSTP1	D	GSTP1	glutathione S-transferase pi 1	Cytoplasm	enzyme
ID1541-2	ID1060-2	-2,501	-2,401	-2,651	-1,508	-1,193	-1,146	GSTP1	D	GSTP1	glutathione S-transferase pi 1	Cytoplasm	enzyme
ID843-5	ID549-5	-1,444	-1,597	-1,492	-1,309	-1,372	-1,253	HDAC2		HDAC2	histone deacetylase 2	Nucleus	transcription regulator
ID306795-2	ID762-2	-1,508	-1,346	-1,323	-5,070	-1,504	-1,898	HDGF	D	HDGF	hepatoma-derived growth factor	Extracellular Space	growth factor
ID1194	ID863	-1,580	-1,450	-1,439	-1,598	-1,159	-1,143	HDGF	D	HDGF	hepatoma-derived growth factor	Extracellular Space	growth factor
ID88373	ID868	-1,938	-1,819	-1,723	-1,785	-1,272	-1,348	HDGF	D	HDGF	hepatoma-derived growth factor	Extracellular Space	growth factor
ID1240-3	ID899-3	-1,617	-1,631	-1,547	-1,195	-1,149	-1,126	HDGF	D	HDGF	hepatoma-derived growth factor	Extracellular Space	growth factor
ID878-2	ID620-2	-1,404	-1,539	-1,373	-1,261	-1,211	-1,155	HMCS1		HMGCSE1	3-hydroxy-3-methylglutaryl-CoA synthase 1 (soluble)	Cytoplasm	enzyme
ID229521-1	ID33186-1	-1,017	-1,187	-1,393	-1,850	-1,414	-1,322	HNRH1	D	HNRNPH1	heterogeneous nuclear ribonucleoprotein H1 (H)	Nucleus	other
ID921-2	ID622-2	-1,202	-1,395	-1,470	-1,610	-1,469	-1,221	HNRH1	D	HNRNPH1	heterogeneous nuclear ribonucleoprotein H1 (H)	Nucleus	other
ID923-1	ID632-1	-1,452	-1,444	-1,575	-1,561	-1,538	-1,304	HNRH1	D	HNRNPH1	heterogeneous nuclear ribonucleoprotein H1 (H)	Nucleus	other
ID918-1	ID636-1	1,108	-1,176	-1,419	-1,743	-1,442	-1,329	HNRH1	D	HNRNPH1	heterogeneous nuclear ribonucleoprotein H1 (H)	Nucleus	other
ID471051-1	ID661-1	-1,070	-1,169	-1,283	-2,810	-1,452	-1,291	HNRH1	D	HNRNPH1	heterogeneous nuclear ribonucleoprotein H1 (H)	Nucleus	other
ID956-2	ID675-2	-1,507	-1,510	-1,514	-1,788	-1,434	-1,220	HNRH1	D	HNRNPH1	heterogeneous nuclear ribonucleoprotein H1 (H)	Nucleus	other
ID934-2	ID684-2	-1,335	-1,433	-1,399	-3,437	-1,460	-1,241	HNRH1	D	HNRNPH1	heterogeneous nuclear ribonucleoprotein H1 (H)	Nucleus	other
ID229521-2	ID33186-2	-1,017	-1,187	-1,393	-1,850	-1,414	-1,322	HNRH2	D	HNRNPH2	heterogeneous nuclear ribonucleoprotein H2 (H)	Nucleus	other
ID922-2	ID637-2	-1,390	-1,494	-1,468	-3,301	-1,505	-1,288	HNRH2	D	HNRNPH2	heterogeneous nuclear ribonucleoprotein H2 (H)	Nucleus	other

*doubles: duplicates (same identification but different spots) are marked with a "D"

LZ-ID	KZ-ID	0min	30min	60min	24h	48h	72h	Protein *	Symbol in IPA	Entrez Gene Name	Location	Type(s)
ID493	ID1943	-1,132	-1,795	-1,735	-2,432	-1,295	-1,334	HNRNLL2	HNRNPULL2	heterogeneous nuclear ribonucleoprotein U-like 2	Nucleus	other
ID458	ID2016	-1,165	-1,817	-1,689	-2,615	-1,507	-1,496	HNRNLL2	HNRNPULL2	heterogeneous nuclear ribonucleoprotein U-like 2	Nucleus	other
ID494	ID2227	-1,145	-2,012	-1,883	-2,748	-1,433	-1,387	HNRNLL2	HNRNPULL2	heterogeneous nuclear ribonucleoprotein U-like 2	Nucleus	other
ID1203	ID217712	-2,382	-2,667	-2,431	1,131	-1,394	-1,057	HNRPC	HNRNPC	heterogeneous nuclear ribonucleoprotein C (C1/C2)	Nucleus	other
ID305540-1	ID835-1	-2,578	-4,750	-2,699	1,122	-1,347	-1,083	HNRPC	HNRNPC	heterogeneous nuclear ribonucleoprotein C (C1/C2)	Nucleus	other
ID854-2	ID64007-2	1,387	1,274	1,389	1,759	1,228	1,222	HNRPF	HNRNPFF	heterogeneous nuclear ribonucleoprotein F	Nucleus	other
ID977-2	ID687-2	1,519	1,535	1,525	1,329	-1,144	-1,139	HNRPF	HNRNPFF	heterogeneous nuclear ribonucleoprotein F	Nucleus	other
ID770	ID518	1,869	2,250	1,928	4,309	4,339	3,164	HNRPK	HNRNPK	heterogeneous nuclear ribonucleoprotein K	Nucleus	other
ID787	ID530	1,316	1,658	1,408	1,618	1,509	1,316	HNRPK	HNRNPK	heterogeneous nuclear ribonucleoprotein K	Nucleus	other
ID878-3	ID620-3	-1,404	-1,539	-1,373	-1,261	-1,211	-1,155	HNRPK	HNRNPK	heterogeneous nuclear ribonucleoprotein K	Nucleus	other
ID201269-2	ID81237-2	-8,373	-6,196	-7,125	-1,519	-1,978	-1,691	HNRPK	HNRNPK	heterogeneous nuclear ribonucleoprotein K	Nucleus	other
ID479-2	ID116600-2	-1,568	-1,765	-1,880	-3,815	-1,575	-1,395	HNRPU	HNRNPU	heterogeneous nuclear ribonucleoprotein U (scaffold attachment factor A)	Nucleus	transporter
ID415-1	ID230-1	-1,285	-1,517	-1,734	-1,547	-2,220	-2,095	HNRPU	HNRNPU	heterogeneous nuclear ribonucleoprotein U (scaffold attachment factor A)	Nucleus	transporter
ID10099-1	ID1752140-1	-2,358	-2,181	-1,615	1,436	1,582	2,064	HOOK3	HOOK3	hook homolog 3 (Drosophila)	Cytoplasm	other
ID485	ID273	-1,487	-1,744	-1,748	-1,616	-1,305	-1,171	HS105	HSPH1	heat shock 105kDa/110kDa protein 1	Cytoplasm	other
ID477-1	ID279-1	-1,387	-1,493	-1,616	-1,578	-1,500	-1,318	HS105	HSPH1	heat shock 105kDa/110kDa protein 1	Cytoplasm	other
ID486	ID283	-1,585	-1,739	-1,743	-1,708	-1,451	-1,293	HS105	HSPH1	heat shock 105kDa/110kDa protein 1	Cytoplasm	other
ID507-2	ID289-2	-1,784	-1,926	-1,857	-2,078	-1,654	-1,475	HS105	HSPH1	heat shock 105kDa/110kDa protein 1	Cytoplasm	other

* doubles: duplicates (same identification but different spots) are marked with a “D“

LZ-ID	KZ-ID	0min	30min	60min	24h	48h	72h	Protein *	Symbol in IPA	Entrez Gene Name	Location	Type(s)	
ID20414	ID131273	-1,062	-1,181	-1,105	1,392	1,743	1,586	HS90A	D	HSP90AA1	heat shock protein 90kDa alpha (cytosolic), class A member 1	Cytoplasm	other
ID10923	ID141710	-1,455	-1,679	-1,568	-1,405	-1,707	-1,393	HS90A	D	HSP90AA1	heat shock protein 90kDa alpha (cytosolic), class A member 1	Cytoplasm	other
ID10099-2	ID1752140-2	-2,358	-2,181	-1,615	1,436	1,582	2,064	HS90A	D	HSP90AA1	heat shock protein 90kDa alpha (cytosolic), class A member 1	Cytoplasm	other
ID3931	ID349	-1,323	-1,846	-1,468	-1,022	1,241	1,094	HS90A	D	HSP90AA1	heat shock protein 90kDa alpha (cytosolic), class A member 1	Cytoplasm	other
ID553	ID351	-1,720	-2,040	-1,825	-1,025	1,395	1,488	HS90A	D	HSP90AA1	heat shock protein 90kDa alpha (cytosolic), class A member 1	Cytoplasm	other
ID575	ID356	-1,393	-1,556	-1,382	-1,326	-1,385	-1,179	HS90A	D	HSP90AA1	heat shock protein 90kDa alpha (cytosolic), class A member 1	Cytoplasm	other
ID559-1	ID357-1	-1,505	-2,088	-1,781	-1,565	-1,488	-1,410	HS90A	D	HSP90AA1	heat shock protein 90kDa alpha (cytosolic), class A member 1	Cytoplasm	other
ID584-3	ID368-3	-1,062	-1,038	-1,113	-2,256	-1,077	-1,129	HS90A	D	HSP90AA1	heat shock protein 90kDa alpha (cytosolic), class A member 1	Cytoplasm	other
ID628	ID375	1,761	1,831	1,828	2,658	2,852	2,274	HS90A	D	HSP90AA1	heat shock protein 90kDa alpha (cytosolic), class A member 1	Cytoplasm	other
ID618-2	ID376-2	-1,143	-1,130	-1,216	-1,586	-1,197	-1,309	HS90A	D	HSP90AA1	heat shock protein 90kDa alpha (cytosolic), class A member 1	Cytoplasm	other
ID629-2	ID378-2	-1,107	-1,066	-1,151	-1,583	-1,197	-1,297	HS90A	D	HSP90AA1	heat shock protein 90kDa alpha (cytosolic), class A member 1	Cytoplasm	other
ID622-2	ID400-2	-1,653	-1,807	-1,627	-1,755	-1,425	-1,261	HS90A	D	HSP90AA1	heat shock protein 90kDa alpha (cytosolic), class A member 1	Cytoplasm	other
ID627-1	ID401-1	1,278	1,241	1,305	1,599	1,818	1,574	HS90A	D	HSP90AA1	heat shock protein 90kDa alpha (cytosolic), class A member 1	Cytoplasm	other
ID577-3	ID371-3	1,199	1,052	1,210	-1,504	-1,065	-1,169	HS90B		HSP90AB1	heat shock protein 90kDa alpha (cytosolic), class B member 1	Cytoplasm	other
ID490	ID278	-1,545	-1,618	-1,603	-1,590	-1,173	-1,022	HSP74	D	HSPA4	heat shock 70kDa protein 4	Cytoplasm	other
ID491	ID288	-1,800	-1,825	-1,823	-1,833	-1,386	-1,221	HSP74	D	HSPA4	heat shock 70kDa protein 4	Cytoplasm	other
ID92002-3	ID208438-3	-1,923	-1,463	-1,707	-1,341	1,012	-1,160	HSP7C	D	HSPA8	heat shock 70kDa protein 8	Cytoplasm	enzyme
ID681-4	ID448-4	1,145	1,086	1,050	1,593	1,355	1,439	HSP7C	D	HSPA8	heat shock 70kDa protein 8	Cytoplasm	enzyme

* doubles: duplicates (same identification but different spots) are marked with a "D"

LZ-ID	KZ-ID	0min	30min	60min	24h	48h	72h	Protein *	Symbol in IPA	Entrez Gene Name	Location	Type(s)
ID710-1	ID485-1	1,735	1,726	1,632	1,535	1,400	1,340	HSP7C	D	HSPA8	heat shock 70kDa protein 8	Cytoplasm enzyme
ID453-1	ID013-1	-1,162	-1,254	-1,006	-10,673	-1,079	-1,128	HSPB1	D	HSPB1	heat shock 27kDa protein 1	Cytoplasm other
ID468-2	ID016-2	1,423	1,570	1,481	-1,012	-1,196	-1,298	HSPB1	D	HSPB1	heat shock 27kDa protein 1	Cytoplasm other
ID492-1	ID12926-1	-1,233	-1,144	-1,078	-2,537	-1,063	-1,061	HSPB1	D	HSPB1	heat shock 27kDa protein 1	Cytoplasm other
ID364-1	ID171-1	-1,054	1,111	1,009	1,582	1,061	1,045	HYOU1	D	HYOU1	hypoxia up-regulated 1	Cytoplasm other
ID376	ID188	-1,015	1,044	1,034	2,076	1,365	1,301	HYOU1	D	HYOU1	hypoxia up-regulated 1	Cytoplasm other
ID5403	ID207	-1,688	-2,174	-1,866	-2,268	-1,395	-1,241	HYOU1	D	HYOU1	hypoxia up-regulated 1	Cytoplasm other
ID427	ID235	-1,261	-1,361	-1,238	-1,560	-1,118	-1,145	ICAL	D	CAST	calpastatin	Cytoplasm peptidase
ID430	ID236	-1,263	-1,400	-1,319	-1,576	-1,164	-1,347	ICAL	D	CAST	calpastatin	Cytoplasm peptidase
ID428-1	ID241-1	-1,336	-1,613	-1,409	-1,790	-1,410	-1,334	ICAL	D	CAST	calpastatin	Cytoplasm peptidase
ID126195	ID242	-1,273	-1,259	-1,128	-1,536	-1,067	-1,100	ICAL	D	CAST	calpastatin	Cytoplasm peptidase
ID475	ID261617	-1,547	-1,728	-1,469	-1,847	-1,420	-1,179	ICAL	D	CAST	calpastatin	Cytoplasm peptidase
ID1154-2	ID803-2	-1,398	-1,498	-1,463	-1,664	-1,239	-1,183	IDH3A	D	IDH3A	isocitrate dehydrogenase 3 (NAD+)-alpha	Cytoplasm enzyme
ID1196	ID846	-1,296	-1,504	-1,260	-1,437	-1,358	-1,230	IF2A		EIF2S1	eukaryotic translation initiation factor 2, subunit 1 alpha, 35kDa	Cytoplasm translation regulator
ID1030-2	ID739-2	-2,081	-2,031	-1,790	-1,645	-1,315	-1,240	IF4A1		EIF4A1	eukaryotic translation initiation factor 4A1	Cytoplasm translation regulator
ID617-1	ID140011-1	-1,499	-1,630	-1,560	-1,143	-1,267	-1,120	IF4B		EIF4B	eukaryotic translation initiation factor 4B	Cytoplasm translation regulator
ID1697	ID1134	-1,730	-1,439	-1,465	-1,644	-1,449	-1,189	IF5A1		EIF5A	eukaryotic translation initiation factor 5A	Cytoplasm translation regulator
ID1139-1	ID552252-1	1,216	-1,085	-1,046	-3,172	-1,064	-1,014	IIEU	D	SERPINB1	serpin peptidase inhibitor, clade B (ovalbumin), member 1	Cytoplasm other
ID1032-3	ID758-3	-2,095	-2,071	-1,735	-8,220	-1,526	-1,278	IIEU	D	SERPINB1	serpin peptidase inhibitor, clade B (ovalbumin), member 1	Cytoplasm other
ID1093-2	ID785-2	-1,990	-1,976	-1,565	-4,586	-1,251	-1,246	IIEU	D	SERPINB1	serpin peptidase inhibitor, clade B (ovalbumin), member 1	Cytoplasm other
ID1137-2	ID799-2	1,163	1,168	1,128	-3,538	-1,361	-1,242	IIEU	D	SERPINB1	serpin peptidase inhibitor, clade B (ovalbumin), member 1	Cytoplasm other
ID3406	ID226092	1,722	2,346	2,024	2,275	1,713	1,752	IMA7		KPNA6	karyopherin alpha 6 (importin alpha 7)	Nucleus transporter

* doubles: duplicates (same identification but different spots) are marked with a "D"

LZ-ID	KZ-ID	0min	30min	60min	24h	48h	72h	Protein *	Symbol in IPA	Entrez Gene Name	Location	Type(s)
ID1449-1	ID9855-1	-1,583	-1,585	-1,360	-1,226	-1,164	-1,190	1433B	YWHAB	tyrosine 3-monoxyxygenase/trypophan 5-monoxyxygenase activation protein, beta polypeptide	Cytoplasm	other
ID1373-2	ID74214-2	-1,400	-1,668	-1,390	2,154	1,020	1,015	1433E	YWHAE	tyrosine 3-monoxyxygenase/trypophan 5-monoxyxygenase activation protein, epsilon polypeptide	Cytoplasm	other
ID1449-2	ID9855-2	-1,583	-1,585	-1,360	-1,226	-1,164	-1,190	1433G	D YWHAG	tyrosine 3-monoxyxygenase/trypophan 5-monoxyxygenase activation protein, gamma polypeptide	Cytoplasm	other
ID1425	ID986	-1,564	-1,558	-1,462	-1,191	-1,189	-1,071	1433G	D YWHAG	tyrosine 3-monoxyxygenase/trypophan 5-monoxyxygenase activation protein, gamma polypeptide	Cytoplasm	other
ID1429-1	ID991-1	-1,781	-1,668	-1,498	-1,454	-1,325	-1,219	1433T	YWHAQ (includes EG: 10971)	tyrosine 3-monoxyxygenase/trypophan 5-monoxyxygenase activation protein, theta polypeptide	Cytoplasm	other
ID348681-2	ID964-2	1,233	1,243	1,323	1,606	1,108	1,127	1433Z	D YWHAZ	tyrosine 3-monoxyxygenase/trypophan 5-monoxyxygenase activation protein, zeta polypeptide	Cytoplasm	enzyme
ID1429-2	ID991-2	-1,781	-1,668	-1,498	-1,454	-1,325	-1,219	1433Z	D YWHAZ	tyrosine 3-monoxyxygenase/trypophan 5-monoxyxygenase activation protein, zeta polypeptide	Cytoplasm	enzyme
ID768-2	ID508-2	1,888	2,288	1,981	4,371	4,553	3,410	2AAA	D PPP2R1A	protein phosphatase 2, regulatory subunit A, alpha	Cytoplasm	phosphatase
ID801	ID517	1,188	1,516	1,247	1,623	1,704	1,549	2AAA	D PPP2R1A	protein phosphatase 2, regulatory subunit A, alpha	Cytoplasm	phosphatase
ID828-3	ID566-3	1,799	2,398	2,061	3,217	3,072	2,468	2AAA	D PPP2R1A	protein phosphatase 2, regulatory subunit A, alpha	Cytoplasm	phosphatase
ID767-1	ID501-1	1,942	2,566	2,128	4,545	4,749	3,764	2AAB	PPP2R1B	protein phosphatase 2, regulatory subunit A, beta	unknown	phosphatase
ID1358-2	ID946-2	-1,327	-1,211	-1,119	-1,739	-1,585	-1,613	3HIDH	D HIBADH	3-hydroxyisobutyrate dehydrogenase	Cytoplasm	enzyme
ID1399-1	ID973-1	-1,522	-1,606	-1,380	-1,164	-1,023	-1,055	3HIDH	D HIBADH	3-hydroxyisobutyrate dehydrogenase	Cytoplasm	enzyme
ID1433-2	ID998-2	-1,004	1,049	1,044	1,733	1,184	1,177	6PGL	PGLS	6-phosphogluconolactonase	Cytoplasm	enzyme
ID1372-5	ID957-5	-1,396	-1,506	-1,330	-1,447	-1,159	-1,066	TPM3L				
ID362224-2	ID157676-2	1,137	1,473	1,517	1,260	-1,197	-1,056	ACL6A	D ACTL6A	actin-like 6A	Nucleus	other

* doubles: duplicates (same identification but different spots) are marked with a "D"

x

LZ-ID	KZ-ID	0min	30min	60min	24h	48h	72h	Protein *	Symbol in IPA	Entrez Gene Name	Location	Type(s)
ID712	ID472	1,643	1,604	1,431	-1,296	1,091	-1,-110	LMNBI	D	LMNBI	lamin B1	Nucleus other
ID708	ID477	1,968	1,732	1,799	-1,042	1,142	-1,-082	LMNBI	D	LMNBI	lamin B1	Nucleus other
ID537545-1	ID484+1	2,340	1,560	2,338	-1,031	1,032	-1,-195	LMNBI	D	LMNBI	lamin B1	Nucleus other
ID1337-1	ID921-1	-1,736	-1,514	-1,586	-1,778	-1,745	-1,-563	LZTFL1	LZTFL1	leucine zipper transcription factor-like 1	unknown	other
ID691-1	ID493-1	1,783	1,653	1,603	1,188	2,052	2,115	MAOX	ME1	malic enzyme 1, NADP(+)-dependent, cytosolic	Cytoplasm enzyme	
ID44539	ID1628016	1,565	1,702	1,695	1,079	-1,050	1,771	MARCS	MARCKS	myristoylated alanine-rich protein kinase C substrate	Plasma Membrane	other
ID1355-1	ID940-1	-1,503	-1,408	-1,245	-1,168	-1,218	-1,-169	MARE1	MAPRE1	microtubule-associated protein, RP/EB family, member 1	Cytoplasm	other
ID768-1	ID508-1	1,888	2,288	1,981	4,371	4,553	3,410	MCM6	MCM6	minichromosome maintenance complex component 6	Nucleus	enzyme
ID585-1	ID370-1	-1,203	-1,175	-1,241	-2,337	-1,398	-1,-360	MDIL1	MAD1L1	MAD1 mitotic arrest deficient-like 1 (yeast)	Nucleus	other
ID2711	ID1113	-1,007	1,243	1,099	-1,805	-1,733	-1,-565	MLRM				
ID1647	ID1120	1,066	1,422	1,148	-1,714	-1,739	-1,-672	MLRM				
ID1041	ID23675	-1,511	-1,447	-1,322	-4,610	-1,169	-1,-087	MP2K2	MAP2K2	mitogen-activated protein kinase 2	Cytoplasm	kinase
ID902-2	ID651-2	-1,072	-1,110	-1,060	-2,550	-1,537	-1,-427	MPPA	PMPCA	peptidase (mitochondrial processing) alpha	Cytoplasm	peptidase
ID627-2	ID401-2	1,278	1,241	1,305	1,599	1,818	1,574	MRE11	MRE11A	MRE11 meiotic recombination 11 homolog A (S. cerevisiae)	Nucleus	enzyme
ID508-1	ID333-1	-1,647	-1,719	-1,794	-1,787	-1,396	-1,-459	MSH2	MSH2	mutS homolog 2, colon cancer, nonpolyposis type 1 (E. coli)	Nucleus	enzyme
ID1630-1	ID1106-1	-1,661	-1,125	-1,053	-1,313	-1,158	-1,-185	MTND	AD11	acireductone dioxygenase 1	Nucleus	other
ID197182-1	ID113950-1	-1,483	-1,672	-1,722	-1,891	-1,222	-1,-133	MVP	D	MVP	major vault protein	Nucleus
ID540509	ID114127	-1,366	-1,385	-1,478	-1,701	-1,150	-1,-237	MVP	D	MVP	major vault protein	other
ID487	ID133980	-1,386	-1,493	-1,686	-1,788	-1,305	-1,-079	MVP	D	MVP	major vault protein	other
ID7894-1	ID284+1	-1,190	-1,294	-1,308	-1,656	-1,105	-1,-075	MVP	D	MVP	major vault protein	other
ID460-1	ID285-1	-1,956	-2,020	-2,086	-2,326	-1,432	-1,-262	MVP	D	MVP	major vault protein	other

* doubles: duplicates (same identification but different spots) are marked with a "D"

LZ-ID	KZ-ID	0min	30min	60min	24h	48h	72h	Protein *	Symbol in IPA	Entrez Gene Name	Location	Type(s)
ID466-2	ID290-2	-1,886	-2,030	-2,055	-2,464	-1,588	-1,426	MVP	D	MVP	major vault protein	Nucleus other
ID584-2	ID368-2	-1,062	-1,038	-1,113	-2,256	-1,077	-1,129	MXI	D	MXI	myxovirus (influenza virus) resistance 1, interferon-inducible protein p78 (mouse)	Nucleus enzyme
ID17545	ID63908	-1,094	1,215	-1,027	2,350	2,521	1,707	MXI	D	MXI	myxovirus (influenza virus) resistance 1, interferon-inducible protein p78 (mouse)	Nucleus enzyme
ID379418-1	ID67833-1	-1,981	-2,365	-2,069	-2,136	-1,454	-1,344	MYG1		C12ORF10	chromosome 12 open reading frame 10	unknown other
ID31063-1	ID8294-1	-1,980	-1,592	-1,597	-4,548	-1,465	-1,337	MYH13		MYH13	myosin, heavy chain 13, skeletal muscle	Cytoplasm other
ID1052-3	ID21899-3	-2,208	-1,741	-1,987	-1,464	-1,214	-1,204	MYL3		MYL3	myosin, light chain 3, alkali; ventricular, skeletal, slow	Cytoplasm other
ID405	ID190	-1,192	-1,522	-1,362	-1,403	-1,002	-1,279	NASP		NASP	nuclear autoantigenic sperm protein (histone-binding)	Nucleus other
ID1632-1	ID1099-1	-1,657	-1,393	-1,298	-1,084	-1,190	-1,033	NDKA		NME1	non-metastatic cells 1, protein (NM23A) expressed in	Nucleus kinase
ID697-3	ID32180-3	1,395	1,302	1,200	1,928	2,741	2,515	NDUS1		NDUFS1	NADH dehydrogenase (ubiquinone) Fe-S protein 1, 75kDa (NADH-coenzyme Q reductase)	Cytoplasm enzyme
ID20028	ID139690	-1,226	-1,120	-1,290	1,605	1,034	-1,004	NEBU	D	NEB	nebulin	Cytoplasm other
ID617-2	ID14011-2	-1,499	-1,630	-1,560	-1,143	-1,267	-1,120	NEBU	D	NEB	nebulin	Cytoplasm other
ID1478-2	ID1020-2	1,183	1,548	1,334	3,117	1,567	1,532	NNMT		NNMT	nicotinamide N-methyltransferase	Cytoplasm enzyme
ID1702	ID1122	-1,154	3,445	1,277	1,187	1,064	1,142	CALM		CALM1	calmodulin 1 (phosphorylase kinase, delta)	Plasma Membrane other
ID929-1	ID373575-1	-1,718	-2,260	-1,647	-1,167	-1,296	-1,073	NPIL1	D	NAPIL1	nucleosome assembly protein 1-like 1	Nucleus other
ID845	ID570	1,593	1,800	1,701	2,911	3,002	2,225	NPIL1	D	NAPIL1	nucleosome assembly protein 1-like 1	Nucleus other
ID926	ID652	-1,616	-1,961	-1,602	-1,230	-1,327	-1,131	NPIL1	D	NAPIL1	nucleosome assembly protein 1-like 1	Nucleus other
ID842	ID565	1,981	2,159	1,964	3,474	3,646	2,756	NPIL4	D	NAPIL4	nucleosome assembly protein 1-like 4	Nucleus other
ID846	ID571	1,804	1,949	1,807	2,918	3,114	2,378	NPIL4	D	NAPIL4	nucleosome assembly protein 1-like 4	Nucleus other
ID1224	ID308638	-1,141	-1,747	-1,750	-1,352	-1,027	-1,152	NPM	D	NPM1 (includes EG-4869)	nucleophosmin (nucleolar phosphoprotein B23, numatrin)	Nucleus transcription regulator

*doubles: duplicates (same identification but different spots) are marked with a "D"

LZ-ID	KZ-ID	0min	30min	60min	24h	48h	72h	Protein *	Symbol in IPA	Entrez Gene Name	Location	Type(s)	
ID1188-3	ID853-3	1,433	1,566	1,321	-1,108	-1,009	1,149	NPM	D	NPM1 (includes EG-4869)	nucleophosmin (nucleolar phosphoprotein B23; numatrin)	Nucleus	transcription regulator
ID3227-1	ID222773-1	1,645	2,181	1,814	2,324	2,129	1,778	NUCB1	D	NUCB1	nucleobindin 1	Cytoplasm	other
ID825-3	ID576-3	1,373	1,803	1,549	2,220	2,095	1,735	NUCB1	D	NUCB1	nucleobindin 1	Cytoplasm	other
DD520	ID327	-1,387	-1,594	-1,633	-1,623	-1,262	-1,302	NUCL	NCL		nucleolin	Nucleus	other
ID50273-1	ID432714-1	3,264	2,811	3,212	1,702	2,033	1,547	NSAP	SYNCRIP		synaptotagmin binding, cytosolic RNA interacting protein	Nucleus	other
ID31063-2	ID8294-2	-1,980	-1,592	-1,597	-4,548	-1,465	-1,337	SEPT15	Sep 15, 2011		15 kDa selenoprotein	Cytoplasm	enzyme
ID1055-2	ID745-2	1,434	1,868	2,008	3,559	2,018	1,392	IF34	D	EIF3G	eukaryotic translation initiation factor 3, subunit G	Cytoplasm	translation regulator
ID1058-2	ID746-2	-1,328	-1,428	-1,093	-1,921	-1,982	-1,711	IF34	D	EIF3G	eukaryotic translation initiation factor 3, subunit G	Cytoplasm	translation regulator
ID1240-1	ID899-1	-1,617	-1,631	-1,547	-1,195	-1,149	-1,126	IF31		EIF3J	eukaryotic translation initiation factor 3, subunit J	Cytoplasm	translation regulator
ID1167-2	ID831-2	-1,483	-1,567	-1,492	-1,458	-1,296	-1,155	TXNL2	D	GLRX3	glutaredoxin 3	Cytoplasm	enzyme
ID31063-4	ID8294-4	-1,980	-1,592	-1,597	-4,548	-1,465	-1,337	OAT	OAT		ornithine aminotransferase	Cytoplasm	enzyme
ID970	ID28739	-1,782	-1,599	-1,509	-2,615	-2,078	-1,678	ODO2	DLST		dihydrodipoamide Ssuccinyltransferase (E2 component of 2-oxo-glutarate complex)	Cytoplasm	enzyme
ID1282-1	ID893-1	1,025	1,154	-1,000	-2,111	-1,597	-1,478	ODPB		PDHB	pyruvate dehydrogenase (lipoyamide) beta	Cytoplasm	enzyme
ID717-1	ID479-1	2,032	1,882	1,805	3,754	3,838	3,261	HSP71					
ID710-2	ID485-2	1,735	1,726	1,632	1,535	1,400	1,340	HSP71					
ID3760	ID1597780	1,790	2,245	2,093	6,598	3,037	3,697	GRP78	D	HSPA5	heat shock 70kDa protein 5 (glucose-regulated protein, 78kDa)	Cytoplasm	other
ID10719	ID1751624	3,510	-1,809	5,736	3,096	1,844	1,616	GRP78	D	HSPA5	heat shock 70kDa protein 5 (glucose-regulated protein, 78kDa)	Cytoplasm	other
ID366771	ID228225	2,438	1,455	2,220	-1,446	-1,080	-1,207	GRP78	D	HSPA5	heat shock 70kDa protein 5 (glucose-regulated protein, 78kDa)	Cytoplasm	other
ID120878-1	ID229319-1	1,790	1,060	1,280	-1,034	1,004	-1,135	GRP78	D	HSPA5	heat shock 70kDa protein 5 (glucose-regulated protein, 78kDa)	Cytoplasm	other

* doubles: duplicates (same identification but different spots) are marked with a "D"

LZ-ID	KZ-ID	0min	30min	60min	24h	48h	72h	Protein *	Symbol in IPA	Entrez Gene Name	Location	Type(s)	
ID661	ID230383	1,327	1,691	1,468	3,234	1,905	2,031	GRP78	D	HSPA5	heat shock 70kDa protein 5 (glucose-regulated protein, 78kDa)	Cytoplasm	other
ID105671-1	ID236729-1	-1,230	1,089	-1,270	1,713	1,139	1,254	GRP78	D	HSPA5	heat shock 70kDa protein 5 (glucose-regulated protein, 78kDa)	Cytoplasm	other
ID662	ID410	1,148	1,561	1,240	2,128	1,453	1,472	GRP78	D	HSPA5	heat shock 70kDa protein 5 (glucose-regulated protein, 78kDa)	Cytoplasm	other
ID658	ID451791	1,241	1,223	1,159	1,575	1,150	1,152	GRP78	D	HSPA5	heat shock 70kDa protein 5 (glucose-regulated protein, 78kDa)	Cytoplasm	other
ID594	ID606664	1,970	1,843	1,832	-1,167	1,010	-1,194	GRP78	D	HSPA5	heat shock 70kDa protein 5 (glucose-regulated protein, 78kDa)	Cytoplasm	other
ID622-1	ID400-1	-1,653	-1,807	-1,627	-1,755	-1,425	-1,261	GSPT1		GSPT1	G to S phase transition 1	Cytoplasm	translation regulator
ID554833	ID112565	-1,726	-2,164	-2,127	-2,681	-1,772	-1,756	UBE1	D	UBA1	ubiquitin-like modifier activating enzyme 1	Cytoplasm	enzyme
ID466-1	ID290-1	-1,886	-2,030	-2,055	-2,464	-1,588	-1,426	UBE1	D	UBA1	ubiquitin-like modifier activating enzyme 1	Cytoplasm	enzyme
ID201269-1	ID81237-1	-8,373	-6,196	-7,125	-1,519	-1,978	-1,691	UQCRC1	D	UQCRC1	ubiquinol-cytochrome c reductase core protein I	Cytoplasm	enzyme
ID550-2	ID313-2	-2,077	-1,997	-1,890	-1,785	-1,412	-1,356	P3H1		LEPRE1	leucine proline-enriched proteoglycan (leprecan) 1	Nucleus	enzyme
ID558	ID40308	1,230	1,254	1,063	-3,207	-1,245	-1,171	P3H3		LEPREL2	leprecan-like 2	Nucleus	enzyme
ID17422-1	ID563-1	1,456	1,747	1,625	-1,215	1,024	1,013	P4HA1		P4HA1	prolyl 4-hydroxylase, alpha polypeptide 1	Cytoplasm	enzyme
ID812-1	ID577-1	1,117	1,137	1,214	1,038	-1,180	-1,155	P4HA2		P4HA2	prolyl 4-hydroxylase, alpha polypeptide II	Cytoplasm	enzyme
ID1401-2	ID996-2	-1,644	-1,432	-1,290	-1,364	-1,407	-1,312	GD1R		ARHGDI α	Rho GDP dissociation inhibitor (GDI) α	Cytoplasm	other
ID876	ID607	-1,813	-1,539	-1,773	-1,259	-1,322	-1,275	TBAK	D	TUBA1B	tubulin, alpha 1b	Cytoplasm	other
ID977-3	ID687-3	1,519	1,535	1,525	1,329	-1,144	-1,139	TBAK	D	TUBA1B	tubulin, alpha 1b	Cytoplasm	other
ID1032-1	ID758-1	-2,095	-2,071	-1,735	-8,220	-1,526	-1,278	PA2G4		PA2G4	proliferation-associated 2G4, 38kDa	Nucleus	transcription regulator
ID302775-2	ID1691858-2	-1,345	-1,539	-1,425	-1,370	-1,263	-1,186	PABP2		PABPN1	poly(A) binding protein, nuclear 1	Nucleus	other

*doubles: duplicates (same identification but different spots) are marked with a "D"

LZ-ID	KZ-ID	0min	30min	60min	24h	48h	72h	Protein *	Symbol in IPA	Entrez Gene Name	Location	Type(s)
ID1511	ID1032	-1,730	-1,683	-1,525	-3,202	-1,149	-1,114	PARK7	PARK7	Parkinson disease (autosomal recessive, early onset) 7	Nucleus	other
ID1304	ID912	-1,394	-1,615	-1,301	-1,293	-1,115	-1,236	PCNA	proliferating cell nuclear antigen		Nucleus	other
ID824	ID553	1,357	1,430	1,429	2,085	1,423	1,354	PDIA1	P4HB	prolyl 4-hydroxylase, beta polypeptide	Cytoplasm	enzyme
ID2239	ID555	1,726	1,722	1,830	3,392	1,787	1,754	PDIA1	P4HB	prolyl 4-hydroxylase, beta polypeptide	Cytoplasm	enzyme
ID230824	ID80041	-1,048	-1,093	1,099	1,741	1,254	1,230	PDIA1	P4HB	prolyl 4-hydroxylase, beta polypeptide	Cytoplasm	enzyme
ID691-3	ID493-3	1,783	1,653	1,603	1,188	2,052	2,115	PDIA3	PDIA3	protein disulfide isomerase family A, member 3	Cytoplasm	peptidase
ID17422-3	ID563-3	1,456	1,747	1,625	-1,215	1,024	1,013	PDIA3	PDIA3	protein disulfide isomerase family A, member 3	Cytoplasm	peptidase
ID808-3	ID585-3	1,312	1,504	1,384	1,100	1,191	1,112	PDIA3	PDIA3	protein disulfide isomerase family A, member 3	Cytoplasm	peptidase
ID836-1	ID597-1	1,176	1,244	1,158	2,193	2,370	1,426	PDIA3	PDIA3	protein disulfide isomerase family A, member 3	Cytoplasm	peptidase
ID864-1	ID616-1	1,416	1,236	1,282	1,539	1,138	1,113	PDIA3	PDIA3	protein disulfide isomerase family A, member 3	Cytoplasm	peptidase
ID854-1	ID64007-1	1,387	1,274	1,389	1,759	1,228	1,222	PDIA3	PDIA3	protein disulfide isomerase family A, member 3	Cytoplasm	peptidase
ID120878-2	ID229319-2	1,790	1,060	1,280	-1,034	1,004	-1,135	PDIA4	PDIA4	protein disulfide isomerase family A, member 3	Cytoplasm	peptidase
ID681-3	ID448-3	1,145	1,086	1,050	1,593	1,355	1,439	PDIA4	PDIA4	protein disulfide isomerase family A, member 4	Cytoplasm	enzyme
ID660	ID454	1,645	1,630	1,502	1,906	2,632	2,132	PDIA4	PDIA4	protein disulfide isomerase family A, member 4	Cytoplasm	enzyme
ID717-2	ID479-2	2,032	1,882	1,805	3,754	3,838	3,261	PDIA4	PDIA4	protein disulfide isomerase family A, member 4	Cytoplasm	enzyme
ID370380	ID92503	1,913	2,278	1,957	1,501	1,899	1,774	PDIA4	PDIA4	protein disulfide isomerase family A, member 4	Cytoplasm	enzyme
ID677-3	ID677-3	1,489	1,479	1,623	1,430	1,112	1,076	PDIA6	PDIA6	protein disulfide isomerase family A, member 6	Cytoplasm	enzyme
ID1243-3	ID848-3	-1,689	-1,599	-1,540	-1,203	-1,136	1,014	PDXK	PDXK	pyridoxal (pyridoxine, vitamin B6) kinase	Cytoplasm	kinase

* doubles: duplicates (same identification but different spots) are marked with a “D“

LZ-ID	KZ-ID	0min	30min	60min	24h	48h	72h	Protein *	Symbol in IPA	Entrez Gene Name	Location	Type(s)	
ID17364-2	ID65569-2	1,400	1,555	1,435	1,282	1,277	1,099	PEPD	PEPD	peptidase D	Cytoplasm	peptidase	
ID1522	ID1046	-1,433	-1,247	-1,370	-1,960	-1,194	-1,186	PFD3	VBP1	von Hippel-Lindau binding protein 1	Cytoplasm	other	
ID1468-1	ID1016-1	1,423	1,570	1,481	-1,012	-1,196	-1,298	PHB	D	PHB (includes EG5245)	Nucleus	transcription regulator	
ID348681-1	ID964-1	1,233	1,243	1,323	1,606	1,108	1,127	PHB	D	PHB (includes EG5245)	prohibitin	Nucleus	
ID16655	ID1175	-1,473	-1,196	-1,188	-1,365	1,471	3,447	PHP14	PHPT1	phosphohistidine phosphatase 1	Cytoplasm	phosphatase	
ID1492-2	ID12926-2	-1,233	-1,144	-1,078	-2,537	-1,063	1,061	PLMT	PCMT1	protein-L-isospartate (D-aspartate) O-methyltransferase	Cytoplasm	enzyme	
ID25674	ID1752165	1,205	1,218	1,238	1,627	1,053	1,199	PLOD3	D	PLOD3	procollagen-lysine, 2-oxoglutarate 5-dioxygenase 3	Cytoplasm	enzyme
ID577-2	ID371-2	1,199	1,052	1,210	-1,504	-1,065	-1,169	PLOD3	D	PLOD3	procollagen-lysine, 2-oxoglutarate 5-dioxygenase 3	Cytoplasm	enzyme
ID384077-1	ID525-1	1,479	1,835	1,524	-1,160	1,053	1,046	PLST	PLS3	plastin 3	Cytoplasm	other	
ID843-1	ID549-1	-1,444	-1,597	-1,492	-1,309	-1,372	-1,253	PNCB	NAPRT1	nicotinate phosphoribosyltransferase domain containing 1	unknown	enzyme	
ID1443	ID1002	-1,328	-1,058	-1,090	-3,878	-1,156	-1,083	PNPO	PNPO	pyridoxamine 5'-phosphate oxidase	unknown	enzyme	
ID1272	ID20440	1,161	1,258	1,099	-3,334	-1,429	-1,315	PP1A	PPP1CA	protein phosphatase 1, catalytic subunit, alpha isozyme	Cytoplasm	phosphatase	
ID1030-1	ID739-1	-2,081	-2,031	-1,790	-1,645	-1,315	-1,240	PP1R7	PPP1R7	protein phosphatase 1, regulatory (inhibitor) subunit 7	Nucleus	phosphatase	
ID415-2	ID230-2	-1,285	-1,517	-1,734	-1,547	-2,220	-2,095	PPCE	D	PREP	prolyl endopeptidase	Cytoplasm	peptidase
ID446	ID611058	-1,385	-1,718	-1,677	-2,098	-1,893	-1,705	PPCE	D	PREP	prolyl endopeptidase	Cytoplasm	peptidase
ID452477	ID91803	1,337	1,484	1,429	2,054	3,248	2,338	PPCE	D	PREP	prolyl endopeptidase	Cytoplasm	peptidase
ID671	ID394	-1,148	1,029	-1,076	1,560	-1,277	-1,552	PPM1G	PPM1G	protein phosphatase Mg2+/Mn2+ dependent, 1G	Nucleus	phosphatase	
ID1084-2	ID405639-2	-1,491	-1,707	-1,100	-1,896	-1,407	-1,010	PPME1	PPME1	protein phosphatase methylesterase 1	unknown	enzyme	
ID844-1	ID582-1	-1,297	-1,027	-1,177	-2,854	-1,107	-1,019	PP5	D	PP5C	protein phosphatase 5, catalytic subunit	Nucleus	phosphatase
ID893-3	ID633-3	-1,315	-1,304	-1,290	-3,680	-1,248	-1,060	PPP5	D	PPP5C	protein phosphatase 5, catalytic subunit	Nucleus	phosphatase
ID1243-1	ID848-1	-1,689	-1,599	-1,540	-1,203	-1,136	1,014	PPP6	PPP6C	protein phosphatase 6, catalytic subunit	Nucleus	phosphatase	
ID1541-1	ID1060-1	-2,501	-2,401	-2,651	-1,508	-1,193	-1,146	PRDX2	PRDX2	peroxiredoxin 2	Cytoplasm	enzyme	

* doubles: duplicates (same identification but different spots) are marked with a "D"

LZ-ID	KZ-ID	0min	30min	60min	24h	48h	72h	Protein *	Symbol in IPA	Entrez Gene Name	Location	Type(s)	
ID1510	ID1040	-2,193	-2,300	-2,033	-4,838	-1,491	-1,331	PRDX3	PRDX3	peroxiredoxin 3	Cytoplasm	enzyme	
ID1497	ID1031	-1,721	-1,038	-1,085	1,284	1,071	1,137	PRDX4	PRDX4	peroxiredoxin 4	Cytoplasm	enzyme	
ID469498-1	ID519949-1	1,667	1,660	1,718	1,249	1,137	1,163	PRS4	PSMC1	proteasome (prosome, macropain) 26S subunit, ATPase, 1	Nucleus	peptidase	
ID302775-3	ID1691858-3	-1,345	-1,539	-1,425	-1,370	-1,263	-1,186	PRS6A	PSMC3	proteasome (prosome, macropain) 26S subunit, ATPase, 3	Nucleus	transcription regulator	
ID1446-2	ID1004-2	-1,623	-1,452	-1,338	-1,514	-1,425	-1,335	PSA3	PSMA3	proteasome (prosome, macropain) subunit, alpha type, 3	Cytoplasm	peptidase	
ID1460	ID1006	1,208	1,508	1,296	1,431	1,128	1,125	PSB7	D	proteasome (prosome, macropain) subunit, beta type, 7	Cytoplasm	peptidase	
ID422947-2	ID974-2	-1,126	-1,228	-1,174	-1,414	-1,661	-1,495	PSB7	D	proteasome (prosome, macropain) subunit, beta type, 7	Cytoplasm	peptidase	
ID1553-2	ID1081-2	-1,401	-1,431	-1,537	1,030	-1,113	-1,084	PSB9	PSMB9	proteasome (prosome, macropain) subunit, beta type, 9 (large multifunctional peptidase 2)	Cytoplasm	peptidase	
ID1140	ID801	-1,430	-1,790	-1,711	-1,449	-1,317	-1,157	PSD13	PSMD13	proteasome (prosome, macropain) 26S subunit, non-ATPase, 13	Cytoplasm	peptidase	
ID1244	ID21409	1,003	-1,010	-1,189	-2,766	-1,164	-1,116	PSDE	D	PSMD14	proteasome (prosome, macropain) 26S subunit, non-ATPase, 14	Cytoplasm	peptidase
ID1352-2	ID932-2	1,149	1,201	1,247	-3,179	1,116	-1,049	PSDE	D	PSMD14	proteasome (prosome, macropain) 26S subunit, non-ATPase, 14	Cytoplasm	peptidase
ID566	ID332	-1,344	-1,553	-1,455	-1,264	-1,260	-1,098	PSMD2	PSMD2	proteasome (prosome, macropain) 26S subunit, non-ATPase, 2	Cytoplasm	other	
ID276677	ID689	-1,071	-1,271	-1,374	-2,044	-1,408	-1,331	PSMD4	PSMD4	proteasome (prosome, macropain) 26S subunit, non-ATPase, 4	Cytoplasm	other	
ID955-1	ID156763-1	-1,761	-1,393	1,020	-1,692	-1,413	-1,572	PSMD5	D	PSMD5	proteasome (prosome, macropain) 26S subunit, non-ATPase, 5	Cytoplasm	other
ID954-1	ID700-1	-1,249	-1,165	-1,160	-1,608	-1,216	-1,133	PSMD5	D	PSMD5	proteasome (prosome, macropain) 26S subunit, non-ATPase, 5	Cytoplasm	other
ID1399-2	ID973-2	-1,522	-1,606	-1,380	-1,164	-1,023	-1,055	PSME1	D	PSME1	proteasome (prosome, macropain) activator subunit I (PA28 alpha)	Cytoplasm	other
ID1433-1	ID998-1	-1,004	1,049	1,044	1,733	1,184	1,177	PSME1	D	PSME1	proteasome (prosome, macropain) activator subunit I (PA28 alpha)	Cytoplasm	other

* doubles: duplicates (same identification but different spots) are marked with a “D“

LZ-ID	KZ-ID	0min	30min	60min	24h	48h	72h	Protein *	Symbol in IPA	Entrez Gene Name	Location	Type(s)	
ID1373-1	ID74214-1	-1,400	-1,668	-1,390	2,154	1,020	1,015	PSME2	D	PSME2	proteasome (prosome, macropain) activator subunit 2 (PA28 beta)	Cytoplasm	peptidase
ID1392	ID967	-1,671	-1,886	-1,581	-1,197	-1,062	-1,080	PSME2	D	PSME2	proteasome (prosome, macropain) activator subunit 2 (PA28 beta)	Cytoplasm	peptidase
ID1409-1	ID982-1	-2,012	-1,783	-1,654	-1,369	-1,201	-1,068	PSME2	D	PSME2	proteasome (prosome, macropain) activator subunit 2 (PA28 beta)	Cytoplasm	peptidase
ID934-3	ID684-3	-1,335	-1,433	-1,399	-3,437	-1,460	-1,241	PTN1		PTPN1	protein tyrosine phosphatase, non-receptor type 1	Cytoplasm	phosphatase
ID906-2	ID654-2	-1,168	1,058	-1,218	-1,590	-1,528	-1,449	PTRF		PTRF	polymerase I and transcript release factor	Nucleus	transcription regulator
ID458579	ID96362	-1,347	-1,805	-1,643	-1,895	-1,623	-1,525	PUR4		PFAS	phosphoribosylformylglycinamide synthase	Cytoplasm	enzyme
ID381	ID199	-1,569	-1,979	-1,845	-2,049	-1,297	-1,442	DYNA	D	DCTN1	dynactin 1	Cytoplasm	other
ID477-2	ID279-2	-1,387	-1,493	-1,616	-1,578	-1,500	-1,318	GPIA1		CAPRIN1	cell cycle associated protein 1	Plasma Membrane	other
ID751	ID463	2,128	2,669	2,053	4,233	4,113	2,992	TRXR1	D	TXNRD1	thioredoxin reductase 1	Cytoplasm	enzyme
ID849	ID586	-1,107	-1,012	1,002	-2,605	-1,036	1,079	TRXR1	D	TXNRD1	thioredoxin reductase 1	Cytoplasm	enzyme
ID837	ID587	-1,108	1,227	1,007	-7,888	1,078	1,179	TRXR1	D	TXNRD1	thioredoxin reductase 1	Cytoplasm	enzyme
ID22200	ID380246	2,009	2,131	1,935	3,046	3,131	2,409	TBA3	D	TUBA1A	tubulin, alpha 1a	Cytoplasm	other
ID16669	ID1183	-1,754	-1,512	-1,263	-1,309	1,699	3,751	TXNL5		TXNDC17	thioredoxin domain containing 17	Cytoplasm	enzyme
ID1137-3	ID799-3	1,163	1,168	1,128	-3,538	-1,361	-1,242	DNJBB		DNAJB11	DnaJ (Hsp40) homolog, subfamily B, member 11	Cytoplasm	other
ID364-2	ID171-2	-1,054	1,111	1,009	1,582	1,061	1,045	OXR1	D	HYOU1	hypoxia up-regulated 1	Cytoplasm	other
ID1703	ID1142	-1,520	-1,130	-1,144	1,028	-1,022	1,144	HSB11		HSPB11	heat shock protein family B (small), member 11	unknown	other
ID373121	ID1752611	1,145	1,055	1,088	-1,556	-1,330	-1,227	QCR1	D	UQCRC1	ubiquinol-cytochrome c reductase core protein 1	Cytoplasm	enzyme
ID714	ID435	1,975	2,340	2,024	3,496	3,702	2,744	RANB3		RANBP3	RAN binding protein 3	Nucleus	other
ID1446-1	ID1004-1	-1,623	-1,452	-1,338	-1,514	-1,425	-1,335	RANG		RANBP1	RAN binding protein 1	Nucleus	other
ID932	ID653	1,286	1,208	1,151	-1,510	-1,229	-1,322	RBBP4		RBBP4	retinoblastoma binding protein 4	Nucleus	enzyme

*doubles: duplicates (same identification but different spots) are marked with a "D"

LZ-ID	KZ-ID	0min	30min	60min	24h	48h	72h	Protein *	Symbol in IPA	Entrez Gene Name	Location	Type(s)	
ID953-2	ID690-2	1,055	1,077	1,043	-1,660	-1,371	-1,466	RBBP7	RBBP7	retinoblastoma binding protein 7	Nucleus	transcription regulator	
ID1596-2	ID1088-2	1,049	-1,307	-1,279	-1,903	-1,861	-1,936	RBM8A	RBM8A	RNA binding motif protein 8A	Nucleus	other	
ID459	ID252707	-1,385	-1,745	-1,516	-1,819	-1,247	-1,239	RCN1	D	RCN1	reticulocalbin 1, EF-hand calcium binding domain	Cytoplasm	
ID280677	ID319408	1,389	1,419	1,485	2,327	1,653	1,676	RCN1	D	RCN1	reticulocalbin 1, EF-hand calcium binding domain	Cytoplasm	
ID935	ID668	-2,058	-2,062	-1,843	-1,585	-1,343	-1,424	RD23A	RAD23A	RAD23 homolog A (<i>S. cerevisiae</i>)	Nucleus	other	
ID94683	ID330639	1,488	1,710	1,540	1,400	1,113	-1,093	RD23B	RAD23B	RAD23 homolog B (<i>S. cerevisiae</i>)	Nucleus	other	
ID1375	ID952	-1,403	-1,476	-1,312	-1,967	-1,760	-1,603	RFA2	D	RPA2	replication protein A2, 32kDa	Nucleus	other
ID1367	ID954	1,101	1,065	1,076	-3,382	1,326	1,334	RFA2	D	RPA2	replication protein A2, 32kDa	Nucleus	other
ID526716	ID21716	-1,486	-1,846	-1,857	-4,843	-1,082	-1,009	RFC2	RFC2	replication factor C (activator 1), 40kDa	Nucleus	other	
ID851	ID575	1,848	1,930	1,804	2,811	2,876	2,247	RHG01	D	ARHGAP1	Rho GTPase activating protein 1	Cytoplasm	
ID844-2	ID582-2	-1,297	-1,027	-1,177	-2,854	-1,107	-1,019	RHG01	D	ARHGAP1	Rho GTPase activating protein 1	Cytoplasm	
ID922-1	ID637-1	-1,390	-1,494	-1,468	-3,301	-1,505	-1,288	RHG01	D	ARHGAP1	Rho GTPase activating protein 1	Cytoplasm	
ID1005	ID714	-2,942	-2,464	-1,984	-2,315	-1,648	-1,339	RINI	RNHI	ribonuclease/angiogenin inhibitor 1	Cytoplasm	other	
ID1139-3	ID552252-3	1,216	-1,085	-1,046	-3,172	-1,064	-1,014	ROAA	D	HNRNPAB	heterogeneous nuclear ribonucleoprotein A/B	Nucleus	enzyme
ID1128-3	ID790-3	-1,304	-1,416	-1,400	-1,561	-1,229	-1,050	ROAA	D	HNRNPAB	heterogeneous nuclear ribonucleoprotein A/B	Nucleus	enzyme
ID1137-4	ID799-4	1,163	1,168	1,128	-3,538	-1,361	-1,242	ROAA	D	HNRNPAB	heterogeneous nuclear ribonucleoprotein A/B	Nucleus	enzyme
ID92002-4	ID208438-4	-1,923	-1,463	-1,707	-1,341	1,012	-1,160	RSSA	RPSA	ribosomal protein SA	Plasma Membrane	transmembrane receptor	
ID888-2	ID617-2	-1,323	-1,335	-1,358	-1,812	-1,188	-1,087	RUVBL1	RUVBL1	RuvB-like 1 (E. coli)	Nucleus	transcription regulator	
ID201269-3	ID81237-3	-8,373	-6,196	-7,125	-1,519	-1,978	-1,691	RUVBL2	RUVBL2	RuvB-like 2 (E. coli)	Nucleus	transcription regulator	
ID1042	ID747	-1,789	-1,716	-1,504	-1,484	-1,244	-1,027	SAHH	D	AHCY	adenosylhomocysteinate	Cytoplasm	
ID1032-2	ID758-2	-2,095	-2,071	-1,735	-8,220	-1,526	-1,278	SAHH	D	AHCY	adenosylhomocysteinate	Cytoplasm	

* doubles: duplicates (same identification but different spots) are marked with a “D“

LZ-ID	KZ-ID	0min	30min	60min	24h	48h	72h	Protein *	Symbol in IPA	Entrez Gene Name	Location	Type(s)	
ID703	ID466	1,362	1,509	1,350	2,518	1,913	1,519	SCFD1	SCFD1	sec1 family domain containing 1	Cytoplasm	transporter	
ID1139-2	ID552252-2	1,216	-1,085	-1,046	-3,172	-1,064	-1,014	SCMC1	D	SLC25A24	solute carrier family 25 (mitochondrial carrier; phosphate carrier), member 24	Cytoplasm	other
ID1093-1	ID785-1	-1,990	-1,976	-1,565	-4,586	-1,251	-1,246	SCMC1	D	SLC25A24	solute carrier family 25 (mitochondrial carrier; phosphate carrier), member 24	Cytoplasm	other
ID937	ID670	-1,917	-1,897	-1,619	-2,259	-1,435	-1,212	SCRN1	SCRN1	secernin 1	Cytoplasm	other	
ID697-1	ID32180-1	1,395	1,302	1,200	1,928	2,741	2,515	SDC10					
ID921-1	ID622-1	-1,202	-1,395	-1,470	-1,610	-1,469	-1,221	SEPT8	SEPT8	septin 8	Extracellular Space	other	
ID92002-1	ID208438-1	-1,923	-1,463	-1,707	-1,341	1,012	-1,160	SET	D	SET	SET nuclear oncogene	Nucleus	phosphatase
ID1052-1	ID321899-1	-2,208	-1,741	-1,987	-1,464	-1,214	-1,204	SET	D	SET	SET nuclear oncogene	Nucleus	phosphatase
ID306795-1	ID762-1	-1,508	-1,346	-1,323	-5,070	-1,504	-1,898	SET	D	SET	SET nuclear oncogene	Nucleus	phosphatase
ID90190	ID820	-1,957	-6,220	-1,780	-1,696	1,096	1,036	SET	D	SET	SET nuclear oncogene	Nucleus	phosphatase
ID9421	ID118966	-1,085	1,159	1,023	3,350	1,699	1,479	SF3B2	D	SF3B2	splicing factor 3b, subunit 2, 145kDa	Nucleus	other
ID354	ID179	-1,326	-1,796	-1,907	-5,408	-1,548	-1,571	SF3B2	D	SF3B2	splicing factor 3b, subunit 2, 145kDa	Nucleus	other
ID355	ID180	-1,448	-1,841	-1,865	-4,263	-1,752	-1,824	SF3B2	D	SF3B2	splicing factor 3b, subunit 2, 145kDa	Nucleus	other
ID43526	ID1752943	1,052	1,051	1,017	-1,664	1,008	-1,328	SFRS1	D	SRSF1	serine/arginine-rich splicing factor 1	Nucleus	other
ID1337-2	ID921-2	-1,736	-1,514	-1,586	-1,778	-1,745	-1,563	SFRS1	D	SRSF1	serine/arginine-rich splicing factor 1	Nucleus	other
ID1345-2	ID926-2	2,250	2,388	2,197	2,275	1,848	1,635	SFRS2	SRSF2	serine/arginine-rich splicing factor 2	Nucleus	transcription regulator	
ID1572	ID1076	1,346	1,033	-1,069	-11,240	-2,151	-3,187	SFRS3	D	SRSF3	serine/arginine-rich splicing factor 3	Nucleus	other
ID506742	ID1494392	-3,151	-2,605	-2,433	1,183	-1,685	-1,580	SFRS3	D	SRSF3	serine/arginine-rich splicing factor 3	Nucleus	other
ID955-2	ID156763-2	-1,761	-1,393	1,020	-1,692	-1,413	-1,572	SH3GL1	D	SH3GL1	SH3-domain GRB2-like 1	Cytoplasm	other
ID13083-2	ID160314-2	-3,336	-3,320	-1,891	-1,634	-1,403	-1,320	SH3G1	D	SH3GL1	SH3-domain GRB2-like 1	Cytoplasm	other
ID954-2	ID700-2	-1,249	-1,165	-1,160	-1,608	-1,216	-1,133	SH3G1	D	SH3GL1	SH3-domain GRB2-like 1	Cytoplasm	other
ID379418-2	ID67833-2	-1,981	-2,365	-2,069	-2,136	-1,454	-1,344	SHLB1	SH3GLB1	SH3-domain GRB2-like endophilin B1	Cytoplasm	enzyme	
ID972	ID405631	-1,562	-1,661	-1,405	-1,919	-1,339	-1,313	SHLB2	(includes EG: 56904)	SH3GLB2	SH3-domain GRB2-like endophilin B2	Cytoplasm	other

* doubles: duplicates (same identification but different spots) are marked with a “D”

LZ-ID	KZ-ID	0min	30min	60min	24h	48h	72h	Protein *	Symbol in IPA	Entrez Gene Name	Location	Type(s)	
ID3111-4	ID619-4	-1,509	-1,424	-1,314	-1,325	-1,109	1,047	SMCE1	SMARCE1	SWI/SNF related, matrix associated, actin dependent regulator of chromatin, subfamily e, member 1	Nucleus	transcription regulator	
ID1167-3	ID831-3	-1,483	-1,567	-1,492	-1,458	-1,296	-1,155	SNAG	NAPG	N-ethylmaleimide-sensitive factor attachment protein, gamma	Cytoplasm	transporter	
ID44851-3	ID515333-3	1,052	-1,549	-1,213	-1,186	-1,163	-1,159	SNX6	D	SNX6	Cytoplasm	transporter	
ID918-3	ID636-3	1,108	-1,176	-1,419	-1,743	-1,442	-1,329	SNX6	D	SNX6	Cytoplasm	transporter	
ID956-1	ID675-1	-1,507	-1,510	-1,514	-1,788	-1,434	-1,220	SNX6	D	SNX6	Cytoplasm	transporter	
ID1632-3	ID1099-3	-1,657	-1,393	-1,298	-1,084	-1,190	-1,033	SODC	D	SOD1	superoxide dismutase 1, soluble	Cytoplasm	enzyme
ID508072	ID1463581	-1,592	-1,316	-1,311	-6,941	-1,614	-1,628	SODC	D	SOD1	superoxide dismutase 1, soluble	Cytoplasm	enzyme
ID1589	ID1084	1,248	1,253	1,099	-1,857	-1,437	-1,432	SORCN	SRI	sorcin	Cytoplasm	transporter	
ID1143	ID822	-1,263	-1,226	-1,176	1,663	1,085	1,160	SPB6	SERPINB6	serpin peptidase inhibitor, clade B (ovalbumin), member 6	Cytoplasm	other	
ID1337-3	ID921-3	-1,736	-1,514	-1,586	-1,778	-1,745	-1,563	SPEE	SRM	spermidine synthase	unknown	enzyme	
ID1083	ID782	-1,730	-1,728	-1,621	-1,350	-1,272	-1,250	SPS1	SEPHS1	selenophosphate synthetase 1	unknown	enzyme	
ID92002-2	ID2084382	-1,923	-1,463	-1,707	-1,341	1,012	-1,160	SPSY	D	SMS	spermine synthase	unknown	enzyme
ID1121-1	ID791-1	-2,318	-1,878	-1,737	-1,679	-1,415	-1,224	SPSY	D	SMS	spermine synthase	unknown	enzyme
ID557	ID352	-1,465	-1,768	-1,568	-1,760	-1,362	-1,216	SRC8	D	CTTN	contactin	Plasma Membrane	other
ID559-3	ID357-3	-1,505	-2,088	-1,781	-1,565	-1,488	-1,410	SRC8	D	CTTN	contactin	Plasma Membrane	other
ID1630-2	ID1106-2	-1,661	-1,125	-1,053	-1,313	-1,158	-1,185	SSRD	SSR4	signal sequence receptor, delta (translocon-associated protein delta)	Cytoplasm	other	
ID853	ID578	1,959	2,328	1,989	3,381	3,359	2,552	STABP	STAMBPP	STAM binding protein	Nucleus	enzyme	
ID1553-1	ID1081-1	-1,401	-1,431	-1,537	1,030	-1,113	-1,084	STAM1	STAM	signal transducing adaptor molecule (SH3 domain and ITAM motif) 1	Cytoplasm	other	
ID826-2	ID572-2	1,581	1,577	1,776	1,543	1,383	1,242	STK3	STK3	serine/threonine kinase 3	Cytoplasm	kinase	
ID1119-1	ID807-1	1,448	1,405	1,448	2,291	1,463	1,355	STML2	STOML2	stomatin (EPB72)-like 2	Plasma Membrane	other	
ID1689	ID1136	-1,345	-1,501	-1,184	-1,851	-1,444	-1,456	STMN1	STMN1	stathmin 1	Cytoplasm	other	

* doubles: duplicates (same identification but different spots) are marked with a "D"

LZ-ID	KZ-ID	0min	30min	60min	24h	48h	72h	Protein *	Symbol in IPA	Entrez Gene Name	Location	Type(s)	
ID1161	ID817	-1,861	-1,918	-1,671	-1,628	-1,457	-1,293	STRAP	D	STRAP	serine/threonine kinase receptor associated protein	Plasma Membrane	other
ID305540-2	ID835-2	-2,578	-4,750	-2,699	1,122	-1,347	-1,083	STRAP	D	STRAP	serine/threonine kinase receptor	Plasma Membrane	other
ID1058-1	ID746-1	-1,328	-1,428	-1,093	-1,921	-1,982	-1,711	SUCB1		SUCLA2	succinate-CoA ligase, ADP-forming, beta subunit	Cytoplasm	enzyme
ID691-2	ID493-2	1,783	1,653	1,603	1,188	2,052	2,115	SWP70		SWAP70	SWAP switching B-cell complex 70kDa subunit	Cytoplasm	other
ID460-2	ID285-2	-1,956	-2,020	-2,086	-2,326	-1,432	-1,262	SYAC	AARS		alanyl-tRNA synthetase	Cytoplasm	enzyme
ID929-2	ID373575-2	-1,718	-2,260	-1,647	-1,167	-1,296	-1,073	SYAP1	SYAP1		synapse associated protein 1	Nucleus	other
ID934-1	ID684-1	-1,335	-1,433	-1,399	-3,437	-1,460	-1,241	SYDC	DARS		aspartyl-tRNA synthetase	Cytoplasm	enzyme
ID673-1	ID442-1	-1,649	-1,404	-1,539	2,963	-1,158	1,041	SYG	GARS		glycyl-tRNA synthetase	Cytoplasm	enzyme
ID908	ID666	-1,267	-1,182	-1,262	-1,967	-1,510	-1,280	SYHC	HARS		histidyl-tRNA synthetase	Cytoplasm	enzyme
ID625-3	ID385-3	-1,210	-1,270	-1,159	4,079	-1,183	-1,075	SYK	D	KARS	lysyl-tRNA synthetase	Cytoplasm	enzyme
ID683-1	ID455-1	1,657	1,946	1,676	2,808	2,279	1,922	SYK	D	KARS	lysyl-tRNA synthetase	Cytoplasm	enzyme
ID469498-2	ID519949-2	1,667	1,660	1,718	1,249	1,137	1,163	SYWC	D	WARS	tryptophanyl-tRNA synthetase	Cytoplasm	enzyme
ID885	ID623	-1,594	-1,452	-1,391	-1,777	-1,131	1,068	SYWC	D	WARS	tryptophanyl-tRNA synthetase	Cytoplasm	enzyme
ID29100	ID1752670	-1,268	-1,681	-1,401	-1,979	-1,697	-1,437	TADBP	D	TARDBP	TAR DNA binding protein	Nucleus	transcription regulator
ID1084-1	ID405639-1	-1,491	-1,707	-1,100	-1,896	-1,407	-1,010	TADBP	D	TARDBP	TAR DNA binding protein	Nucleus	transcription regulator
ID1078-3	ID749-3	-1,015	1,071	1,005	-1,529	-1,464	-1,283	TADBP	D	TARDBP	TAR DNA binding protein	Nucleus	transcription regulator
ID1046-2	ID83121-2	12,137	9,453	7,307	1,021	-1,083	-1,075	TADBP	D	TARDBP	TAR DNA binding protein	Nucleus	transcription regulator
ID1183-2	ID841-2	-1,630	-1,537	-1,458	-1,593	-1,097	-1,009	TALDO1			transaldolase 1	Cytoplasm	enzyme
ID17364-1	ID65569-1	1,400	1,555	1,435	1,282	1,277	1,099	TBA1A	D	TUBA1A	tubulin, alpha 1a	Cytoplasm	other
ID904-1	ID161198-1	-1,181	1,096	-1,394	-1,475	-1,524	-1,192	TBA1B	D	TUBA1B	tubulin, alpha 1b	Cytoplasm	other
ID402687	ID32346	-1,276	-1,055	-1,342	-1,923	-1,514	TBA1B	D	TUBA1B	tubulin, alpha 1b	Cytoplasm	other	
ID836-2	ID597-2	1,176	1,244	1,158	2,193	2,370	1,426	TBA1B	D	TUBA1B	tubulin, alpha 1b	Cytoplasm	other

* doubles: duplicates (same identification but different spots) are marked with a "D"

LZ-ID	KZ-ID	0min	30min	60min	24h	48h	72h	Protein *	Symbol in IPA	Entrez Gene Name	Location	Type(s)
ID906-1	ID654-1	-1,168	1,058	-1,218	-1,590	-1,528	-1,449	TBA1C	tubulin, alpha 1c	Cytoplasm	other	
ID906-3	ID654-3	-1,168	1,058	-1,218	-1,590	-1,528	-1,449	TBA4A	tubulin, alpha 4a	Cytoplasm	other	
ID3111-3	ID619-3	-1,509	-1,424	-1,314	-1,325	-1,109	1,047	TBB2A	tubulin, beta 2A	Cytoplasm	other	
ID3111-1	ID619-1	-1,509	-1,424	-1,314	-1,325	-1,109	1,047	TBB2C	D	TUBB2C	Cytoplasm	other
ID875-1	ID625-1	-1,780	-1,712	-1,507	-1,657	-1,154	-1,268	TBB2C	D	TUBB2C	Cytoplasm	other
ID917-2	ID642-2	-1,667	-1,456	-1,369	-1,594	-1,204	-1,182	TBB2C	D	TUBB2C	Cytoplasm	other
ID875-2	ID625-2	-1,780	-1,712	-1,507	-1,657	-1,154	-1,268	TBB3	tubulin, beta 3	Cytoplasm	other	
ID904-2	ID61198-2	-1,181	1,096	-1,394	-1,475	-1,524	-1,192	TBB5	D	TUBB	tubulin, beta	Cytoplasm
ID875-3	ID625-3	-1,780	-1,712	-1,507	-1,657	-1,154	-1,268	TBB5	D	TUBB	tubulin, beta	Cytoplasm
ID917-1	ID642-1	-1,667	-1,456	-1,369	-1,594	-1,204	-1,182	TBB5	D	TUBB	tubulin, beta	Cytoplasm
ID906-4	ID634-4	-1,168	1,058	-1,218	-1,590	-1,528	-1,449	TBB5	D	TUBB	tubulin, beta	Cytoplasm
ID3111-2	ID619-2	-1,509	-1,424	-1,314	-1,325	-1,109	1,047	TBB6	tubulin, beta 6	Cytoplasm	other	
ID893-2	ID633-2	-1,315	-1,304	-1,290	-3,680	-1,248	-1,060	TBG1	tubulin, gamma 1	Cytoplasm	other	
ID29990	ID30353	1,556	1,999	1,725	1,020	1,197	1,107	TCPA	D	TCP1	t-complex 1	Cytoplasm
ID7422-2	ID563-2	1,456	1,747	1,625	-1,215	1,024	1,013	TCPA	D	TCP1	t-complex 1	Cytoplasm
ID888-1	ID617-1	-1,323	-1,335	-1,358	-1,812	-1,188	-1,087	TCPB	D	CCT2	chaperonin containing TCP1, subunit 2 (beta)	Cytoplasm
ID586647-2	ID7535-2	-1,030	-1,050	-1,073	-2,819	-1,225	-1,120	TCPB	D	CCT2	chaperonin containing TCP1, subunit 2 (beta)	Cytoplasm
ID843-3	ID549-3	-1,444	-1,597	-1,492	-1,309	-1,372	-1,253	TCPE	D	CCT5	chaperonin containing TCP1, subunit 5 (epsilon)	Cytoplasm
ID405373-1	ID635677-1	1,780	1,608	1,634	1,039	1,080	1,169	TCPE	D	CCT5	chaperonin containing TCP1, subunit 5 (epsilon)	Cytoplasm
ID760	ID510	-1,222	-1,184	-1,260	-2,092	-1,253	-1,170	TCPG	D	CCT3	chaperonin containing TCP1, subunit 3 (gamma)	Cytoplasm
ID771	ID519	1,223	1,462	1,261	-3,065	-1,026	1,082	TCPG	D	CCT3	chaperonin containing TCP1, subunit 3 (gamma)	Cytoplasm
ID843-4	ID549-4	-1,444	-1,597	-1,492	-1,309	-1,372	-1,253	TCPQ		CCT8	chaperonin containing TCP1, subunit 8 (theta)	Cytoplasm

* doubles: duplicates (same identification but different spots) are marked with a "D"

LZ-ID	KZ-ID	0min	30min	60min	24h	48h	72h	Protein *	Symbol in IPA	Entrez Gene Name	Location	Type(s)
ID1576	ID1082	1,012	-1,080	-1,088	-1,431	-1,222	-1,280	TCTP	TPT1 (includes EG:7178)	tumor protein, translationally-controlled 1	Cytoplasm	other
ID2310	ID1086	-1,422	-1,283	-1,246	-1,952	-1,437	-1,536	TEBP	PTGES3 (includes EG:10728)	prostaglandin E synthase 3 (cytosolic)	Cytoplasm	enzyme
ID540	ID300	-1,263	-1,405	-1,395	-1,825	-1,328	-1,256	TERA	D VCP	valosin-containing protein	Cytoplasm	enzyme
ID9875	ID344	-1,438	-1,530	-1,527	-1,992	-1,483	-1,267	TERA	D VCP	valosin-containing protein	Cytoplasm	enzyme
ID681-2	ID448-2	1,145	1,086	1,050	1,593	1,355	1,439	TF65	RELA	v-ret reticuloendotheliosis viral oncogene homolog A (avian)	Nucleus	transcription regulator
ID414193	ID802	-1,181	-1,097	-1,126	-1,664	-1,169	-1,087	THOC3	THOC3	THO complex 3	Nucleus	other
ID479-1	ID116600-1	-1,568	-1,765	-1,880	-3,815	-1,575	-1,395	TIF1B	D TRIM28	tripartite motif-containing 28	Nucleus	transcription regulator
ID478-2	ID274-2	-1,510	-1,719	-1,726	-2,192	-1,343	-1,246	TIF1B	D TRIM28	tripartite motif-containing 28	Nucleus	transcription regulator
ID469-2	ID275-2	-1,513	-1,795	-1,785	-2,124	-1,358	-1,263	TIF1B	D TRIM28	tripartite motif-containing 28	Nucleus	transcription regulator
ID7894-2	ID284-2	-1,190	-1,294	-1,308	-1,656	-1,105	-1,075	TIF1B	D TRIM28	tripartite motif-containing 28	Nucleus	transcription regulator
ID488	ID286	-1,288	-2,097	-2,251	-2,568	-1,423	-1,514	TIF1B	D TRIM28	tripartite motif-containing 28	Nucleus	transcription regulator
ID471051-2	ID661-2	-1,070	-1,169	-1,283	-2,810	-1,452	-1,291	TIF1B	D TRIM28	tripartite motif-containing 28	Nucleus	transcription regulator
ID449-3	ID985-3	-1,583	-1,585	-1,360	-1,226	-1,164	-1,190	TIF1B	D TRIM28	tripartite motif-containing 28	Nucleus	transcription regulator
ID537545-2	ID484-2	2,340	1,560	2,338	-1,031	1,032	-1,195	TKT	TKT	transketolase	Cytoplasm	enzyme
ID774	ID495	2,046	2,505	1,966	3,921	3,849	2,761	TML2	TOMIL2	target of myb1-like 2 (chicken)	unknown	transporter
ID463-2	ID1014-2	-1,566	-1,283	-1,287	-3,216	-1,085	-1,105	TPIS	TPI1	triosephosphate isomerase 1	Cytoplasm	enzyme
ID55610-1	ID313265-1	1,009	-1,265	-1,102	-1,638	-1,879	-1,511	TPM1	D TPM1	tropomyosin 1 (alpha)	Cytoplasm	other
ID1315	ID902	1,148	1,042	1,038	-1,362	-1,551	-1,287	TPM1	D TPM1	tropomyosin 1 (alpha)	Cytoplasm	other
ID1372-3	ID957-3	-1,396	-1,506	-1,330	-1,447	-1,159	-1,066	TPM1	D TPM1	tropomyosin 1 (alpha)	Cytoplasm	other
ID87491	ID304592	-1,761	-2,128	-1,510	1,227	-1,136	-1,002	TPM2	D TPM2	tropomyosin 2 (beta)	Cytoplasm	other

* doubles: duplicates (same identification but different spots) are marked with a "D"

LZ-ID	KZ-ID	0min	30min	60min	24h	48h	72h	Protein *	Symbol in IPA	Entrez Gene Name	Location	Type(s)	
ID55610-2	ID313265-2	1,009	-1,265	-1,102	-1,638	-1,879	-1,511	TPM2	TPM2	tropomyosin 2 (beta)	Cytoplasm	other	
ID1240-4	ID899-4	-1,617	-1,631	-1,547	-1,195	-1,149	-1,126	TPM2	TPM2	tropomyosin 2 (beta)	Cytoplasm	other	
ID1372-4	ID957-4	-1,396	-1,506	-1,330	-1,447	-1,447	-1,159	TPM2	TPM2	tropomyosin 2 (beta)	Cytoplasm	other	
ID1372-1	ID957-1	-1,396	-1,506	-1,330	-1,447	-1,447	-1,159	TPM3	TPM3	tropomyosin 3	Cytoplasm	other	
ID1372-2	ID957-2	-1,396	-1,506	-1,330	-1,447	-1,447	-1,159	TPM4	TPM4	tropomyosin 4	Cytoplasm	other	
ID683-2	ID455-2	1,657	1,946	1,676	2,808	2,279	1,922	TRFL	D	LTF	lactotransferrin	Extracellular Space	
ID688	ID456	1,790	2,010	1,912	2,083	2,975	2,384	TRFL	D	LTF	lactotransferrin	Extracellular Space	
ID531704	ID9686	-1,117	-1,027	1,018	-4,366	-1,091	-1,152	TSNAX	TSNAX	translin-associated factor X	Nucleus	transporter	
ID362224-1	ID157676-1	1,137	1,473	1,517	1,260	-1,197	-1,056	TXND5	D	TXND5	thioredoxin domain containing 5 (endoplasmic reticulum)	Cytoplasm	enzyme
ID992-1	ID158562-1	1,317	1,249	1,326	-1,640	-1,591	-1,555	TXND5	D	TXND5	thioredoxin domain containing 5 (endoplasmic reticulum)	Cytoplasm	enzyme
ID13083-1	ID160314-1	-3,336	-3,320	-1,891	-1,634	-1,403	-1,320	TXND5	D	TXND5	thioredoxin domain containing 5 (endoplasmic reticulum)	Cytoplasm	enzyme
ID977-1	ID687-1	1,519	1,535	1,525	1,329	-1,144	-1,139	TXND5	D	TXND5	thioredoxin domain containing 5 (endoplasmic reticulum)	Cytoplasm	enzyme
ID959-2	ID699-2	-1,090	-1,101	-1,031	-1,649	-1,559	-1,602	TXND5	D	TXND5	thioredoxin domain containing 5 (endoplasmic reticulum)	Cytoplasm	enzyme
ID36428	ID43494	1,391	1,480	1,333	-2,797	1,300	1,080	U2AF2	U2 small nuclear RNA auxiliary factor 2 (includes EG: 11338)	U2 small nuclear RNA auxiliary factor 2	Nucleus	other	
ID197182-2	ID113950-2	-1,483	-1,672	-1,722	-1,891	-1,222	-1,133	UBA1	D	UBA1	ubiquitin-like modifier activating enzyme 1	Cytoplasm	enzyme
ID478-1	ID274-1	-1,510	-1,719	-1,726	-2,192	-1,343	-1,246	UBA1	D	UBA1	ubiquitin-like modifier activating enzyme 1	Cytoplasm	enzyme
ID469-1	ID275-1	-1,513	-1,795	-1,785	-2,124	-1,358	-1,263	UBA1	D	UBA1	ubiquitin-like modifier activating enzyme 1	Cytoplasm	enzyme
ID460-3	ID285-3	-1,956	-2,020	-2,086	-2,326	-1,432	-1,262	UBA1	D	UBA1	ubiquitin-like modifier activating enzyme 1	Cytoplasm	enzyme

* doubles: duplicates (same identification but different spots) are marked with a “D“

LZ-ID	KZ-ID	0min	30min	60min	24h	48h	72h	Protein *	Symbol in IPA	Entrez Gene Name	Location	Type(s)	
ID466-3	ID290-3	-1,886	-2,030	-2,055	-2,464	-1,588	-1,426	UBA1	D	UBA1	ubiquitin-like modifier activating enzyme 1	Cytoplasm	enzyme
ID1358-1	ID946-1	-1,327	-1,211	-1,119	-1,739	-1,585	-1,613	UBA1	D	UBA1	ubiquitin-like modifier activating enzyme 1	Cytoplasm	enzyme
ID3542	ID331959	1,239	1,127	1,155	-2,744	-1,983	-1,687	UBAS		UBAS	ubiquitin-like modifier activating enzyme 5	Cytoplasm	enzyme
ID1116	ID793	-1,432	-1,457	-1,338	-2,106	-1,020	-1,042	UBCP1		UBLCP1	ubiquitin-like domain containing CTD phosphatase 1	unknown	phosphatase
ID818	ID561	-1,750	-1,832	-1,645	-1,291	-1,206	-1,068	UBP14		USP14	ubiquitin specific peptidase 14 (tRNA-guanine transglycosylase)	Cytoplasm	peptidase
ID545	ID312	-2,073	-2,017	-1,801	-1,652	-1,272	-1,194	UBP5	D	USP5	ubiquitin specific peptidase 5 (isopeptidase 1)	Cytoplasm	peptidase
ID550-1	ID313-1	-2,077	-1,997	-1,890	-1,785	-1,412	-1,356	UBP5	D	USP5	ubiquitin specific peptidase 5 (isopeptidase 1)	Cytoplasm	peptidase
ID767-2	ID501-2	1,942	2,566	2,128	4,545	4,749	3,764	UBQL1	D	UBQLN1	ubiquilin 1	Cytoplasm	other
ID764	ID502	2,013	2,644	2,178	4,640	4,899	3,736	UBQL1	D	UBQLN1	ubiquilin 1	Cytoplasm	other
ID809	ID151367	-1,647	-1,981	-1,966	-1,339	-1,258	-1,131	ULAI		NAE1	NEDD8 activating enzyme E1 subunit 1	Cytoplasm	enzyme
ID1031	ID23331	-1,177	-1,465	-1,361	-2,982	-1,345	-1,207	VAT1		VAT1	vesicle amine transport protein 1 homolog (T. californica)	Plasma Membrane	transporter
ID864-2	ID616-2	1,416	1,236	1,282	1,539	1,138	1,113	VATB2	D	ATP6V1B2	ATPase, H ⁺ transporting, lysosomal 56/58kDa, V1 subunit B2	Cytoplasm	transporter
ID854-3	ID64007-3	1,387	1,274	1,389	1,759	1,228	1,222	VATB2	D	ATP6V1B2	ATPase, H ⁺ transporting, lysosomal 56/58kDa, V1 subunit B2	Cytoplasm	transporter
ID3227-2	ID222773-2	1,645	2,181	1,814	2,324	2,129	1,778	VIME	D	VIM	vimentin	Cytoplasm	other
ID975	ID712	1,666	1,955	1,776	1,216	1,163	-1,003	VIME	D	VIM	vimentin	Cytoplasm	other
ID1044	ID742	2,180	2,523	2,567	1,295	1,471	1,086	VIME	D	VIM	vimentin	Cytoplasm	other
ID431	ID244	-1,149	-1,424	-1,508	-1,880	-1,414	-1,402	VINC	D	VCL	vinculin	Plasma Membrane	enzyme
ID433	ID247	-1,447	-1,514	-1,532	-13,808	-1,354	-1,213	VINC	D	VCL	vinculin	Plasma Membrane	enzyme

*doubles: duplicates (same identification but different spots) are marked with a "D"

LZ-ID	KZ-ID	0min	30min	60min	24h	48h	72h	Protein *	Symbol in IPA	Entrez Gene Name	Location	Type(s)
ID432	ID451763	-1,241	-1,283	-1,325	-1,730	-1,226	-1,175	VINC	D	VCL	vinculin	Plasma Membrane
ID828-2	ID566-2	1,799	2,398	2,061	3,217	3,072	2,468	VTDB	GC	group-specific component (vitamin D binding protein)	Extracellular Space	enzyme transporter
ID697-4	ID32180-4	1,395	1,302	1,200	1,928	2,741	2,515	WDR72	WD repeat domain 72	zyxin	unknown	other
ID644-2	ID372-2	1,041	-1,155	-1,003	1,589	-1,207	-1,006	ZYX		zyxin	Plasma Membrane	other

* doubles: duplicates (same identification but different spots) are marked with a "D"

6. Table S-2

Summary results from network-analysis using Ingenuity Pathway Analysis (IPA).
Spot-lists of MALDI-TOF-MS identified proteins with statistical significance (all protein spots are included in **Table S-1**) were analysed separately for each time point regarding the biological functions. Statistical comparison of ENTplas treated samples to the corresponding control was in the focus. A fold change of at least 1.5 was considered as significant. Direct and indirect relationships were considered. Resulting network-descriptions, molecular and cellular functions, as well as top tox lists are displayed for each time point and combined in order to visualize time dependent tendencies. The top 5 rankings of cellular functions and toxicities were summarized in **Figure 14**.

Associated Network Functions	0min		30min		60min		24h		48h		72h	
	Score		Score		Score		Score		Score		Score	
1.	Post-Translational Modification, Protein Folding, Cancer	46	Cancer, Reproductive System Disease, Cardiovascular Disease	47	Infection Mechanism, Organismal Development, Lipid Metabolism	52	Cancer, Reproductive System Disease, Cardiovascular Disease	42	Post-Translational Modification, Protein Folding, Infectious Disease	52	Cellular Assembly and Organization, Cancer, Reproductive System Disease	51
2.	Cell Morphology, Cancer, Reproductive System Disease	43	Protein Synthesis, Cancer, RNA Post-Translational Modification	41	Cancer, Reproductive System Disease, Cardiovascular Disease	49	Gene Expression, RNA Post-Translational Modification, Cellular Assembly and Organization	40	Cellular Assembly and Organization, Cancer, Reproductive System Disease	46	DNA Replication, Recombination and Repair, Post-Translational Modification, Protein Folding	49
3.	Cancer, Reproductive System Disease, Cellular Assembly and Organization	43	DNA replication, Recombination and Repair, Energy Production, Nucleic Acid Metabolism	40	Post-Translational Modification, Protein Folding, Cellular Function and Maintenance	47	Amino Acid Metabolism, Post-Translational Modification, Small Molecule Biochemistry	35	Cell Death, Neurological Disease, Infectious Disease, Organismal Injury and Abnormalities	33	Infection Mechanism, Infectious Disease, Amino Acid Metabolism	25
4.	Post-Translational Modification, Protein Degradation, Cell Death	42	Cell Morphology, Genetic Disorder, Neurological Disease	39	Neurological Disease, Cancer, Genetic Disorder	46	Cancer, Cellular Assembly and Organization, Small Molecule Biochemistry	33	DNA Replication, Recombination and Repair, Cardiovascular Disease, Infection Mechanism	31	Cell-to-Cell Signaling and Interaction, Cellular Assembly and Organization, Cellular Function and Maintenance	22
5.	Carbohydrate Metabolism, Small Molecule Biochemistry, Immunological Disease	41	Post-Translational Modification, Protein Folding, Amino Acid Metabolism	39	Post-Translational Modification, Protein Folding, Genetic Disorder	26	Tumor Morphology, Cell Death, DNA Replication, Recombination and Repair	33	Protein Synthesis, Skeletal and Muscular System Development and Function, Tissue Morphology	28	Cell Death, Infection Mechanism, Cell Cycle	19
Molecular and Cellular Functions	p-value/Molecules		p-value/Molecules		p-value/Molecules		p-value/Molecules		p-value/Molecules		p-value/Molecules	
1.	Cell Death	3.26E-11 – 2.71E-02 / 101	Post-Translational Modification	8.29E-14 – 2.71E-02 / 42	Post-Translational Modification	1.95E-15 – 2.54E-02 / 37	Post-Translational Modification	1.11E-11 – 2.48E-02 / 40	Cell Death	1.90E-06 – 4.01E-02 / 49	Cellular Growth and Proliferation	6.58E-07 – 4.91E-02 / 32
2.	Post-Translational Modification	3.26E-11 – 2.71E-02 / 55	Protein Folding	8.29E-14 – 1.62E-02 / 16	Protein Folding	1.95E-15 – 1.28E-02 / 16	Protein Folding	1.11E-11 – 2.88E-04 / 14	Cellular Growth and Proliferation	2.41E-06 – 3.22E-02 / 35	Cell Death	7.20E-07 – 4.91E-02 / 43
3.	Protein Folding	4.65E-11 – 2.71E-02 / 43	Cell Death	4.05E-13 – 2.73E-02 / 110	Cell Death	7.86E-10 – 2.63E-02 / 86	Cell Death	1.14E-10 – 2.86E-02 / 96	Cellular Assembly and Organization	2.44E-06 – 4.26E-02 / 35	Cellular Assembly and Organization	3.40E-06 – 4.64E-02 / 33
4.	Cellular Growth and Proliferation	2.32E-08 – 1.59E-02 / 40	Cellular Growth and Proliferation	1.18E-07 – 2.46E-02 / 67	Cellular Function and Maintenance	2.89E-08 – 2.54E-02 / 31	Cellular Growth and Proliferation	1.43E-10 – 2.25E-02 / 67	DNA Replication, Recombination and Repair	7.10E-06 – 3.47E-02 / 21	DNA Replication, Recombination and Repair	3.40E-06 – 3.87E-02 / 20
5.	Cellular Function and Maintenance	2.32E-08 – 1.37E-02 / 15	Cellular Function and Maintenance	2.71E-07 – 2.70E-02 / 35	Cellular Growth and Proliferation	1.77E-07 – 2.54E-02 / 52	Cellular Function and Maintenance	1.50E-08 – 2.48E-02 / 31	Cellular Movement	3.79E-05 – 4.01E-02 / 23	RNA Post-Translational Modification	1.63E-04 – 6.77E-03 / 6
Top Tox Lists	p-value/Ratio		p-value/Ratio		p-value/Ratio		p-value/Ratio		p-value/Ratio		p-value/Ratio	
1.	Oxidative Stress	1.2E-05 / 7/57 (0.123)	Oxidative Stress Response Mediated by Nrf2	1.95E-03 / 10/205 (0.049)	Oxidative Stress	7.95E-04 / 5/57 (0.088)	Oxidative Stress Response Mediated by Nrf2	8.63E-05 / 12/205 (0.059)	Oxidative Stress Response Mediated by Nrf2	6.69E-03 / 6/205 (0.029)	Mechanism of Gene Regulation by Peroxisome Proliferators via PPAR-Alpha	3.94E-03 / 4/95 (0.042)
2.	Oxidative Stress Response Mediated by Nrf2	5.28E-04 / 10/205 (0.049)	Oxidative Stress	2.28E-03 / 5/57 (0.088)	Oxidative Stress Response Mediated by Nrf2	4.93E-03 / 8/205 (0.039)	Nitric Oxide Receptor Signaling	5.79E-04 / 9/151 (0.06)	Mechanism of Gene Regulation by Peroxisome Proliferators via PPAR-Alpha	7.57E-03 / 4/95 (0.042)	Oxidative Stress	6.77E-03 / 3/57 (0.053)
3.	Mitochondrial Dysfunction	7.42E-03 / 6/125 (0.048)	Mitochondrial Dysfunction	4.31E-03 / 7/125 (0.056)	Mitochondrial Dysfunction	2.22E-02 / 5/125 (0.04)	Oxidative Stress	1.86E-03 / 5/57 (0.088)	Oxidative Stress	1.12E-02 / 3/57 (0.053)	Oxidative Stress Response Mediated by Nrf2	1.28E-02 / 5/205 (0.024)
4.	Mechanism of Gene Regulation by Peroxisome Proliferators via PPAR-Alpha	4.13E-02 / 4/95 (0.042)	G2/M Transition of the Cell Cycle	1.89E-02 / 3/35 (0.086)	Mechanism of Gene regulation by Peroxisome Proliferators via PPAR Alpha	1.22E-01 / 3/95 (0.032)	Mechanism of Gene Regulation by Peroxisome Proliferators via PPAR Alpha	1.6E-02 / 5/95 (0.053)	PPAR-Alpha/RXR Activation	4.69E-02 / 4/166 (0.024)	PPAR-Alpha/RXR Activation	2.63E-02 / 4/166 (0.024)
5.	G2/M Transition of the Cell Cycle	8.24E-02 / 2/35 (0.057)	Cholesterol Biosynthesis	2.71E-02 / 2/16 (0.125)	Aryl Hydrocarbon Receptor Signaling	1.29E-01 / 4/151 (0.026)	PPAR-Alpha/RXR Activation	4.46E-02 / 6/166 (0.036)	PXR/RXR Activation	1.06E-01 / 2/68 (0.029)	PXR/RXR Activation	7.76E-02 / 2/68 (0.029)

7. Movie S-1 (see DVD)

Timeline of resulting Voronoi Treemaps for ENTplas treated vs. untreated S9 epithelial cells. Identified proteins were assorted into individualised KEGG-BRITE hierarchy. Every tile in that structural hierarchy, representing one identified protein, was coloured by logarithmised, normalized expression values (% volume, normalized by the specific Cy-2-standard) of ENTplas treated samples divided by expression values of untreated controls from Delta-2D quantities. The isoluminant divergent colour gradient encodes expression changes: white coloured tiles show expressions, which correspond a fold change of '1'. Blue shaded tiles represent proteins with negative fold change (lower expression in ENTplas treated samples in comparison to the untreated controls) and shades of orange represent proteins with higher fold change than '1'. Saturation of blue and orange is reached at an expression rate five times higher or lower than the corresponding control. The six different time points 0 h, 0.5 h, 1 h, 24 h, 48 h and 72 h are displayed.

8. Movie S-2 (see DVD)

Timeline of resulting Voronoi Treemaps for ENTplas treated vs. untreated S9 epithelial cells. Identified proteins were assorted into individualised KEGG-BRITE hierarchy. The “oxidative stress” section was excerpted and is presented exclusively. Every tile in that structural hierarchy, representing one identified protein, was coloured by logarithmised, normalized expression values (% volume, normalized by the specific Cy-2-standard) of ENTplas treated samples divided by expression values of untreated controls from Delta-2D quantities. The isoluminant divergent colour gradient encodes expression changes: white coloured tiles show expressions, which correspond a fold change of ‘1’. Blue shaded tiles represent proteins with negative fold change (lower expression in ENTplas treated samples in comparison to the untreated controls) and shades of orange represent proteins with higher fold change than ‘1’. Saturation of blue and orange is reached at an expression rate five times higher or lower than the corresponding control. The six different time points 0 h, 0.5 h, 1 h, 24 h, 48 h and 72 h are displayed.

Danksagung

Ich möchte mich hiermit bei all denjenigen bedanken, die an der Entstehung dieser Arbeit beteiligt waren und mir mit ihrem persönlichen Einsatz dabei geholfen haben diese fertigzustellen. Dabei gilt Herrn Professor Dr. med. Werner Hosemann der Dank für die Überlassung des Themas dieser Promotion.

Ganz besonders möchte ich Dr. Christian Scharf für die Betreuung während der gesamten Bearbeitungszeit und darüber hinaus bedanken. Unsere Gespräche und Diskussionen haben mir sehr geholfen mich in die Thematik einzuarbeiten und die Techniken der Molekularbiologie, Massenspektrometrie, Statistik und Mikrobiologie zu verstehen. Deine Anmerkungen und Verbesserungsvorschläge haben diese Arbeit letztendlich zu der gemacht, die sie nun ist. Schließlich danke ich dir für die besondere Betreuung in Hinsicht auf die Massenspektrometrie.

Große Anteile an dieser Arbeit hat auch Dr. Jörg Bernhardt. Nur durch seine Hilfe - und die seines Mitarbeiters Henry Mehlan - konnten die Ergebnisse so visualisiert werden, wie sie es verdient haben. Darüber hinaus halfen deine Anmerkungen und Korrekturen sehr, diese Arbeit zu verfeinern. Auch allen anderen Korrektoren möchte ich an dieser Stelle herzlich danken: Prof. Dr. Uwe Völker, Prof. Dr. Thomas von Woedtke, PD Dr. Georg Daeschlein, PD OA Dr. Achim Beule, Prof. Dr. rer. nat. Robert Jack und Dipl. Nat. Stefanie Arnold konnten dieser Arbeit ihren Feinschliff verpassen. Vielen Dank für die Geduld und die sehr hilfreichen Verbesserungsvorschläge und Kommentare.

Des weiteren gebührt Katrin Darm mein ganz besonderer Dank. Nur durch ihre exzellente Durchführung der proteomischen Versuche konnte diese Arbeit überhaupt erstellt werden. Ihre nette, freundliche und selbstlose Art war stets erfrischend und machte die Arbeit im Labor gleich etwas angenehmer. Letzteres trifft auch uneingeschränkt auf Frau Wolter zu. Sie hatte die sicherlich schwierige Aufgabe den unbedarften Studenten mit den Arbeitstechniken der Molekularbiologie vertraut zu machen. Sie tat dies stets mit ihrer inneren Ruhe und Ausgeglichenheit und kümmerte sich auch über die Einweisungsphase hinaus stets rührend um mich. Dafür möchte ich mich ganz besonders bei ihr bedanken! Dem Rest der Labortruppe und den temporär anwesenden Austauschstudenten gilt mein Dank für die Unterstützung und Unterhaltung während teilweise sehr langwierigen Arbeiten und Tagen im Labor.

Ebenfalls nicht unerwähnt sollten die Mitarbeiter der Firma Decodon um Matthias Berth bleiben. Nur durch ihre Hilfe konnten die großen Datenmengen bewältigt werden.

Dem Graduiertenkolleg 840 der Universität Greifswald gilt der Dank für die wissenschaftliche und finanzielle Unterstützung zur Durchführung dieser Arbeit. Ich wurde als eher untypisches Mitglied sehr freundlich aufgenommen und konnte viel aus den Veranstaltungen und Diskussionen lernen.

Nicht zuletzt danke ich meiner Familie für die uneingeschränkte persönliche und auch finanzielle Unterstützung, die mir meinen beruflichen Werdegang überhaupt erst ermöglicht haben. Die Geduld, die ihr oft für mich aufbringen musstet und die stetigen aufmunternden Worte haben mir viel geholfen. All dies hat dazu beigetragen, dass es überhaupt zu dieser Arbeit kommen konnte.

Dir, Eva, gilt zum Schluss mein herzlichster Dank. Ich danke dir dafür, dass du immer geduldig mit mir warst und mich immer in jeder Hinsicht unterstützt und aufgemuntert hast, wenn dies nötig w